EXPERIMENTAL AND THERMODYNAMIC STUDIES OF IONIC LIQUIDS FOR CARBON DIOXIDE SEPARATION

A Thesis

Submitted to the Faculty of Graduate Studies and Research

In Partial Fulfillment of the Requirement for the

Degree of Master of Applied Science in

Industrial Systems Engineering

University of Regina

By

Tursun John Uygur

Regina, Saskatchewan, Canada

March 2013

UNIVERSITY OF REGINA

FACULTY OF GRADUATE STUDIES AND RESEARCH

SUPERVISORY AND EXAMINING COMMITTEE

Tursun John Uygur, candidate for the degree of Master of Applied Science in Industrial Systems Engineering **,** has presented a thesis titled, ***Experimental and Thermodynamic Studies of Ionic Liquids for Carbon Dioxide Separation,*** in an oral examination held on March 5, 2013. The following committee members have found the thesis acceptable in form and content, and that the candidate demonstrated satisfactory knowledge of the subject material.

External Examiner:	Dr. Hussameldin Ibrahim, Process Systems Engineering
Supervisor:	Dr. Amr Henni, Industrial Systems Engineering
Committee Member:	Dr. Ezeddin Shirif, Petroleum Systems Engineering
Committee Member:	*Dr. Mohamed Ismail, Industrial Systems Engineering
Chair of Defense:	Dr. Cameron Louis, Faculty of Arts

*Not present at defense

ABSTRACT

Capturing greenhouse gases and preventing climate change are becoming imperative global issues. There is a growing awareness that carbon dioxide emission from fossil fuel combustion is the biggest contributor to this environmental phenomenon. One of the most effective and potential solutions of reducing carbon dioxide emission is to capture it from industrial gas streams, such as flue gases. Among the most commonly used technologies, gas absorption via chemical solvent is the most promising technology due to its capacity to handle a large volume of carbon dioxide. Nevertheless, aqueous alkanolamines have shortcomings that make the process costly and environmentally unfriendly. Recently, ionic liquids started playing a significant role in overcoming these inadequacies.

The main objective of this research is to determine the solubility of carbon dioxide in conventional ionic liquids. During this work, a gravimetric microbalance was used to measure the solubility of carbon dioxide in 1,3-Diethoxyimidazolium bis(trifluoromethylsulfonyl)imide [[(ETO)2IM][Tf2N]], 1,3Dimethoxyimidazolium bis(trifluoromethylsulfonyl)imide [[DMIM][Tf2N]], 1-Butyl-1-methylpiperidinium bis(trifluoromethylsulfonyl)imide [[BMPIP][Tf2N]], 1-Butyl-3-methylimidazolium trifluoromethanesulfonate [[BMIM][TfO]] and 1-Butyl-3 methylimidazolium dibutyl phosphate [([BMIM][DBP]] at 298.15, 313.15 and 323.15 over a pressure range of 100 mbar to 20000 mbar. Critical properties of ionic liquids are estimated by group contribution methods, and estimated values were in agreement with

published results. The Peng-Robinson (PR) equation of state and the non-random two-liquid (NRTL) models were used to correlate the experimental results. Consistency tests for obtained NRTL results are also presented.

ACKNOWLEDGEMENTS

First and foremost, I would like to thank Dr. Amr Henni for his valuable and thoughtful guidance, wise advice and encouraging support throughout my graduate program at the University of Regina.

Next, I would like to express my sincere thanks to Drs. David deMontigny, Ezeddin Shirif, and Ataullah Khan for challenging me in their lectures and helping during my studies. I also would like to express my appreciation to Mr. Kazi-Zamshad Sumon and Dr. Aravind V. Rayer for training me on all the experimental laboratory set ups and helping me with Aspen HYSYS.

Finally, my deepest gratitude must go to my mom, wife, sister, and brother. Without your support, patience, understanding, and unwavering optimism, I would not have made it to this point. Your love and support means the world to me.

LIST OF CONTENTS

LIST OF TABLES

LIST OF FIGURES

LIST OF SYMBOLS AND ABBREVIATIONS

Abbreviations:

AAD	Average absolute deviation
EoS	Equation of state
NRTL	Non-random two-liquid models
PVT	Pressure volume temperature
RTILs	Room Temperature ionic liquids
TSILs	Task-specific ionic liquids
VLE	Vapour-liquid equilibrium

Greek symbols:

γ	Activity coefficient
ρ	Density (kg/m^3)
Δ	represents a change
Ω	Acentric factor

Subscripts:

1	Component 1
2	Component 2
b	Boiling point
c	Critical
i	i-th component
j	j-th component

Symbols:

F	Fugacity (bar)
H	Henry's constant (bar)
K	Binary interaction coefficient from equation of state
M	Molar mass (g/mole)
P	Pressure (bar)
R	Universal gas constant (cm^3.bar/mole .K)
T	Temperature (K)
x	Mole fraction in liquid phase

CHAPTER 1

INTRODUCTION

1.1 General Introduction

There is not an absolute universal agreement on the cause of global climate change, but there is growing consensus that global warming is happening, and many climate scientists and scholars believe that a major cause is the anthropogenic carbon dioxide emission into the atmosphere. Fossil fuels currently supply over 86% of the energy needs of the United States, and a similar percentage of the energy is used worldwide because of their low cost, relatively easier availability, high energy density, and the existing reliable technology for energy production (EIA, 2006a, b).

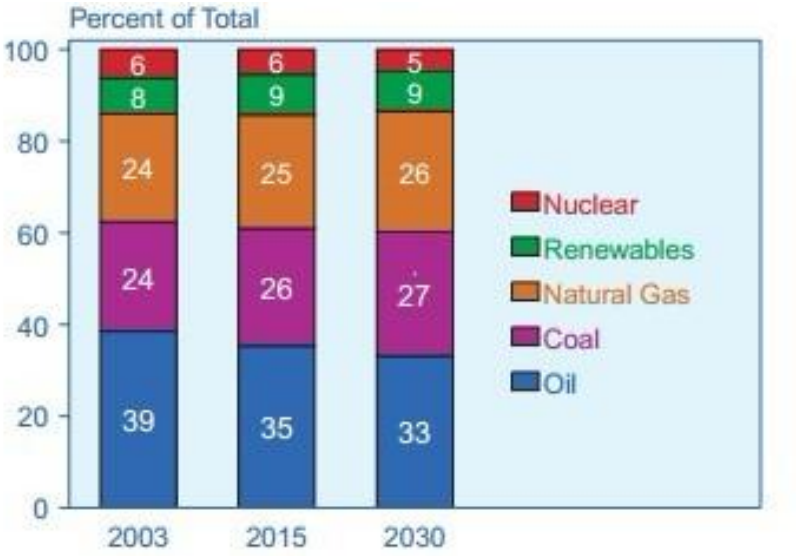

Figure1.1: Fuel Shares of World Marketed Energy Use, 2003, 2015, and 2030 Note: Fuel shares may not add up to 100 percent due to independent rounding. Sources: 2003: Energy Information Administration (EIA).International Energy Annual 2003 (May-July 2005), website: www.eia.doe.gov/iea/. 2015 and 2030: EIA, System for the Analysis of Global Energy Markets (2006) (Original in color)

Global carbon dioxide emissions increased from 22.5 billion tons in1990 to 31.5 billion tons in 2008 (NEAA, 2009). China has overtaken the United States and become the number one CO_2 emitter in 2006 because of its high economic booming rate and coal-dominated energy reliance (Gregg et al., 2008; NEAA, 2009). The Energy Information Administration (EIA) within the U. S. Department of Energy (DOE) estimates that consumption of fossil fuels (coal, petroleum, and natural gas) will increase by 27% over the next 20 years, thereby increasing U.S. CO_2 emissions from the current 6000 million tons per year to 8000 million tons per year by 2030. Although U.S. carbon dioxide emissions are projected to increase, they will decrease from 23% of the world's total in 2003 to 19% in 2030 (EIA, 2006a). Specifically, the EIA estimates that the combined carbon dioxide emissions from China and India in 2030 from coal use will be three times that of the Unites States (China, 8286 million tons of carbon dioxide; India, 1371 million tons of carbon dioxide; U.S., 3226 million tons of carbon dioxide) (EIA, 2006b). This illustrates that no single country can sufficiently reduce GHGs to stabilize global atmospheric concentrations. The efforts must be united and cost effective to sustain domestic and global economic growth while reducing GHG emissions; in order to approach stability, the industry needs new technology that costs less, is more efficient, and causes less harm to the workers and the environment.

The combustion of fossil fuels produces carbon dioxide, a GHG with an increasing potential for by-product end-use in the industrial and energy production sectors. One approach that holds great promise for reducing GHG

emissions is carbon capture and sequestration (CCS). Under this concept, carbon dioxide would be captured from large point sources, such as power plants and natural gas, and injected into geologic formations, such as depleted oil and gas fields, saline formations, and unlikeable coal seams (Klara et al, 2003). Capturing carbon dioxide and using it as a by-product would not only have economic benefits but would simultaneously mitigate global climate change concerns.

1.2 Commonly Used Solvents

1.2.1 Chemical Solvent

Alkanolamines, as various available chemical solvents, have been Used for last couple decades for capturing carbon dioxide from natural gas streams in the gas and oil industry, especially monoethanolamine and diethanolamine, which have achieved a pinnacle position in the gas sweetening industry. This method presents several serious drawbacks, such as intensive energy consumption, cost increases, degradation at high temperature and corrosion. The first two drawbacks are two of the main shortcomings that stop companies from capturing a large amount of acid gases from flue gas. Monoethanolamine is particularly reactive with carbon dioxide and H2S, and can absorb instantaneously. Unfortunately, monoethanolamine reacts irreversibly with organic sulfur compounds, such as carbonyl sulfide, carbon disulfide, and mercaptans. The relatively high vapor pressure and low thermal stability of

monoethanolamine causes significant amount of solvent loss in the regeneration unit. Moreover, amines, especially primary amines, cause serious corrosion to some parts of the gas sweetening unit where the concentration and temperature of acid gas are relatively high. Hence, the utilization of a primary amine in gas sweetening requires the application of corrosion inhibitors, and an amine unit may have to be built with special materials, such as stainless steels (Anne et al., 2010). A simplified process flow sheet for absorption in alkanolamine-based solvents is showed in Figure 1.2.

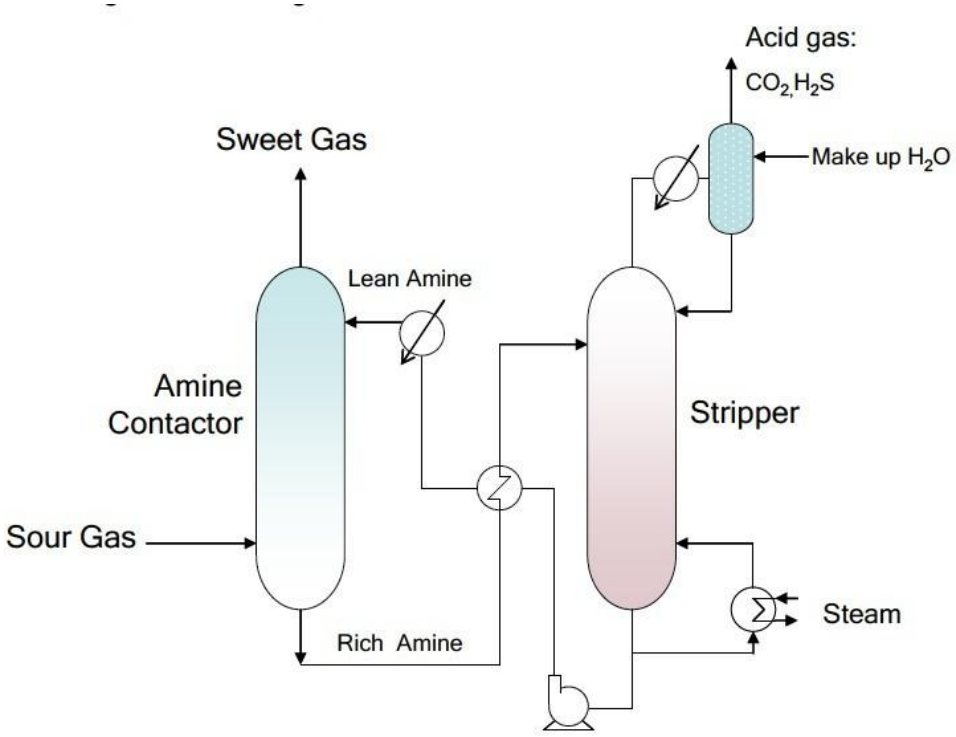

Figure 1.2: Typical Gas Sweetening Process with Alkanolamines (Kohl, et al., 1997) (Original in color)

1.2.2 Physical Solvent

IFPEXOL ©, Selexol ©, *N*-methyl-2-pyrrolidone (Purisol process), methanol (Rectisol process) and propylene carbonate (Fluor solvent process) are the most commonly accepted and widely used solvents for gas treatment. They depend upon a high acid gas partial pressure for solubility and subsequent pressure reduction for regeneration. Energy requirements and degradation for these processes are significantly reduced because heat regeneration is not necessarily required. Absorbed acid gas could be stripped by simple pressure reduction, which keeps the operating cost relatively low. However, the main drawback of these physical solvents is only effective at partial pressures, higher than 5 bars (Singh et al., 2010). Moreover, they have very high affinity to heavy hydrocarbon (especially true of aromatics and unsaturated hydrocarbons), resulting in high hydrocarbons contents in the acid gas stream and subsequent hydrocarbon losses from the treated gas stream. The basic process flow scheme of a physical solvent is shown in Figure 1.3.

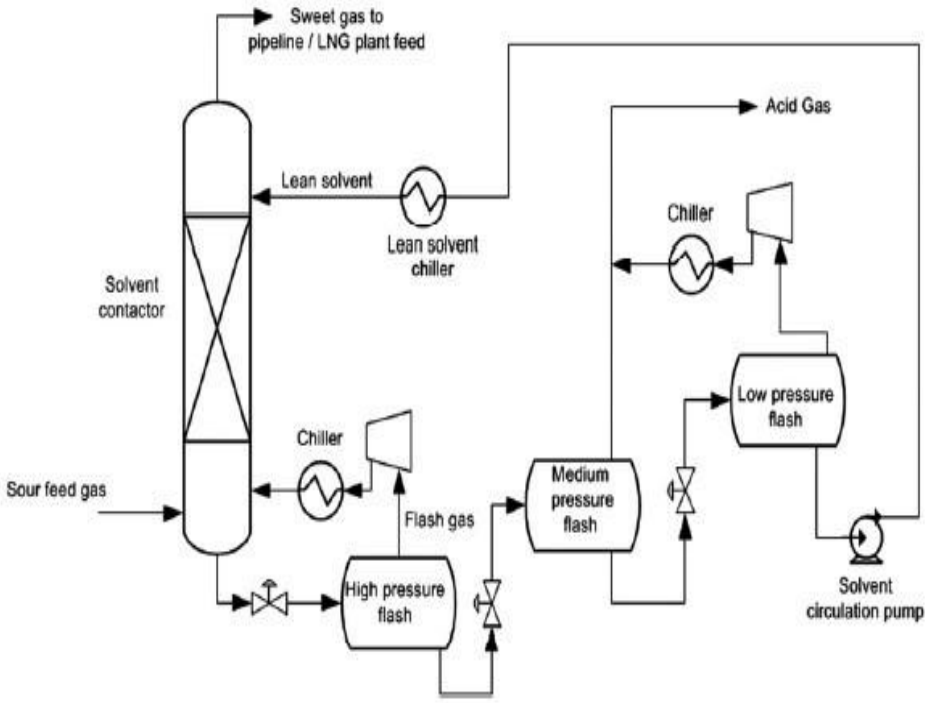

Figure 1.3: Flow Diagram of a Typical Physical Solvent Process for Absorption of CO_2 and Other Acid Gases from Natural Gas (GPSA Engineering Data Book, 2004).

1.2.3 Hybrid Solvent

By combining both physical and chemical solvents, some vendors have developed gas sweetening solvents and processes that take advantage of the benefits of both. One of the most successful and typical hybrid separation processes used in the oil and gas field is the Sulfinol process, licensed by Shell, which uses a mixture of a physical solvent (sulfolane), a chemical solvent [either MDEA (Sulfinol-M) or DIPA (Sulfinol-D)], and water. This process makes the solvent more efficient with lower energy consumption and circulation rates. Moreover, the process has a high acid gas loading and causes less corrosion to the sweetening unit. However, it has a higher co-absorption of heavier hydrocarbons since the physical solvent (sulfolane) has relatively higher affinity to heavy hydrocarbons.

1.3 Effective and Efficient Solvent for Industrial Use

In order to absorb carbon dioxide from natural and flue gas, the promising absorption solvent should have the following characteristics:

- Low vapour pressure and high thermo stability for reducing make-up volume, degradation and contamination of the gas stream with a volatile solvent (Yang et al., 2008).
- Economical in the sense that it regenerates with less energy consumption.
- Doesn’t cause corrosion to gas sweetening unit and equipment.
- Not toxic to operator and environmentally friendly.

- Has high selectivity to acid gas, and absorbs hydrocarbon as little as possible.
- Low circulation rate with low viscosity.
- Foaming should be minimized.

Although, over the last for few decades amine sweetening technology is has been called an unbeaten technology for removing acid gas from natural gas, scientists and engineers have recently developed relatively more effective and efficient technologies. Most of them are based on combining alkanolamines with physical solvents, which means they most likely also bring their disadvantages while they bring their advantages.

1.4 Ionic Liquids and Gas Separations

1.4.1 Ionic Liquids

Most of Room Temperature Ionic Liquids (RTILs), also known as liquid organic, molten, or fused salts, are a class of non-molecular ionic solvents with low melting points and vapour pressures, and with thermal stabilities of some ionic liquids of up to 500K (Heintz et al., 2005). The accepted definition of an RTIL is any salt that has a melting point lower than ambient temperature (Welton, 1999). However, ionic liquid (IL) is often applied to any compound that has a melting point lower than 100°C. The cations are large, bulky asymmetric organic molecules; such as pridinium, imidazolium, pyrrolidinium and phosphonium. On the other hand, the anions are usually small inorganic structures, such as

hexafluorophosphate [PF_6^-], tetrafluoroborate [BF_4], tris(trifluoromethylsulfonyl) methide [$(CF_3SO_2)_3C^-$], bis(trifluoromethylsulfonyl) imide [$(CF_3SO_2)_2N^-$], bis(methylsulfonyl) imide [$(CH_3SO_2)_2N^-$], triflate [$CF_3SO_3^-$], acetate [$CH_3CO_2^-$], trifluoroacetate [$CF_3CO_2^-$], dicyanamide [$(CN)_2N$], nitrate [NO_3^-], chloride [Cl^-], bromide [Br^-], or iodide [I^-]. Some typical common examples of ionic liquids classes are shown in Figure 1.4.

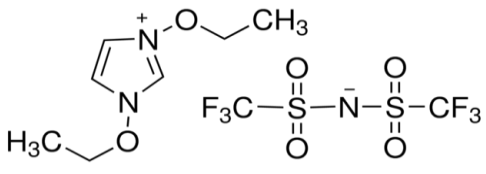

1,3-Diethoxyimidazolium bis(trifluoromethylsulfonyl)imide [(ETO)2IM][Tf2N]

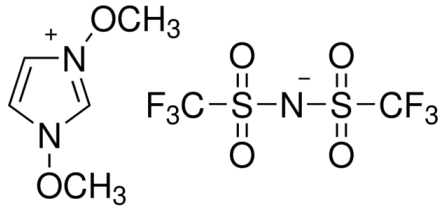

1,3-Dimethoxyimidazolium bis(trifluoromethylsulfonyl)imide [DMIM][Tf2N]

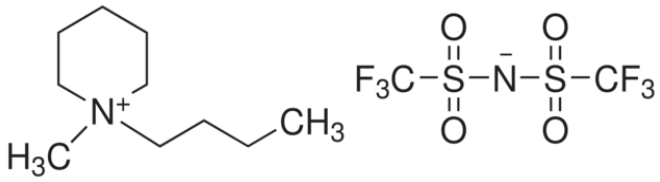

1-Butyl-1-methylpiperidinium bis(trifluoromethylsulfonyl)imide [BMPIP][Tf2N]

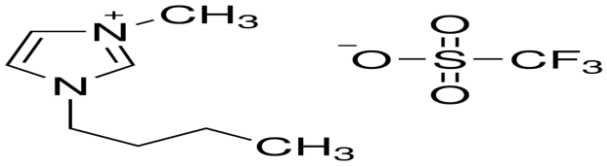

1-Butyl-3-methylimidazolium trifluoromethanesulfonate [[BMIM][TfO]]

Figure 1.4: Schematic of Typical Example Classes of Ionic Liquids.

1.4.2 Development of Ionic Liquids

In 1982, Wilkes first reported on ambient-temperature ionic liquids based on the 1-alkyl-3-methylimidazolium cation (Wilkes et al., 1982). Since then, various types of ionic liquids containing a variety of cations and anions of different sizes have been synthesized in order to have specific characteristics for certain applications. Ionic liquids can be custom synthesized to be miscible or immiscible and have a unique combination of cations and anions which influences the various physical and chemical properties of ionic liquids; hence, they have been described as designable solvents (Freemantle, 1998). Statistically and theoretically, the range of available anion and cation combinations could provide up to 10^{18} different RTILs (Carmichael et al., 2000). As a result of this impetus, the research and application of ionic liquids have been booming in the last ten years.

Bates et al. (2002) added a primary amine chain on the cation of an imidazolium based ionic liquid and synthesized a task-specific ionic liquid (TSIL) so that the solvent can chemically absorb carbon dioxide with higher solubility, and the result of the solubility measurement was approximately 0.5 mol carbon dioxide per mol of solvent at 1 atm at room temperature (~295 K). Gurkan and co-researchers have shown that phosphonium-based amino acid ionic liquids at 1 atm at room temperature (~295 K) can react with carbon dioxide in a 1:1 stoichiometry, achieving higher molar capacities than cation-fuctionalized ionic liquids or even aqueous amine absorbents (Gurkan et al., 2010). Different types of functional moieties, such as amines, alcohols,

carboxylic groups and nitriles, have been synthesized based on conventional and measured solubility in the literature. The ability to fine-tune the properties of ionic liquids by combining cations and anions with functional moieties in ionic liquids permits solvent design. Such research and promising strategies help the synthesis and development of task-specific ionic liquids to fulfill specific functional requirements.

1.4.3 Gas Separations

One of the main potential applications of ionic liquids is to use them for selectively separating gas mixtures since ionic liquids are non-volatile (Sumon et al., 2011). They would not contaminate the gas stream, pollute the environment and harm workers. This unique property means that ionic liquids have an innate advantage over traditional solvents currently used for gas sweetening from natural and flue gas. Whether applied in traditional absorbers or in supported-liquid membrane systems, knowledge of the gas solubility in ionic liquids is required (Cadena et al., 2003). The purpose of this work is to measure the solubility of carbon dioxide in ionic liquids and correlate the experimental data with thermodynamic models.

CHAPTER 2

EXPERIMENTAL METHODS

2.1 Materials

Five different ionic liquids, listed in Table 2.1, were used in this work. They were purchased from Sigma-Aldrich and EMD Millipore Canada. Their purities were removed before sending carbon dioxide to the reactor, although the purities already ranged from 96% to 98%.

Carbon dioxide was purchased from Praxair Inc. (Regina) with a mass purity of 99.99%.

Table 2.1: Studied Ionic Liquids in This Work with Their Shorthand Notation, CAS Number, and Structure

Ionic Liquids	Shorthand Name	CAS number	Structure
1-Butyl-3-methylimidazolium dibutyl phosphate	[BMIM][DBP]	663199-28-8	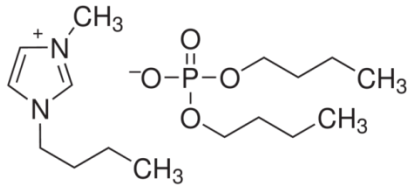
1,3-Diethoxyimidazolium bis(trifluoromethylsulfonyl)imide	[(ETO)2IM] [Tf2N]	1017254-66-8	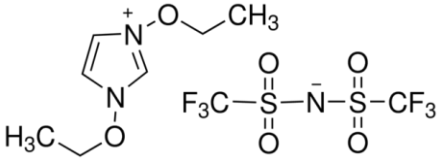
1,3-Dimethoxyimidazolium bis(trifluoromethyl-sulfonyl)imide	[DMIM][Tf2N]	951021-03-7	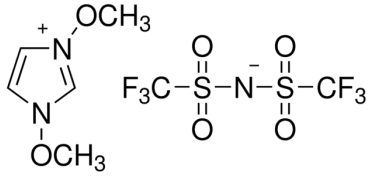
1-Butyl-1-methylpiperidinium bis(trifluoromethylsulfonyl)imide	[BMPIP][Tf2N]	623580-02-9	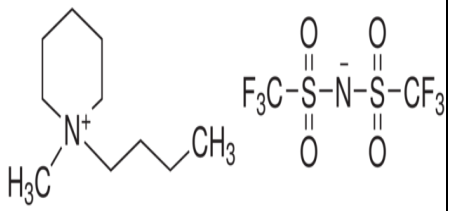
1-Butyl-3-methylimidazolium trifluoromethanesulfonate	[BMIM][TfO]	174899-66-2	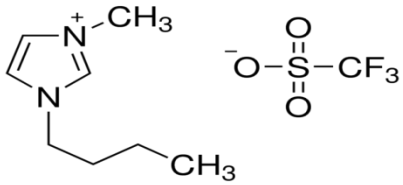
1-Ethyl-3-methylimidazolium (S)-2-aminopropionate	[IE3IM][AMIN]	766537-81-9	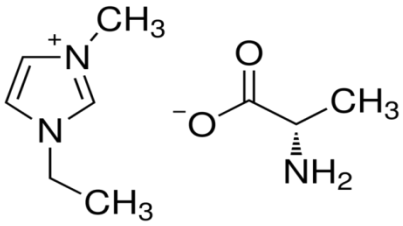

2.2 Density Measurement

The densities of all ionic liquids were measured at temperatures from 278.15 K to 348.15 K and at atmospheric pressure using the DMA 4500, as shown in Figure 2.1. The reproducibility of the measurement was ±0.00005 g/cm^3. A density measurement was performed with an accuracy of ±0.00001g/cm^3. The result of the density measurement is shown in Figure 2.2.

The cell of the density-meter was carefully cleaned with acetone, methanol and distilled water and dried for 30 minutes at 80 °C before injecting ionic liquids.

Figure 2.1: DMA 4500 Density Meter

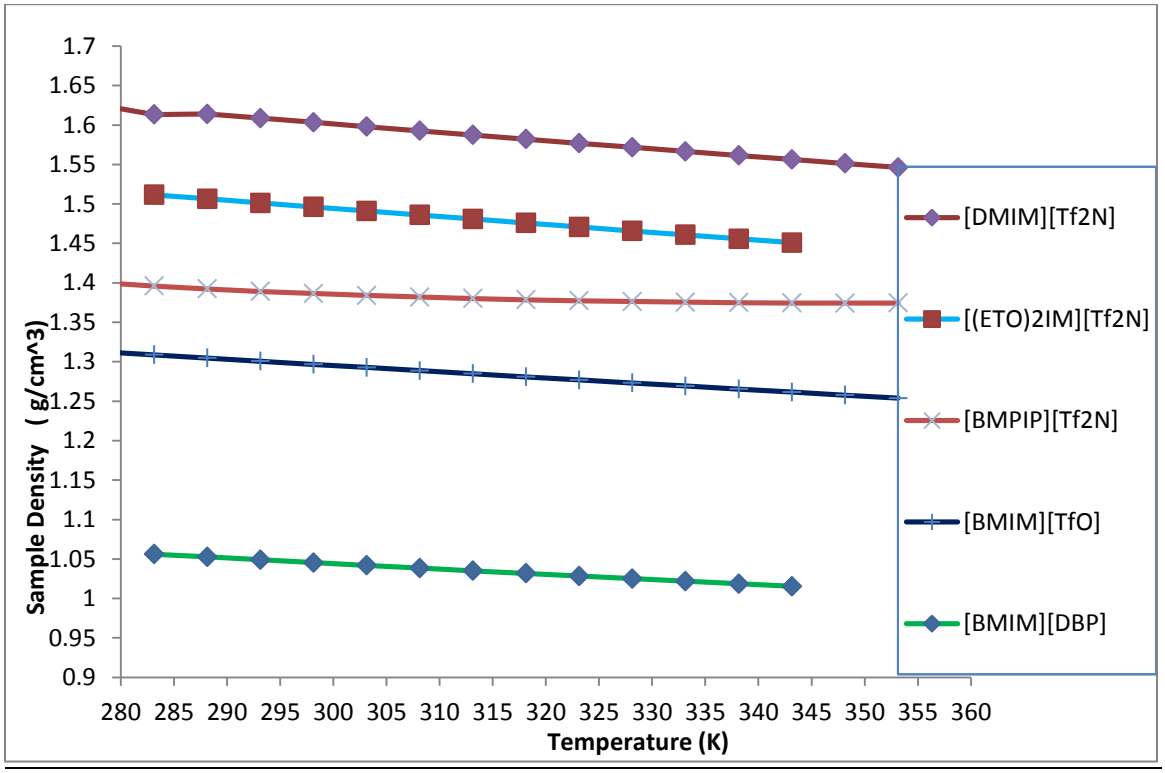

Figure 2.2: Density of Ionic Liquids Used in This Work

2.3 Solubility Measurement

2.3.1 Gravimetric Microbalance

The gas solubility was measured by using an Intelligent Gravimetric Analyzer (IGA 003) from Hiden Analytical, which is shown in Figure in 2. The IGA is a gravimetric microbalance which is capable of measuring absorption isotherms using either vapours in static mode or gases in flowing or static modes. This apparatus has been previously used in absorption experiments and a detailed description of the apparatus can be found elsewhere. A detailed schematic of the apparatus and its components is shown in Figure 2.4.

Figure 2.3: Gravimetric Microbalance

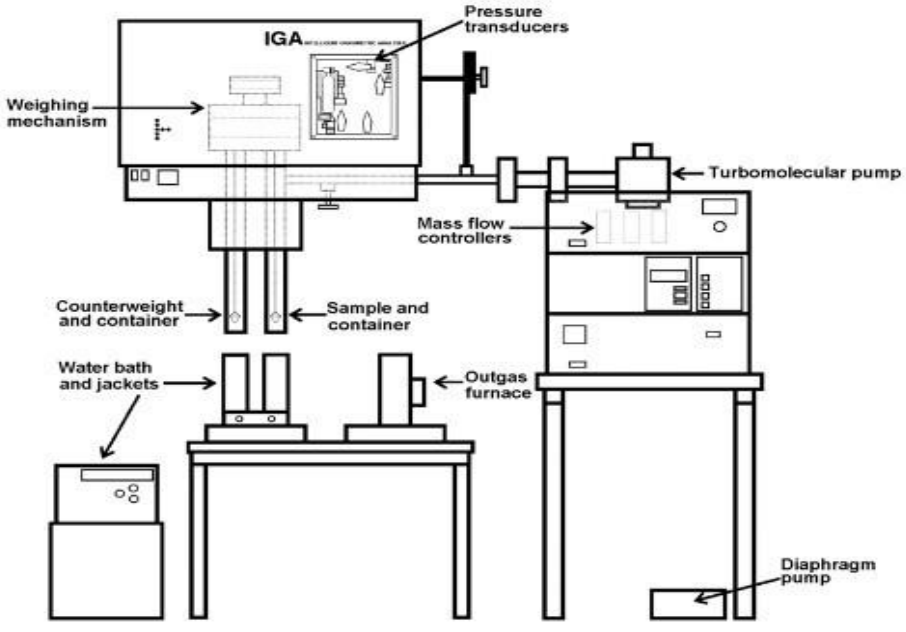

Figure 2.4: Detailed Schematic of Gravimetric Microbalance

Stainless steel foil cylindrical bucket
Approx. height 11mm
diameter 11mm

Figure 2.5: Stainless Steel Foil Cylindrical Bucket

2.3.2 Experimental procedure

In order to minimize buoyancy effects on absorbed mass, the sample pan and counterweight container were symmetrically configured with the exact same stainless steel bucket, as shown in Figure 2.5 with its height and diameter. The sample bucket was filled with approximately 60 to 90 mg of ionic liquids.

After handing the sample bucket onto the chains in the reactor, the reactor vessel was tightly sealed by gaskets and six bolts. The sample was heated and degassed by first pulling a coarse vacuum on the sample with a diaphragm pump and then fully vacuuming the reactor vessel to about 2 milli-bars with a turbo molecular pump The sample was heated to about 60-75°C during this process with an external water jacket, which is connected to an automatically temperature controlled water bath. The sample kept the vacuum at 60-75 °C for a minimum of 10 hours; during this time, the sample weight slowly decreased. It was assumed that the 2%-4% impurity was vacuumed off the ionic liquids, and the purity of sample was roughly close enough to 100% as the residual water, gases, and other unknown components were driven off from the sample. Once the weight of sample had stabilized for approximately 2 hours, the sample was considered fully purified. Then, the sample temperature was set at experimental temperature, and the absorption processes was initiated by sending carbon dioxide when it was stabilized at experimental temperature for approximately 1 hour, as shown in Figure 2.6.

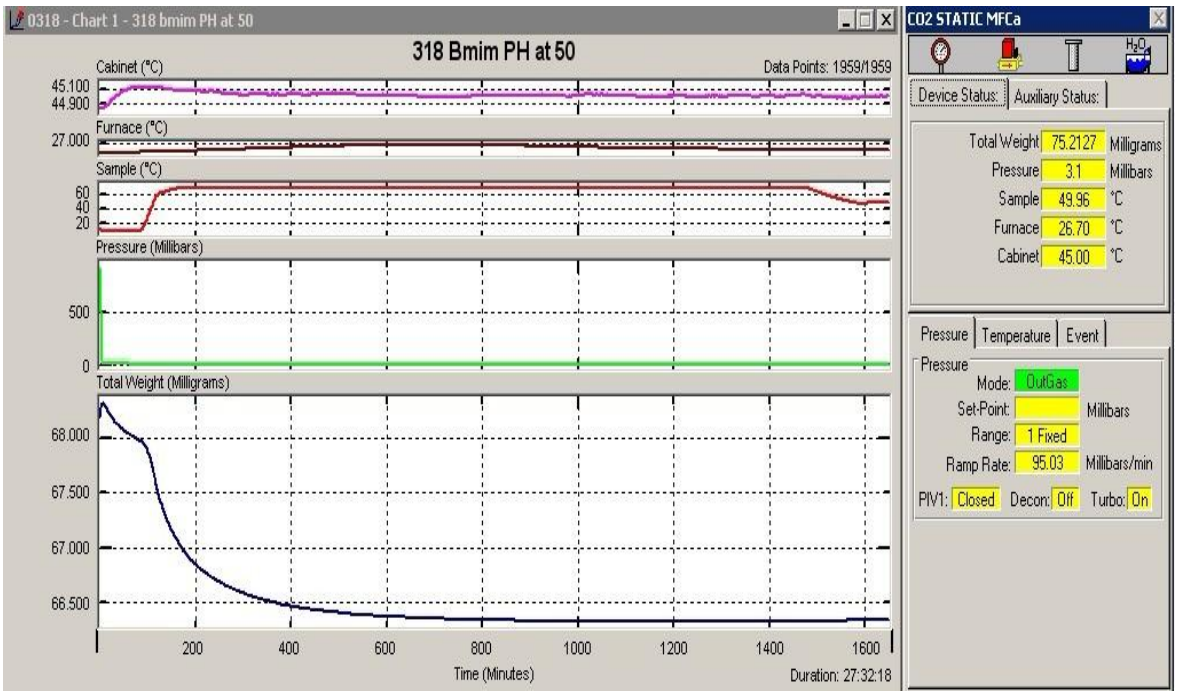

Figure 2.6: Mass Changes in [BMIM][DBP] as a Function of Time Due to Impurity Removal While Treating at Vacuum Pressure at 70 and 50 °C (Original in colour)

During the experiments, the temperature of the reactor vessel was controlled at experimental temperature by a water jacket and constant-temperature water bath. The sample temperature was monitored with a type K platinum thermocouple placed in the reactor vessel and automatically maintained within 0.1 °C of the set point.

2.3.3 Equilibrium Time

One of the most important factors before sending carbon dioxide into the reactor is to make sure sufficient time is given for the system to reach equilibrium. Ionic liquids are known as viscous solvents, so the diffusion of carbon dioxide into the liquid phase can be relatively slow. One of the major advantages of using microbalance for measuring mass change is that the weight change can be monitored my computer screen as a function of time, as shown earlier in Figure 2.6. Monitoring the mass change directly on a screen allows us to determine the time necessary for reaching equilibrium, as shown in Figure 2.7. Thereby, sufficient time could be given before sending carbon dioxide into the reactor vessel via programming. When programming the experiment, the maximum equilibrium time should be at least 30 minutes more than the actual equilibrium time; as shown in Figure 2.7, the maximum equilibrium time, the green line, is about 150 minutes more than the real equilibrium time, the blue line.

The equilibrium time for all samples in this work ranged from 120 to 280 minutes and depended on the ionic liquid, the pressure, and temperature; a more viscous ionic liquid takes a longer time at a lower temperature and pressure.

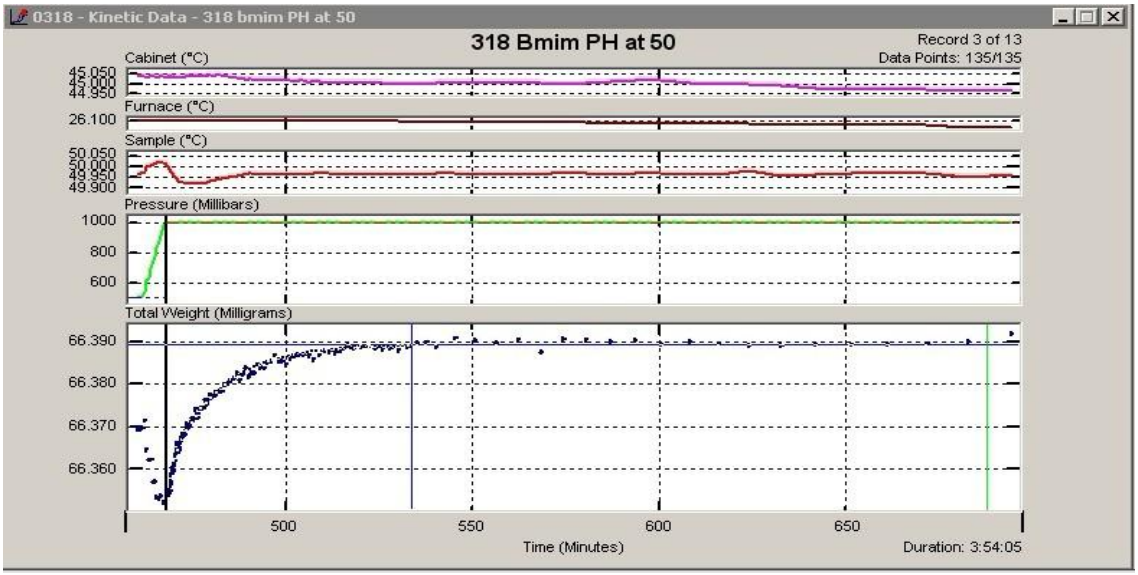

Figure 2.7: Reaching Equilibrium in [BMIM][DBP] as a Function of Time at 1000 Millibars and 50 °C (Original in Colour)

2.4 Buoyancy and Data Correction

One of the most important tasks after measuring the solubility is to account and correlate the effect of buoyancy on the measurements. Thermogravimetric analysis provides a direct and powerful method for assessing both gas solubility and diffusivity, and it must be carefully correlated for a number of gravitational balance forces introduced at high pressure (Pinkerton et al., 2001). These include (Shiflett et al., 2005):

(1) Changes in the buoyant forces due to changes in pressure and temperature.

(2) Aerodynamic drag forces created by the flow of gases.

(3) Changes in the balance sensitivity due to changes in temperature and pressure.

(4) Volumetric changes in the samples due to expansivity (Anthony et al. 2002).

Shiflett et al. (2005) developed an empirical buoyancy correlation equation, as showing equation 2.1, and calculated the upward force buoyancy force using equation 2.1 where the mass of the carbon dioxide displaced is equivalent to the volume of the submersed object V_i multiplied by the carbon dioxide density (p_g) at a measured temperature and pressure and the local gravitational acceleration (g).

$$C_b = \text{Buoyancy} = gV_i p_g(T,P) = g\frac{m_i}{p_i}p_g(T,P) \qquad (2.1)$$

In the binary system, the volume of IL is considered to be a constant, but during the experiment at a high temperature, the volume expansion might be large enough to influence the buoyancy correlation, especially, when light gases are absorbed at a high temperature and low pressure. Shiflett et al. (2005) calculated

the volume of ionic liquid and carbon dioxide using their weights and densities, as shown in equation 2.2-2.6:

$$V_{m_{IL}} = \frac{MW_{IL}}{p_{IL}} \quad (2.2)$$

$$V_{m_{Gas}} = \frac{MW_{gas}}{p_{gas}} \quad (2.3)$$

According to Kai's rule, once the mole fraction of gas (x) is introduced into a binary system, the average molar volume is:

$$V_{m_{av}}(T,P) = V_{m_{IL}}(1-x) + V_{m_{gas}}x \quad (2.4)$$

Then the volume of the ionic liquid could be calculated using the average liquid volume, the moles of the ionic liquid, and the moles of absorbed gas:

$$\text{V (T, P)} = V_{m_{av}}(T,P)\left[\left(\frac{m_{IL}}{MW_{IL}}\right) + \left(\frac{m_{ab-gas}}{MW_{gas}}\right)\right] \quad (2.5)$$

$$\text{V(T, P)}p_{gas}(T,P) = \frac{m_{IL}}{p_{IL}(T_{IL})}p_{gas}\left(T_{IL,}P\right) + \frac{m_{ab-gas}}{p_{ab-gas}(T_{IL})}p_{gas}\left(T_{IL,}P\right) \quad (2.6)$$

The weight measured using microbalance is the mass difference between the sample side (i) and counterweight side. Therefore, once a correction (C_f) due to the sensitivity of the balance, and equation 2.6, because of the expansivity of ionic liquids in liquid phase in binary system, are introduced into equation 2.1, the mass difference between sample side and counterweight side can be expressed as :

IGA measured weight $=\sum_{S_i=1} m_{IL} - \sum_{cw_j} m_{cw_j} - \sum_{s_i=1} \frac{m_{IL}}{p_s} p_{gas}(T_{IL,}P) +$

$\sum_{cw_j=1} \frac{m_{cw}}{p_{cw}} p_{gas}\left(T_{Cw_j}, P\right) + m_{IL} + m_{ab-gas} \frac{m_{IL}}{p_{IL}(T_{IL})} p_{gas}(T_{IL}, P) - \frac{m_{ab-gas}}{p_{ab-gas}(T_{IL})} -$

$C_{f(T_{IL}P)}$ (2.7)

The sample container, sample, and counterweight contribute to mass change more since their densities are relatively less.

In order to better convey an understanding of equation 2.7, the schematic diagram of counterweight and sample side of Hiden Isochema IGA 003 is shown in Figure 2.8, and the basic parameters of microbalance components contributing to Buoyancy Calculation are shown in Figure 2.9.

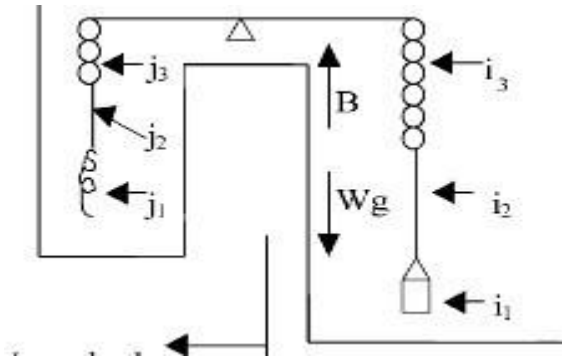

Figure 2.8: Schematic Diagram of Counterweight and Sample Side of Hiden Isochema IGA 003

Table 2.2: Microbalance Components Contributing to Buoyancy Calculation

Subscript	Items	Weight(g)	Materials	Density(g/cm^3)
s	IL	m_{IL}	shown in table 2.1	p_{IL}
a	CO_2	m_{ab-gas}	CO_2	p_{gas}
i_1	bucket	0.6327	stainless steel	7.393103
i_2	wire	0.06524	tungsten	21
i_3	chain	0.3055	gold	19.8
j_1	counter-weight	0.81219	stainless steel	7.9
j_2	hook	0.00582	tungsten	21
j_3	chain	0.239	gold	19.8

CHAPTER 3

SOLUBILITY STUDIES

3.1 Ionic Liquid Treatment and Equilibrium Time

[(ETO)2IM][Tf2N]: The 1,3-Diethoxyimidazolium bis(trifluoromethyl sulfonyl)imide used in the gas solubility measurements was purchased from SIGMA-ALDRICH with 98% purity and was used as received. It is a relatively clear liquid of high density. It was dried under vacuum at 70°C for more than 12 hours in all three experiments before carbon dioxide to sample was sent to the sample chamber. It took about 60 minutes to reach equilibrium under 1000 millibars pressure at 50 °C.

[DMIM][Tf2N]: 1,3-Dimethoxyimidazolium bis(trifluoromethylsulfonyl)imide was also obtained from SIGMA-ALDRICH with 98% high purity and was used as received. Its density is very similar with to that of [(ETO)2IM][Tf2N], and it is a clear liquid with a slight yellow tint. It was dried under vacuum at 65 °C for at least 18 hours before carbon dioxide was sent to the sample chamber. It took approximately 18 minutes to reach equilibrium under 1000 millibars pressure at 50 °C.

[BMIM][TfO] : 1-Butyl-3-methylimidazolium trifluoromethanesulfonate was purchased from EMD Millipore Canada with 98% purity and was used as received. It is relatively less viscous. The sample was transferred into the bucket almost entirely under the effects of gravity without pressing plastic pipette. It was dried under vacuum at 75 °C for at least 10 hours before carbon dioxide was sent

to the sample chamber. It took about 45 minutes for to reach equilibrium under 1000 millbars pressure at 50 °C.

[BMIM][DBP]: 1-Butyl-3-methylimidazolium dibutyl phosphate was obtained from SIGMA-ALDRICH with 96% purity and was used as received. It was the most viscous among all five samples. It is a slightly yellow liquid. It was dried for at least 10 hours at 70 °C under vacuum conditions before carbon dioxide was sent to the sample chamber. It took about 70 minutes to reach equilibrium at 50 °C under atmospheric pressure.

[BMPIP][Tf2N]: 1-Butyl-1-methylpiperidinium bis(trifluoromethyl sulfonyl)imide was purchased from SIGMA-ALDRICH with 97% purity and used as received. It is a clear liquid with a slight yellow tint. It was dried for at least 12 hours at 75 °C under vacuum conditions before send carbon dioxide was sent to the sample chamber. It took about 20 minutes to reach equilibrium at 50 °C under vacuum conditions.

Sufficient equilibrium time was given in all experiments; at least 30 minutes more than the actual equilibrium time. Also, the impurity was removed by drying at high temperature under vacuum pressure. Table 3.1shows the given equilibrium time and treatment time at a certain high temperature for each experiment in this work.

1-Ethyl-3-methylimidazolium (S)-2-aminopropionate(as shown in Table 2.1), a task –specific ionic liquid with a primary amine anion that reacts chemically with carbon dioxide, was purchased from SIGMA-ALDRICH with 96%

purity, and the solubility of carbon dioxide was measured at 298.15K and at 2000 millibars. Unfortunately, the measurement was not completed as planned for three isothermals (298.15K, 313.15K and 323.15K) at 13 pressures (range from 100 to 20000 millibars) because for number of reasons. Firstly, the equilibrium time it needed was too long to be realistically done by IGA. 33000 minutes (23 days) as a maximum equilibrium time was given at 298.15K and at 2000 millibars, but it is clearly shown in Figure 3.1that the weight of the sample was still sharply increasing after the given maximum equilibrium time, which means it did not fully reach equilibrium. Secondly, its thermal stability which is strongly required by IGA was relatively lower than conventional ionic liquids. 68.483 milligrams (at 1000 millibars and at 25°C) of sample was loaded in the bucket, and the shown sample weight after one hour was 65.6753 milligrams (at 2.2 milli bars and 50 °C), and it had not been stabilized even 50 hours later (sample weight was 61.4781mg at 3.6 millibars and 50 °C) as do conventional ionic liquids do. Presumably, the most convincing reason is that the sample was vaporizing since the percentage of decrease (>6%) was unacceptably higher than the impurity of the sample (<4%) even when the weight loss from 68.483 mg to 65.6753 mg was fully considered as a buoyancy effect and was not counted.

Table 3.1: Given Equilibrium Time, Treated Temperature, and Time and Weight Change

Pre-experimental treatment process						Experimental process	
ILS	Experiment Temperature/ °C	Loaded Weight at Ambient T/P (mg)	Treated Temperature At Vacuum (°C)	Treated Hours At vacuum Condition (Hours)	Weight after Treatment at Treated Temperature under Vacuum /(mg)	Given Minimum Equilibrium time Given (Minute)	Given Maximum Equilibrium time (Minute)
[(ETO)2IM][Tf2N]	25.0	65.277	70.0	21	65.107	140	300
	40.0	67.414	70.0	12	67.224	130	200
	50.0	66.960	65.0	29	66.772	100	300
[BMIM][DBP]	25.0	61.671	70.0	22	60.027	220	300
	40.0	52.330	70.0	12	46.860	180	230
	50.0	68.139	70.0	23	66.322	220	300
[BMIM][TfO]	25.0	77.348	70.0	16	77.232	220	400
	40.0	70.907	70.0	12	69.860	100	120
	50.0	76.779	70.0	11	75.688	200	250
[DMIM][Tf2N]	25.0	64.808	65.0	11	64.506	150	300
	40.0	66.007	70.0	10	65.598	120	200
	50.0	62.08	70.0	14	61.932	120	300
[BMPIP][Tf2N]	25.0	78.326	75.0	10	78.116	180	250
	40.0	66.383	75.0	12	66.180	180	250
	50.0	79.093	75.0	11	78.934	180	250

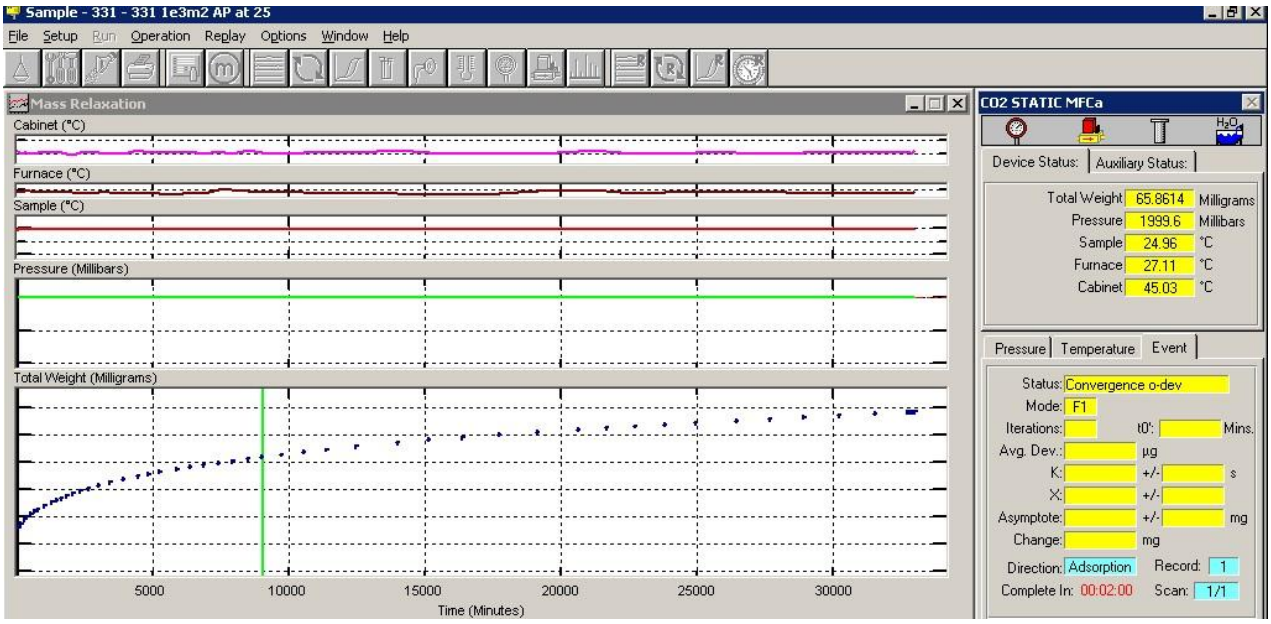

Figure 3.1: Reaching Equilibrium in [IE3IM][AMIN] as a Function of Time at 2000 Millibars and 25 °C (Original in colour)

3.2 Thermodynamic Properties and Solubility Results

3.2.1 Phase Equilibrium

The quantitative description of vapour-liquid equilibrium requires that the properties of vapour phase and liquid phase be known. These properties are then interrelated by the condition of equilibrium. For any component i, the general conditions are:

$$T_V = T_L \tag{3.1}$$

$$P_V = P_L \tag{3.2}$$

Conditions 3.1 and 3.2 also could be described with chemical potentials μ:

$$\mu_i^V(\mathrm{T},\mathrm{P}) = \mu_i^L(\mathrm{T},\mathrm{P}) \tag{3.3}$$

Equation 3.3 expresses the equality of chemical potentials of a component in the vapour and in the liquid for all the components in the system. Chemical potential needs to be changed to measurable physical quantities since chemical potential is not physically measurable. Integrating the chemical potential for a pure ideal gas at a certain constant temperature, we obtain:

$$\int_{\mu_0}^{\mu} d_\mu = \int_{P^O}^{P} V_{av}dp \Rightarrow \mu_i - \mu_i^o = RTln\frac{P}{P^O} \tag{3.4}$$

where μ_i^o refers to the value of μ_i as an ideal gas at unit pressure.

Furthermore, the function f, fugacity, is defined for any isothermal change for any component in any system. For each component i in the system, Equation 3.1 and 3.2 or 3.3 could be written:

$$f_i^V = f_i^L \tag{3.5}$$

Applying Equation 3.5 to Equation 3.4 gives the following:

$$\mu_i^V - \mu_i^L = RTln\frac{f_i^V}{f_i^L} = 0 \quad (3.6)$$

The ratio $\frac{f_i^V}{f_i^L}$ between vapour and liquid phase is an activity of a substance, a. The activity changes when non-ideal molecules interact in a gas or liquid; hence, in an ideal solution, a=1. This is why the fugacity is a well-behaved function with a→1as P→0.

From the definition of fugacity of the components in vapour-liquid mixtures, Equation 3.5 can be written as:

$$\Phi_i y_i P = \gamma_i x_i f_i^o \quad (3.7)$$

where $\Phi_i$is the fugacity coefficient of component i, x_i is the mole fraction of component i in liquid phase, P is the partial pressure in the binary system, y_i is the mole fraction of component i in the vapour phase. γ_i is the activity coefficient of component i and f_i^o is the fugacity at the standard state of component i. Also, y_i could be simplified as y_i≈1since ionic liquids have high thermal stability and negligible vapour pressure.

The fugacity f_{iL}^o of pure liquid I at the system T and P can easily be related to its valor pressure p_i^o at T:

$$f_{iL=}^o P_i^o \Phi_i^o \exp[\frac{V_{iL}}{RT}(P - P_i^o)] \quad (3.8)$$

The exponential factor reflects the effect of P being different from vapour pressure p_i^o, assuming the liquid volume change is V_{iL} when the pressure

changes between p and P_i^o. The quantity Φ_i^o is the fugacity coefficient of the pure i as a saturated fluid at set temperature T and P_i^o.

All experiments in this study were operated under 20 bars, in which condition the IL is not compressible, i.e., no volume changes occur, and the Poynting correction has been neglected in all cases.

Alternatively, if the assumption of ideal gas behavior is not valid, the fugacity coefficient will not be unity and must be calculated. For calculating the fugacity coefficient, the Virial equation of state (EoS) is applied. EOS works better at low to moderate pressure since the pressure is linear with compressibility factor Z. The relation between fugacity coefficient, partial pressure and compressibility factor Z could be expressed as:

$$\ln\Phi=\int_0^P \frac{(Z-1)}{P} dP \qquad (3.9)$$

3.2.2 Henry's Law Constant

Henry's constant, as a proportional constant, is related to the partial pressure of the gaseous and liquids phase at an infinitely dilute system (Prausnitz et al., 1999). The gas solubility in most liquid is too low to be described by Henry's Law. The equation relating the fugacity of the gas component i dissolved in the liquid phase f_I^L and composition x_i is:

$$H_i(T,P) = \lim_{x_{i\to 0}} \frac{f_i^L}{x_i} \qquad (3.10)$$

Henry's Constant,$H_i(T,P)$, is strongly sensitive to and dependent on temperature, but is less sensitive to and dependent on pressure. If the binary system is an ideal vapour-liquid equilibrium (i.e. Φ_i=1;$y_i = 1$), then the fugacity f_I^L

is equal to the total pressure of the vapour liquid equilibrium. In this work, the ionic liquid has high thermal stability and negligible vapour pressure, and Henry's assumption is applicable to the system in this work, so the binary system in this work is studied as an ideal system. For the system studies in this work, Henry's Law could be written as follows:

$$P_i = H_i(T)x_i \quad (3.11)$$

where P_i is partial pressure of carbon dioxide, the unit of Henry's constant is pressure per mole fraction.

The Henry's constant could also be described with the infinite dilution activity coefficient, γ_i, and the pressure of the gas phase:

$$\Phi_i y_i P = \gamma_i x_i f_1^0 \quad (3.12)$$

The ionic liquid and carbon dioxide mixture is considered an ideal mixture, so taking the f_1^0=P_1^{sat}, where P_1^{sat} is the vapour pressure of pure gas at set temperature T, then the Equation 3.12 can be re-written as:

$$P=P_1^{sat}x_i\gamma_i \quad (3.13)$$

Equation 3.13 means that the activity coefficient of gas that is dissolved into ionic liquid phase could be calculated by the measured mole fraction of carbon dioxide in ionic liquids and the pressure created by carbon dioxide above ionic liquid. Henry's constant gives a linear relationship between pressure and solute concentration; hence, it can be calculated from the linear slope of experimental solubility data. The estimated Henry's constant for carbon dioxide in five ionic liquids at three different temperatures that are studied in this work is shown in

Table 3.2. Also, the Henry's constants as function of temperature are shown in Figure 3.2.

Table 3.3 shows a summary of Henry's constants from the literature review.

As shown in Table 3.1, the Henry's Law constants for carbon dioxide in ionic liquids increase with temperature, indicating lower carbon dioxide solubility at higher temperatures.

Table 3.2: Henry's Law Constants for Carbon Dioxide in Ionic Liquids

Ionic Liquids	Temperature (K)	Henry's Constants (bar)
[(ETO)2IM][Tf2N]	298.15	34.64
	313.15	43.79
	323.15	54.07
[BMIM][DBP]	298.15	46.13
	313.15	57.28
	323.15	68.62
[BMIM][TfO]	298.15	47.06
	313.15	65.21
	323.15	78.57
[DMIM][Tf2N]	298.15	40.67
	313.15	54.36
	323.15	66.32
[BMPIP][Tf2N]	298.15	35.70
	313.15	47.16
	323.15	55.85

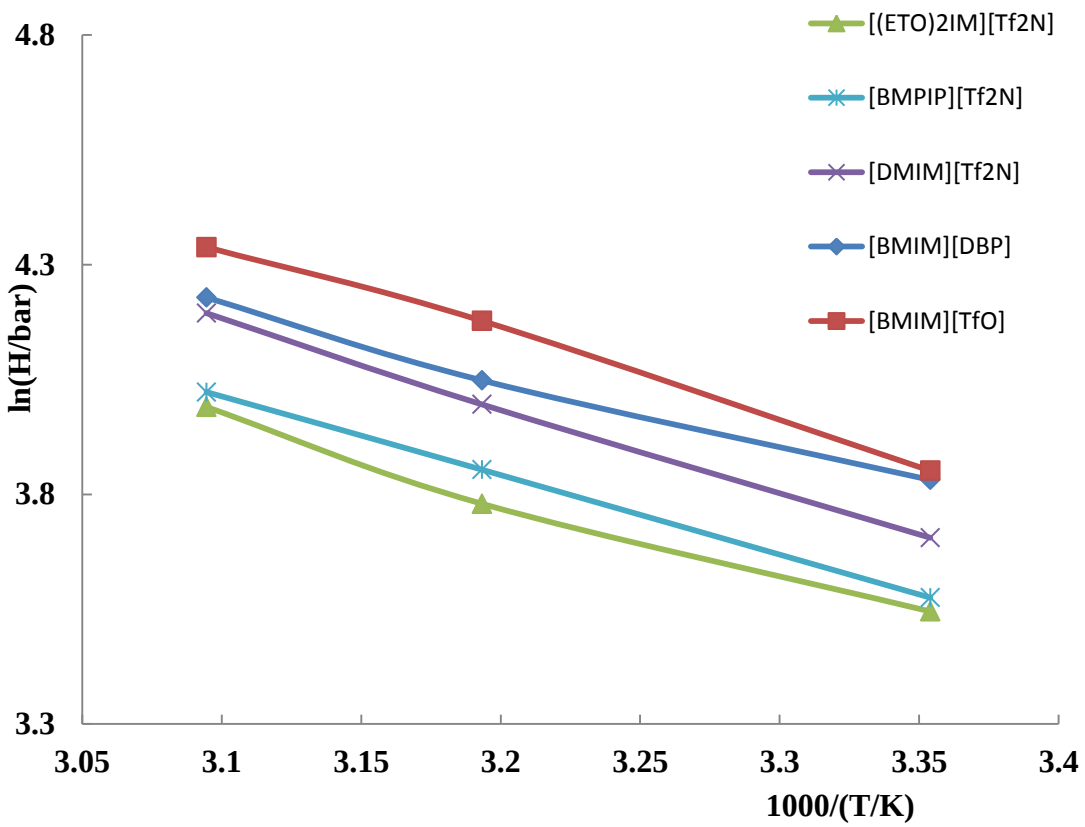

Figure 3.2: Henry's Constants for Carbon Dioxide as a Function of Temperature (Original in colour)

Table 3.3: Literature Summary of Henry's Constants for Carbon Dioxide in Ionic Liquids

Source	Ionic Liquid		T(K)	Henry's Constant (Bar)
	Cation	Anion		
(Anderson et al., 2008)	1-hexyl-3-methylimidazolium	bis(trifluoromethyl sulfonyl)imide	283	25.4
			298	32.8
			333	46.2
	1-hexyl-3methylpyridinium	bis(trifluoromethyl sulfonyl)imide	283	24.2
			298	31.6
			333	45.6
(Anthony et al.,2002, 2005)	1-*n*-butyl-3-methylimidazolium	hexafluorophosphate	283	38.7
			298	53.4
			323	81.3
	1-*n*-butyl-3-methylimidazolium	hexafluorophosphate	283	38.8
			298	53.4
			323	81.3
	1-*n*-butyl-3-methylimidazolium	tetrafluoroborate	283	41.8
			298	59.0
			323	88.6
	1-*n*-butyl-3-methylimidazolium	bis(trifluoromethyl sulfonyl)imide	283	25.3
			298	33.0
			323	48.7

(Anthony et al.,2002, 2005)	methyl-butyl-pyrrolidinium	bis(trifluoromethyl sulfonyl)imide	283	30.2
			298	38.6
			323	56.1
(Finotello et al., 2008)	1-*n*-hexyl-3-methylimidazolium	bis(trifluoromethyl sulfonyl)imide	298	34.5
			313	43.6
			328	53.7
			343	64.8
	1-ethyl-3-methylimidazolium	bis(trifluoromethyl sulfonyl)imide	298	39.5
			313	50.7
			328	63.8
			343	79.0
	1,3-dimethylimidazolium	methyl sulfate	298	131.7
			313	172.3
			328	222.9
			343	263.4
	1-ethyl-3-methylimidazolium	tetrafluoroborate	298	81.1
			313	101.3
			328	131.7
			343	162.1
(Shiflett et al., 2008)	1-*n*-hexyl-3-methylimidazolium	bis(trifluoromethyl sulfonyl)imide IUPAC	282	23.0
			297	30.1
			323	45.5
			348	60.6

(Shiflett et al., 2007)	1-*n*-hexyl-3-methylimidazolium	bis(trifluoromethylsulfonyl)imide EMD	282	22.9
			297	30.4
			323	46.9
			348	61.7
(Shiflett et al., 2005)	1-*n*-butyl-3-methylimidazolium	hexafluorophosphate	283	40.7
			298	55.6
			323	85.5
			348	125.0
	1-n-butyl-3-methylimidazolium	tetrafluoroborate	283	42.9
			298	58.1
			323	91.7
			348	133.3

3.2.3 Derivation for Enthalpy and Entropy of Gas Solubility

Temperature is known to have significant effects on Henry's constants. The derivation of temperature is known to have effects on either the partial molar enthalpy or the partial molar entropy of the solute in the solution. Therefore, enthalpies and entropies of absorption can be determined by the temperature effects on gas solubility. The enthalpy informs the strength of interaction between liquid and gas molecules in liquid phase, whereas the entropy shows the level of ordering that takes place in the vapour and liquid mixture (Prausnitz et al., 1999). They could be expressed as per the following thermodynamic relations (Hildebrand et al., 1962):

$$\Delta h_i = h_i^{mix} - h_i^{pure} = RT(\frac{\partial lnx_i}{\partial lnT})_P(\frac{\partial lna_i}{\partial lnx_i})_{T,P} \quad (3.14)$$

$$\Delta s_i = s_i^{mix} - s_i^{pure} = R(\frac{\partial lnx_i}{\partial lnT})_P(\frac{\partial lna_i}{\partial lnx_i})_{T,P} \quad (3.15)$$

where h_i^{mix} and s_i^{mix} are the partial molar enthalpy and entropy of the carbon dioxide in ionic liquids, h_i^{pure} and s_i^{pure} are the partial molar enthalpy and entropy of pure carbon dioxide in the ideal condition, and a_i is the activity of carbon dioxide in the liquid phase; it is relation with the activity coefficient and the mole fraction is : $a_i = \gamma_i x_i$

If the Henry's Constants is introduced into Equations 3.14 and 3.14 via the dependent factors of pressure and temperature, then the result would be Van's Hoff equations:

$$\Delta h_i = h_i^{mix} - h_i^{pure} = -R(\frac{\partial lnx_i}{\partial(\frac{1}{T})})_P = R(\frac{\partial lnH_i(T)}{\partial(\frac{1}{T})})_P \quad (3.16)$$

$$\Delta s_i = s_i^{mix} - s_i^{pure} = -R(\frac{\partial lnx_i}{\partial(T)})_P = -R(\frac{\partial lnH_i(T)}{\partial ln(T)})_P \quad (3.17)$$

Estimated Enthalpy and Entropy for carbon dioxide in five ionic liquids that are studied in this work are shown in Table 3.4:

Table 3.4: Enthalpy and Entropy for Carbon Dioxide in Ionic Liquids

Ionic Liquids	Enthalpy (kJ/mol)	Entropy (J/mol K)
[(ETO)2IM][Tf2N]	-14.06	-45.43
[BMIM][DBP]	-12.58	-40.63
[BMPIP][Tf2N]	-14.35	-46.29
[DMIM][Tf2N]	-15.61	-50.37
[BMIM][TfO]	-15.72	-50.71

3.3 Solubility Results and Analysis

3.3.1 General solubility discussion

The solubility measurement of carbon dioxide in five ionic liquids (shown in Table 2.1) was accomplished at 298.15, 313.15, and 323.15 K. The experimental results are reported in Figure 3.3 and Tables 3.5 to 3.9.

CO_2 solubility is particularly important because of its common existence in many industrial gas mixtures and the need to separate it from those gas streams in an economic and efficient way. Ionic liquids have one of the highest affinity and selectivity for carbon dioxide, which is why it is essential that we understand how the ionic liquids and carbon dioxide interact in order to design and optimize the process of using ionic liquids (Moore et al., 2000). Moreover, the phase behaviour of CO_2 in ionic liquids is important for the development of several potential ionic liquid designs and applications including extraction of organic solutes (Blanchard et al., 2001), catalytic reactions (Webb et al., 2003) and the separation from CO_2 from gas mixtures (Sumon and Henni, 2011). The thermodynamic phase modeling is expressed in Chapter Four.

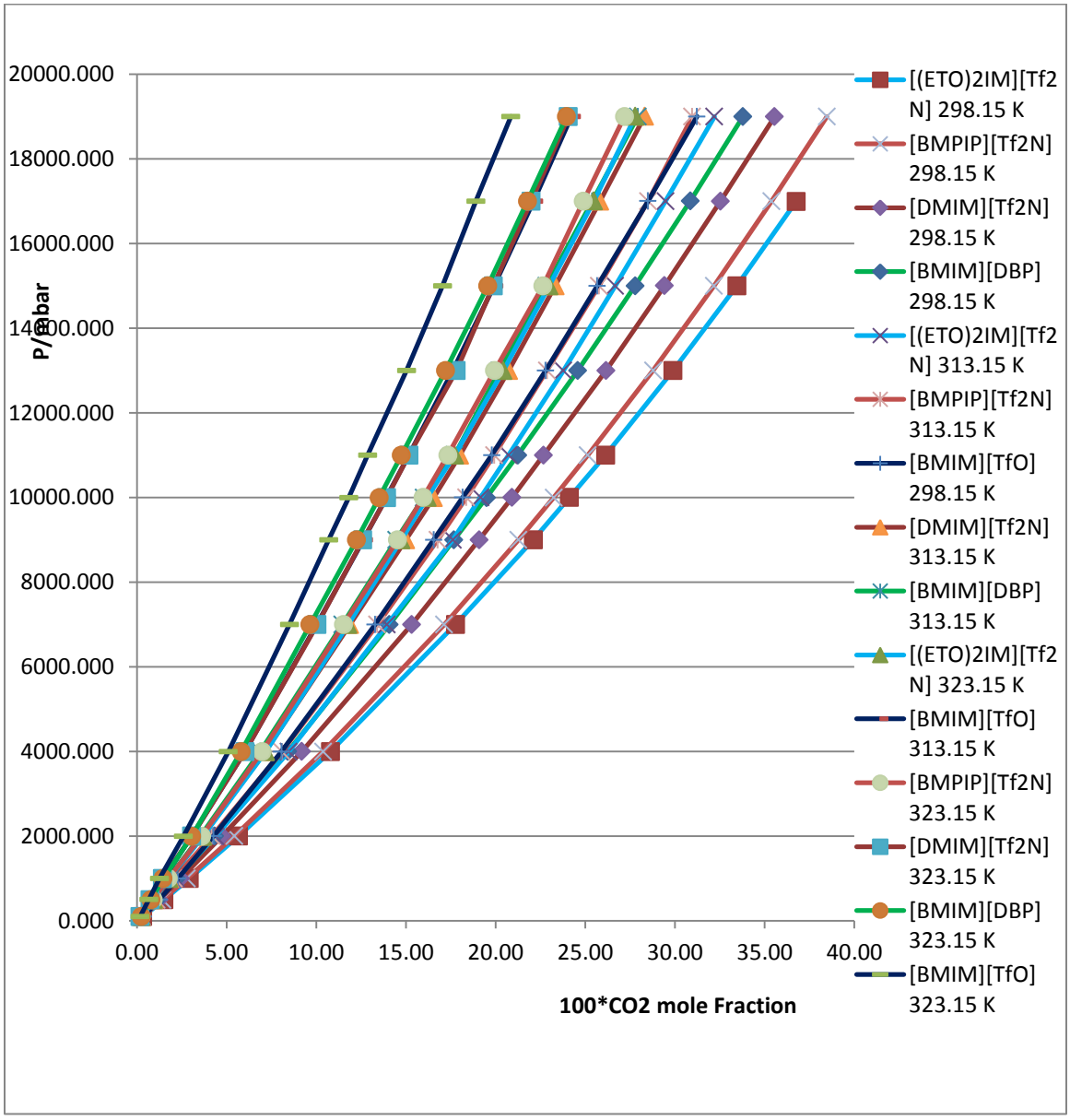

Figure 3.3: Solubility of Carbon Dioxide in [[BMPIP][Tf2N]], [[(ETO)2IM][Tf2N]], [[DMIM][Tf2N]], [BMIM][DBP] and [BMIM][TfO](Original in colour)

Table 3.5: Mole Fraction of Carbon Dioxide in [BMPIP][Tf2N]

398.15 K		313.15 K		323.15 K	
Pressure (mbar)	Mole Fraction of CO_2	Pressure (mbar)	Mole Fraction of CO_2	Pressure (mbar)	Mole Fraction of CO_2
98.872	0.0029	100.073	0.0028	101.007	0.0024
500.833	0.0142	499.898	0.0110	500.966	0.0091
999.013	0.0279	1000.615	0.0207	998.746	0.0175
1999.778	0.0543	1999.778	0.0418	1998.977	0.0361
3998.372	0.1038	3999.173	0.0808	3998.372	0.0698
6998.665	0.1713	6998.933	0.1340	6998.665	0.1152
9000.195	0.2128	8999.795	0.1677	8999.528	0.1454
9998.024	0.2324	9999.093	0.1837	9999.226	0.1596
10999.860	0.2514	10999.590	0.1992	10999.320	0.1734
12998.450	0.2879	12998.850	0.2287	13000.990	0.1994
14998.780	0.3218	14996.380	0.2575	15000.250	0.2264
17000.180	0.3539	16999.110	0.2851	16997.240	0.2489
18996.500	0.3847	18997.700	0.3096	18998.640	0.2719

Table 3.6: Mole Fraction of Carbon Dioxide in [DMIM][Tf2N]

398.15 K		313.15 K		323.15 K	
Pressure (mbar)	Mole Fraction of CO_2	Pressure (mbar)	Mole Fraction of CO_2	Pressure (mbar)	Mole Fraction of CO_2
98.338	0.0027	99.406	0.0024	100.740	0.0018
499.631	0.0125	499.098	0.0096	500.165	0.0073
999.013	0.0242	998.479	0.0182	999.147	0.0142
2000.312	0.0474	1999.511	0.0366	1999.645	0.0306
4000.507	0.0919	3999.306	0.0716	3998.639	0.0603
6998.399	0.1532	6998.532	0.1187	6997.198	0.1005
9000.462	0.1908	8998.460	0.1499	9000.195	0.1259
10001.360	0.2091	9998.158	0.1654	9998.425	0.1393
10998.120	0.2266	11000.660	0.1800	11001.330	0.1516
12996.450	0.2615	12997.780	0.2073	12997.920	0.1780
15002.780	0.2942	14999.580	0.2332	15000.920	0.1987
16996.710	0.3253	17001.240	0.2582	16999.240	0.2198
18996.500	0.3555	19002.640	0.2831	18996.770	0.2405

Table 3.7: Mole Fraction of Carbon Dioxide in [BMIM][TfO]

398.15 K		313.15 K		323.15 K	
Pressure (mbar)	Mole Fraction of CO_2	Pressure (mbar)	Mole Fraction of CO_2	Pressure (mbar)	Mole Fraction of CO_2
99.272	0.0037	100.740	0.0019	101.541	0.0018
501.366	0.0124	499.765	0.0080	501.767	0.0066
999.013	0.0227	999.280	0.0151	998.880	0.0125
1999.778	0.0427	1999.911	0.0304	1999.111	0.0259
3998.506	0.0806	3999.040	0.0603	3998.772	0.0510
6998.933	0.1327	6998.399	0.1001	6999.600	0.0851
9000.996	0.1655	8999.262	0.1264	8999.662	0.1069
9998.959	0.1816	9999.492	0.1390	9998.425	0.1181
10998.920	0.1979	11001.190	0.1516	10999.320	0.1286
13000.190	0.2279	12998.850	0.1761	13000.320	0.1504
14998.510	0.2567	15000.780	0.1991	15000.520	0.1704
17001.910	0.2849	16999.510	0.2212	16998.580	0.1890
18998.500	0.3123	19000.370	0.2423	18997.970	0.2085

Table 3.8: Mole Fraction of Carbon Dioxide in [(ETO)2IM][Tf2N]

398.15 K		313.15 K		323.15 K	
Pressure (mbar)	Mole Fraction of CO_2	Pressure (mbar)	Mole Fraction of CO_2	Pressure (mbar)	Mole Fraction of CO_2
99.806	0.0033	98.605	0.0029	99.939	0.0025
497.763	0.0150	499.765	0.0115	497.496	0.0093
996.611	0.0292	1000.081	0.0218	998.746	0.0179
2000.712	0.0566	1999.244	0.0438	1999.378	0.0368
3998.906	0.1079	3998.639	0.0847	3998.372	0.0718
7000.000	0.1777	6998.265	0.1395	6998.131	0.1177
8999.662	0.2211	9000.596	0.1762	8998.861	0.1473
9999.894	0.2411	9999.226	0.1916	9999.760	0.1618
10999.320	0.2613	10999.990	0.2073	10999.860	0.1772
13000.050	0.2989	12998.320	0.2377	12995.920	0.2042
14998.780	0.3345	14999.580	0.2667	14999.720	0.2299
16994.040	0.3676	16999.110	0.2947	17002.050	0.2547
		18997.570	0.3220	19002.380	0.2779

Table 3.9: Mole Fraction of Carbon Dioxide in [BMIM][DBP]

398.15 K		313.15 K		323.15 K	
Pressure (mbar)	Mole Fraction of CO_2	Pressure (mbar)	Mole Fraction of CO_2	Pressure (mbar)	Mole Fraction of CO_2
96.203	0.0025	99.539	0.0023	99.139	0.0025
498.831	0.0114	500.032	0.0092	501.099	0.0078
999.013	0.0222	998.479	0.0174	998.880	0.0146
1999.778	0.0434	2000.045	0.0354	1999.378	0.0306
3999.707	0.0842	3999.840	0.0688	3998.105	0.0581
6998.665	0.1408	6998.799	0.1145	6997.865	0.0965
8999.395	0.1767	8999.662	0.1446	8999.395	0.1225
9997.357	0.1950	9998.559	0.1599	9997.091	0.1351
10999.990	0.2124	11002.260	0.1771	10998.660	0.1475
12999.250	0.2458	13000.850	0.2022	12996.450	0.1721
15000.250	0.2778	14999.720	0.2283	14995.310	0.1956
17001.780	0.3085	16999.510	0.2539	17000.450	0.2178
19000.910	0.3379	18999.040	0.2793	18999.310	0.2395

Shiflett et al. (2007) measured the solubility of carbon dioxide in1-hexyl-3-methylimidazolium bis(trifluoromethylsulfonyl)imide ([hmim]-[Tf2N]) with the same methods and under similar conditions and Yim et al. (2011) measured in 1-butyl-1-methyl-pyrrolidinium bis(trifluoromethylsulfonyl)imide ([BMP][Tf2N]) at high pressure. The measured solubility of carbon dioxide in [[(ETO)2IM][Tf2N]] in this study has competitive solubility with their reported data. However, Yokozeki et al. (2008) measured acetate anion-based ionic liquid, 1-butyl-3-methylimidazolium acetate [bmim]-[Ac]. The solubility results unsurprisingly show higher solubility than any other RTILs (as shown in Figure 3.4.) that were studied in this work since acetate reacts with carbon dioxide chemically, which means it requires energy to be regenerated. Shen et al. (1992) measured solubility of carbon dioxide in 15.3 wt % MEA aqueous solution at 313.15 K, and the mole fraction of carbon dioxide was 0.423 at 1400 mbar. At under exactly same conditions, the mole fraction of carbon dioxide in [[(ETO)2IM][Tf2N]] was 0.03. The value for [bmim]-[Ac] reported by Yokozeki et al. (2008) was 0.281.

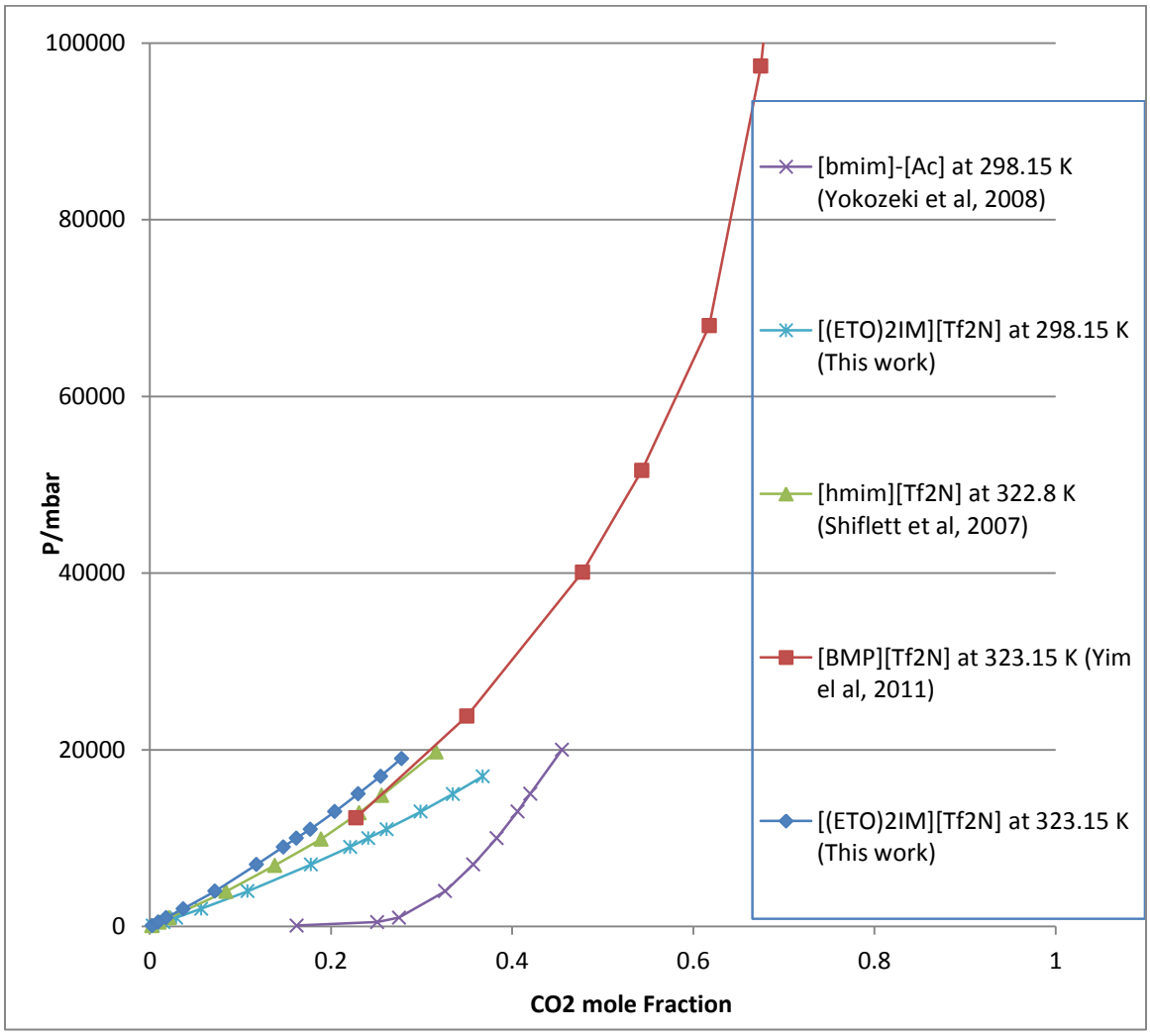

Figure 3.4: Solubility of CO_2 at 323.15 K in [(ETO)2IM][Tf2N], ([hmim]-[Tf2N] and [BMP][Tf2N] and at 298.15 K in [(ETO)2IM][Tf2N]and [bmim]-[Ac] (Original in Colour)

As discussed in section 3.2.2, the solubility and fraction of carbon dioxide in ionic liquids are strongly dependent on pressure and temperature. As shown in Tables 3.4 to 3.8, carbon dioxide is more soluble at lower temperature and higher pressure. This relation was also generally true for carbon dioxide absorption in all physical absorption with ionic liquids in all literature reviewed.

The mass transfer kinetics and mass diffusion of carbon dioxide in ionic liquids are slower at lower temperatures and in more viscous ionic liquids; this means it took longer to reach phase equilibrium.

3.3.2 Effect of Anions and Cations

As mentioned in section 1.4.2, ionic liquids are designable solvents for industrial applications. Hence, the experimental and theoretical studies of cation and anion combinations are essential for modifying and changing either cations or anions. For example, Gutkowski et al. (2006) indicated that the length of the alkyl chain on imidazolium cations has larger effects on carbon dioxide solubility: the solubility increases as the alkyl chain increases on imidazolium. The Henry's Law constants of [DMIM][Tf2N] and [(ETO)2IM][Tf2N]at the same temperature clearly showing that [(ETO)2IM][Tf2N](34.64 bar at 298.15 K) has slightly higher solubility than [DMIM][Tf2N] (40.67 bar at 298.15 K) since it has one more alkyl chain on imidazolium. Aki et al. (2004) and Muldoon et al. (2007) also indicated that the density decreases with alkyl chain increase on imidazolium, and the density of [(ETO)2IM][Tf2N]is slightly lower than the density of [DMIM][Tf2N], as shown in figure 2.3. Crowhurst et al. (2003) indicated that the hydrogen at the 2-

position on the imidazolium ring is one of the most acidic hydrogens on the imidazolium ring. This might explain the solubility differences among imidazolium- based ionic liquids. Weaker interaction between carbon dioxide and the hydrogen on the 2-position of imidazolium ring (Blath et al., 2011) may occur. Figure 3.5 shows the solubility comparison between [(ETO)2IM][Tf2N]and [DMIM][Tf2N].

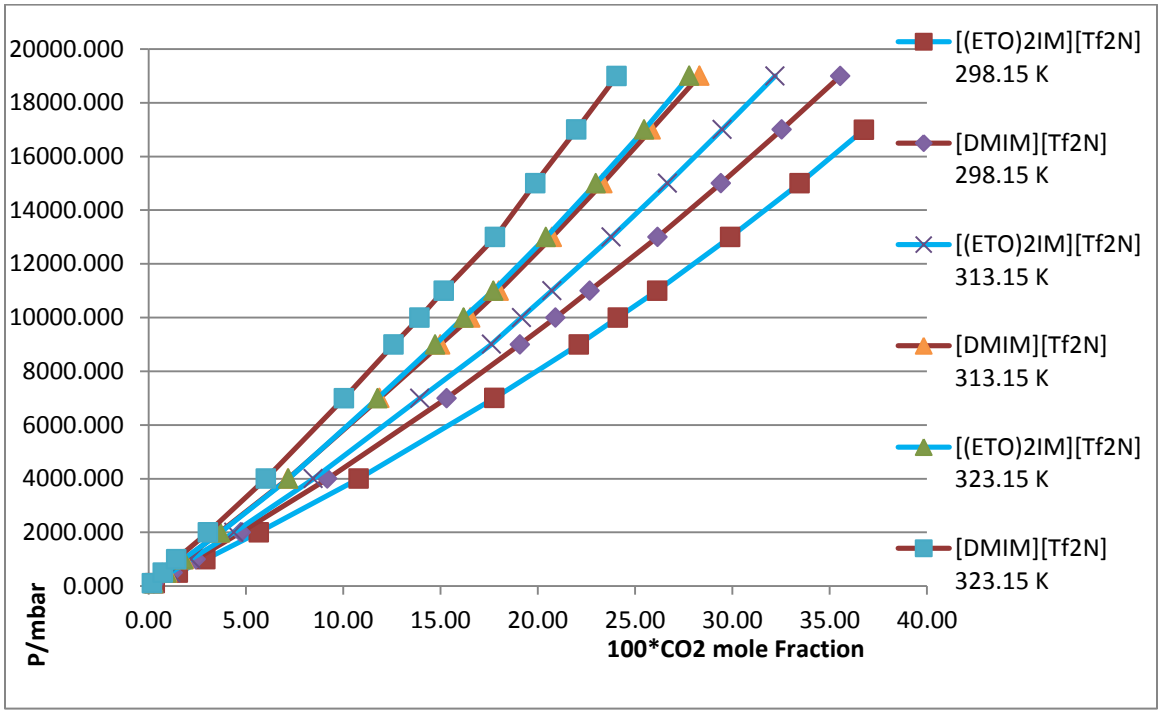

Figure 3.5: Solubility of CO_2 in [(ETO)2IM][Tf2N]and [DMIM][Tf2N] (Original in Colour)

In the design of ionic liquids for carbon absorption fluorination (TF2N) is a proven method of increasing the CO_2 solubility through theoretical research (Sumon and Henni, 2011). Bara et al. in 2009 replaced the anion BF4 with TF2N and found that 1-ethyl-3-methyimidazoliumcation increases the carbon dioxide solubility, corresponding to an increase of 31% (Bara et al, 2009). In this work, the Henry's Law Constant at 298.15 K for Tf2N-based [(ETO)2IM][Tf2N], [DMIM][Tf2N], and [BMPIP][Tf2N]are 34.64, 40.67 and 35.70 bar, respectively, higher than non TF2N-based [BMIM][DBP] (46.13 bar) and [BMIM][TfO](47.06 bar). Hence, the result is consistent with Sumon and Bara's theoretical and experimental conclusions and results.

Shiflett et al. (2007) investigated the influence of anions on solubility via measuring solubility of carbon dioxide in various types of anion-based ionic liquids and drew as conclusion that carbon dioxide solubility for 1-butyl-3-methylimidazolium ([bmim]+)- based ionic liquids at 60 °C increased in the order of nitrate ([NO3]-) < tetrafluoroborate ([BF4]-) < dicyanamide ([DCA]-) _hexafluorophosphate ([PF6]-) _ trifluoromethanesulfonate ([OTF-] 0< bis[(trifluoromethyl)-sulfonyl]imide ([Tf2N]-) < tris(trifluoromethylsulfonyl)methide ([methide]-). However, there was very little research on anion dibutyl phosphate [DPH] in the literature. In order to determine the effect of anion trifluoromethane sulfonate and dibutyl phosphate on carbon dioxide solubility, two ionic liquids (1-Butyl-3-methylimidazolium trifluoromethanesulfonate and 1-Butyl-3-

methylimidazolium dibutyl phosphate) with the exact same cation (1-Butyl-3-methylimidazolium) were chosen in this work. Enthalpy and Henry's Law constant showed anion [DPH] has stronger interaction with carbon dioxide and higher solubility than [OTF]-based ionic liquids, although the phosphate might be the main reason that [BMIM][DBP] is relatively viscous. Figure 3.6 shows the solubility of carbon dioxide in [BMIM][DBP] and [BMIM][TfO].

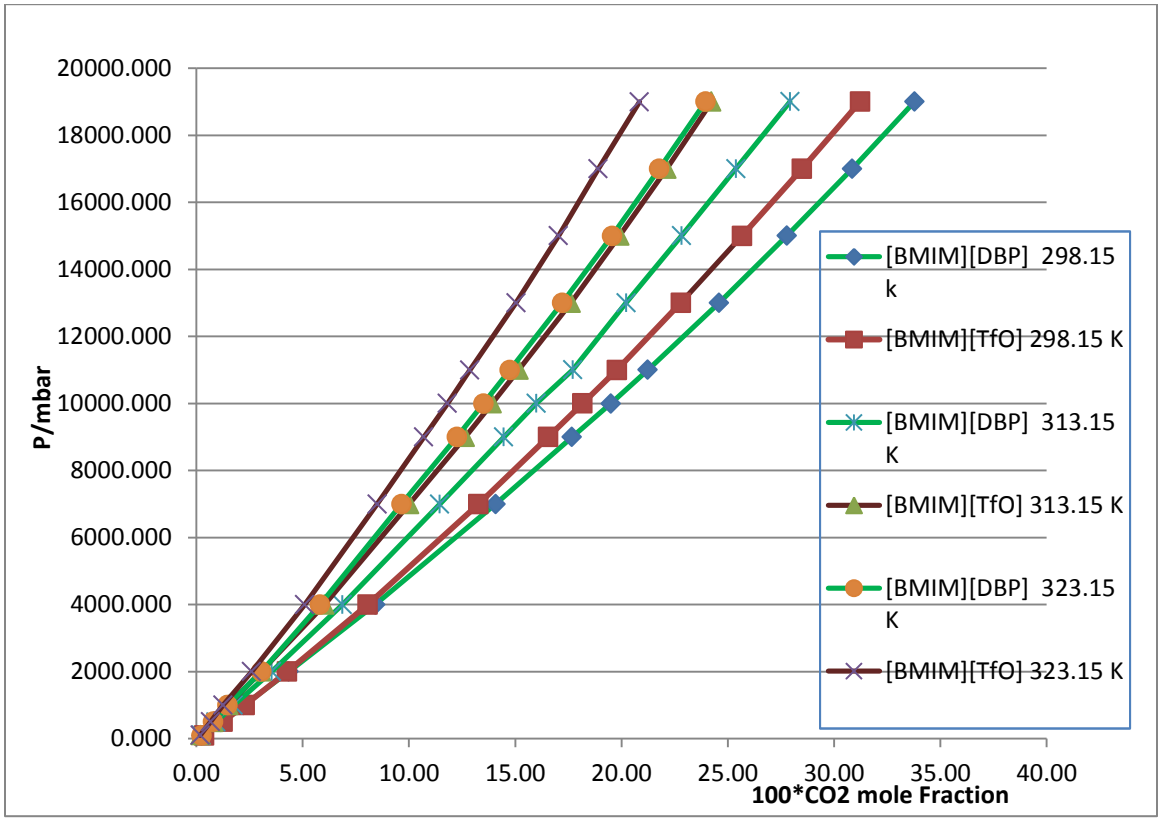

Figure 3.6: Solubility of CO_2 in [BMIM][DBP] and [BMIM][TfO](Original in colour)

CHAPTER 4

Experimental Data Correlation

4.1 Theory:

4.1.1 Equation of State

Cubic equations of state (EoSs), as one the most flexible and accurate available models, are most commonly used in chemical and petroleum industries. They are suitable for representing all thermodynamic and physical properties for pure components, as well as binary and ternary systems. It is also widely applicable for various types of polar as well as nonpolar systems at a wide range of temperatures and pressures. EoS can be written in a general form of five parameters as:

$$P = \frac{RT}{V-b} - \frac{\theta(V-\eta)}{(V-b)(V^2+\delta V+\varepsilon)} \qquad (4.1)$$

where, depending on the equation, the parameters θ, b, η, δ and ε might be constants, including zero as temperature, and component compositions are varied in the mixture systems.

Table 4.1 shows the relation and values for parameters in several modified common cubic EoSs.

Table 4.1: Parameters for Cubic EoS

EoS	δ	ε	θ
Van der Waals (1890)	0	0	a
Redlich and Kwong (1949)	0	0	$a/T_r^{0.5}$
Soave (1972)	b	0	aα($T_{r,\omega}$)
Peng and Robinson (1976)	2b	-b^2	aα($T_{r,\omega}$)
Patel and Teja (1982)	b+c	-bc	aα($T_{r,\omega}$)
Stryjek and Vera (1986)	2b	-b^2	aα($T_{r,\omega}$)

In all cases listed above, parameter b is a positive constant and equal to η. Parameters a and b are dependent on the critical properties of the component and can be expressed as Equations 4.2, 4.3, and 4.4.

$$a = a_c \alpha(T_{r,\omega}) \quad (4.2)$$

$$a_c = C_1 R T_C^2 / P_c \quad (4.3)$$

$$b = C_2 R T_c / P_c \quad (4.4)$$

where the parameter α was used to add the temperature dependence to a. $C_1 and\ C_2$ are constants depending on the type of the EoSs, C_1 is 0.0778 for Peng Robinson (PR 1976) and 0.0833 for Soave Redlich Kwong (SRK 1984) , and C_2 is 0.4572 for PR(1976) and 0.4218 for SRK(1984). In order to estimate the critical parameters of the ionic liquids and their components, a few correlations are available in the literature. $\alpha(T_r)$ is a temperature dependent parameter, where T_r is the reduced temperature that can be expressed as in Table 4.2.

Table 4.2: Reduced Temperature for Cubic EoS

EoS	$\alpha(T_r)$
Van der Waals (1890)	1
Redlich and Kwong (1949)	$1/T_r^{1/2}$
Soave (1972)	$[1+(0.48+1.574\omega-0.176\omega^2)(1-T_r^{\frac{1}{2}})]^2$
Peng and Robinson (1976)	$[1+(0.37464+1.54226\omega-0.2699\omega^2)(1-T_r^{\frac{1}{2}})]^2$
Patel and Teja (1982)	$(1+[1+(0.452413+1.38092\omega-0.295937\omega^2)(1-T_r^{\frac{1}{2}})]^2(1-T_r^{\frac{1}{2}})]^2$
Stryjek and Vera (1986)	$[1+(0.378893+1.4897153\omega-0.17131848\omega^2+0.0196554\omega^3)(1-T_r^{\frac{1}{2}})]^2+k_1(1-T_r)(0.7-T_r)$

4.1.2 Solubility Parameter Theory

When applying the EoS to the Vapour-Liquid Equilibrium, the difficulty is finding the accurate mixture parameters that now depend on the mixture composition. For this reason, the currently available rules are formulated in a manner to yield the minimum deviation between experimental and correlated data.

Cubic EoSs in binary systems include the dispersion forces between two molecular components, and the mixing rules give the EoS composition dependence. Adjustable parameters or binary parameters in the cubic EoS account for specific chemical or physical reactions or interactions, such as, the 2-position hydrogen bonding on the imidazolium ring and carbon dioxide type interactions and complexities because of the size, structure polarity and energies.

In order to adjust the dispersion force and molecular interaction, EoS mixing rules might use one or two of the following interaction parameters: k_{ij}measures the deviation from geometric intermolecular interactions assumed for the unlike cohesive energy parametera_{ij}, and since the standard Peng-Robinson generally produces satisfactory results for nonpolar systems, the geometric mean should be a very good first approximation, so in data analysis, k_{ij} is retained and set as $k_{ij} = k_{ji}$ (Mathias et al., 1983). Meanwhile, j_{ij} measures the deviation from arithmetic intermolecular interaction repulsions

assumed for the unlike repulsive energy parameterb_{ij}. These binary interaction parameters could be positive, negative or zero. Forh_{ij}, there is no established physical meaning since there are not sufficient data on this parameter to establish a trend on its values, and in most published literature, it is set as zero.

For mixtures with composition x_i and total N components, the following equations can be used to calculate a and b in various types of thermodynamic models:

$$a_{mix} = \sum_{i=1}^{N} \sum_{j=1}^{N} x_i x_j a_{ij} \quad (4.5)$$

$$b_{mix} = \sum_{i=1}^{N} x_i b_i \quad (4.6)$$

where a_{ij} could be express as:

$$a_{ij}=(a_i a_j)^{1/2}(1-k_{ij}) \quad (4.7)$$

For mixtures, the volume translation C can be expressed same in the same form as b:

$$c_{mix} = \sum_{i=1}^{N} x_i c_i \quad (4.8)$$

Prausnitz et al. (1999) indicated that there is no volume change (V^E=0) and entropy change (s^E=0) when mixing two liquids at constant temperature and pressure. This theory can be perfectly applied in this study since ionic liquid is less expandable and compressible. The cohesive energy density parameter c can be written as:

$$c=\frac{\Delta u^v}{v^L} \quad (4.9)$$

where Δu^v is the energy change upon isothermal vapourization of a saturated liquid to the ideal gas state.

Generalized Equation 4.9, a Hildebrand and Scatchard equation, can be rewritten for binary mixtures as:

$$(u_{liquid} - u_{ideal\ gas})_{binary\ mixture} = \frac{c_{11}v_1^2x_1^2+2c_{12}v_1v_2x_2x_1+c_{22}v_2^2x_2^2}{x_1x_1+v_2x_2} \qquad (4.10)$$

The excess molar energy change of mixing is defined as

$$u^E = u_{binary\ mixture} - x_1u_1 - u_2x_2 \qquad (4.11)$$

For non-polar molecules, the cohesive energy density parameter c can be:

$$c_{12} = \sqrt{c_{11}c_{22}} \qquad (4.12)$$

For ideal pure solution, the excess molar energy change is zero, ($u_{ideal}^E = 0$), so plotting Equation 4.9 and 4.10 into Equation 4.11, for excess molar energy change for mixture, it would be:

$$u^E = (c_{11} + c_{22} - 2c_{12})(x_1v_1 + v_2x_2)\Phi_1\Phi_2 \qquad (4.13)$$

where the volume fraction Φ_1 and Φ_2 can be written as:

$$\Phi_1 = \frac{x_1v_1}{x_2v_2+x_1v_1} \qquad (4.14)$$

$$\Phi_2 = \frac{x_2v_2}{x_2v_2+x_1v_1} \qquad (4.15)$$

Substituting Equation 4.12 into Equation 4.13, it will then be:

$$u^E = (x_1v_1 + v_2x_2)\Phi_1\Phi_2(\delta_1 - \delta_2)^2 \qquad (4.16)$$

where $\delta_1 and\ \delta_2$ are Hildebrand solubility parameters for two components in a binary system, and that can be defined as:

$$\delta_1 = \sqrt{c_{11}} = (\sqrt{\frac{\Delta u^v}{v}})_1 \quad (4.17)$$

$$\delta_1 = \sqrt{c_{11}} = (\sqrt{\frac{\Delta u^v}{v}})_1 \quad (4.18)$$

At constant pressure and temperature:

$$g^E = u^E + PV^E + Ts^E \quad (4.19)$$

If we apply Prausnitz's theory (V^E=0=s^E), as discussed above, then it can be:

$$g^E = u^E \quad (4.20)$$

For ideal solution:

$$g^E = \sum_i RTln\gamma_i \quad (4.21)$$

Then, for the mixture:

$$\ln\gamma_1 = \frac{v_1\Phi_2^2(\delta_1-\delta_2)^2}{RT} \quad (4.22)$$

$$\ln\gamma_2 = \frac{v_2\Phi_1^2(\delta_2-\delta_1)^2}{RT} \quad (4.23)$$

4.2 Critical Properties and Acentric Factors Estimation

Using an equation of state for correlating the phase behaviour experimental data of gas in ionic liquids is challenging since it requires the critical properties and acentric factors of ionic liquid. Those properties for most ionic liquids are not available in the Aspen database and in the literature. The critical properties of ionic liquids cannot be experimentally measured in many cases because most such compounds start to decompose at temperatures close or up to normal boiling point. Therefore, estimating the critical properties is the only option with most ionic liquids. Researchers have been working on critical

properties estimation methods, and two methods that are most commonly used for estimating ionic liquid properties are discussed in this section.

Joback Method:

Joback reevaluated Lydersen's group contribution method, added several new functional groups, and determined new contribution values. The relations for the critical properties are (Poling et al., 1987):

$$T_C(K) = T_b\{0.584 + 0.965[\sum_k N_k(tck)] - [\sum_k N_k(tck)]^2\} \quad (4.24)$$

$$T_b(K) = [198 + \sum_k N_k(tbk)] \quad (4.25)$$

$$P_C(bar) = [0.113 + 0.0032N_{atoms} - \sum_k N_k(pck)]^{-2} \quad (4.26)$$

$$V_c(cm^3mol^{-1}) = 17.5 + \sum_k N_k\,(vck) \quad (4.27)$$

where the contributions are indicated as tck, pck, and vck. The group identities and Joback's group contributions values for the critical properties are in Table 7.1. The boiling point T_b needs to be calculated using Equation 4.25 in order to estimate T_c.

The Joback method itself does not provide equations for estimating the acentric factor. However, CHEMCAD uses the Lee-Kesler method to estimate the acentric factor, and this is how researchers have been estimating the acentric factor for ionic liquids. The relation with critical properties is:

$$\omega = \frac{-lnP_c - 5.97214 + 6.09648\left(\frac{T_b}{T_c}\right)^{-1} + 1.28862\ln\left(\frac{T_b}{T_c}\right) - 0.169347\left(\frac{T_b}{T_c}\right)^6}{15.2518 - 15.6875\left(\frac{T_b}{T_c}\right)^{-1} - 13.4721ln\left(\frac{T_b}{T_c}\right) + 0.43577\left(\frac{T_b}{T_c}\right)^6} \quad (4.28)$$

where the unit of P_c is [atm].

Valderrama-Robles Method:

Valderramma and Robles (2007) updated Joback's methods and proposed the following correlations for estimating critical properties and acentric factors:

$$T_b(K) = 198.2 + \sum n\Delta T_{bM} \quad (4.29)$$

$$T_c(K) = \frac{T_b}{0.5703+1.0121\sum n\Delta T_M-(\sum n\Delta T_M)^2} \quad (4.30)$$

$$P_c(bar) = \frac{M}{0.2573+(\sum n\Delta P_M)^2} \quad (4.31)$$

$$V_b(cm^3mol^{-1}) = 6.75 + \sum n\Delta V_M \quad (4.32)$$

$$\omega=\frac{(T_b-43)(T_c-43)}{(T_c-T_b)(0.7T_c-43)}\log\left(\frac{P_c}{P_b}\right)-\frac{(T_b-43)}{(T_c-T_b)}\log\left(\frac{P_c}{P_b}\right)+\log\left(\frac{P_c}{P_b}\right) \quad (4.33)$$

where the contributions are indicated as ΔT_M, ΔT_{bM} , ΔP_M, and ΔV_M. M is the molecular weight of the component. Boiling point T_b also needs to be estimated first for T_c. Group contributions for various properties are shown in APPENDIX B.

In this study, the Valderrama-Robles Method was used for predicting the critical properties for all five ionic liquids, and the results are approximately consistent with how ionic liquids should be.

Table 4.3: Critical Properties of Five Ionic Liquids in This Study

Ionic Liquid	ω	T_b(K)	T_c(K)	P_C(bar)	M (g/mol)
[(ETO)2IM][Tf2N]	0.252	873.650	1306.106	28.167	437.340
[DMIM][Tf2N]	0.168	827.890	1288.252	33.270	409.280
[BMIM][DBP]	0.931	785.350	992.216	15.061	348.420
[BMIM][TfO]	0.365	719.460	1043.080	27.133	288.290
[BMPIP][Tf2N]	0.318	849.700	1227.451	23.342	436.430

4.3 Modeling Results with Peng-Robinson Equation of State (1976)

The solubility results of carbon dioxide in five different kinds of ionic liquids were correlated using Aspen HYSYS (2012) with the PR-RoS model. Any properties of the ionic liquids studied in this work are unavailable on the Aspen HYSYS database, assuming the updating of the database and property research on ionic liquids is not catching the speed of ionic liquid creating. Therefore, in all modeling processes of five ionic liquids, 1-Butyl-3-methylimidazolium hexafluorophosphate (CAS number: 174501-64-5) was used/replaced as liquid phase, but all necessary properties were changed to the real properties of the ionic liquids that were studied in this work. Based on the negligible vapour pressure of ionic liquids, all vapour pressure was set as zero. Binary interaction parameters $\mathbf{K_{ij}}$ and $\mathbf{l_{ij}}$ (PRLij) were regressed.

$$AAD\% = \frac{\sum[ABS(\frac{Exp-Reg}{Exp})]}{NP} * 100\% \qquad (4.34)$$

where, Exp and Reg are the experimental and regressed values of partial pressures of carbon dioxide above ionic liquids, and NP are the number of experimental data points. The regressed binary interaction parameters K_{ij}(PRKBV/3) and l_{ij}(PRLij) and the average deviation are listed in Table 4.4.The regressed specific solubility values presented at certain pressures and temperatures are given in Tables 4.5 to 4.19 and Figures 4.1 to 4.15.

Table 4.4: Regressed Binary Interaction Parameters and AAD%

Binary Systems	Temperature (K)	l_{ij}(PRLij)	K_{ij}(PRKBV/3)	AAD%
[(ETO)2IM][Tf2N]--- Carbon Dioxide	298.15	0.00096525	0.02897586	0.41
	313.15	0.00104289	0.05428252	0.40
	323.15	0.00107965	0.07804153	0.35
[BMIM][DBP] --- Carbon Dioxide	298.15	0.00085304	0.07787972	0.46
	313.15	0.00079644	0.11672983	0.05
	323.15	0.00082871	0.12351221	0.40
(bmim)OTF--- Carbon Dioxide	298.15	0.00089531	0.09110709	0.52
	313.15	0.00082301	0.11981021	0.31
	323.15	0.000978	0.1524757	0.29
[DMIM][Tf2N]--- Carbon Dioxide	298.15	0.00053063	0.03599421	0.42
	313.15	0.00068871	0.06405091	0.38
	323.15	0.00069249	0.08229675	0.26
[BMPIP][Tf2N]--- Carbon Dioxide	298.15	0.00054495	0.02674385	0.42
	313.15	0.00068508	0.05403734	0.36
	323.15	0.00074643	0.07071133	0.31

Table 4.5: Regressed and Experimental Solubility Data of Carbon Dioxide in [BMIM][DBP] at 298.15 K

Experimental Mole Fraction of CO_2	Regressed mole fraction of CO_2	Experimental P/(ATM)	Regressed P / (ATM)
0.0025	0.0024	0.095	0.100
0.0114	0.0113	0.492	0.495
0.0222	0.0223	0.986	0.978
0.0434	0.0435	1.974	1.965
0.0842	0.0882	3.947	3.774
0.1408	0.1461	6.907	6.696
0.1767	0.1812	8.882	8.709
0.1950	0.1983	9.867	9.739
0.2124	0.2145	10.856	10.775
0.2458	0.2451	12.829	12.855
0.2778	0.2737	14.804	14.955
0.3085	0.3005	16.779	17.072
0.3379	0.3256	18.752	19.195

Table 4.6: Regressed and Experimental Solubility Data of Carbon Dioxide in [BMIM][DBP] at 313.15 K

Experimental Mole Fraction of CO_2	Regressed mole fraction of CO_2	Experimental P/(ATM)	Regressed P / (ATM)
0.0023	0.0023	0.098	0.098
0.0092	0.0093	0.493	0.493
0.0174	0.0174	0.985	0.985
0.0354	0.0354	1.974	1.974
0.0688	0.0688	3.948	3.947
0.1145	0.1147	6.907	6.895
0.1446	0.1448	8.882	8.872
0.1599	0.1601	9.868	9.859
0.1771	0.1773	10.858	10.847
0.2022	0.2019	12.831	12.846
0.2283	0.2279	14.804	14.821
0.2539	0.2503	16.777	16.952
0.2793	0.2793	18.751	18.752

Table 4.7: Regressed and Experimental Solubility Data of Carbon Dioxide in [BMIM][DBP] at 323.15 K

Experimental Mole Fraction of CO_2	Regressed mole fraction of CO_2	Experimental P/(ATM)	Regressed P / (ATM)
0.0025	0.0023	0.098	0.107
0.0078	0.0078	0.495	0.497
0.0146	0.0147	0.986	0.976
0.0306	0.0316	1.973	1.914
0.0581	0.0612	3.946	3.773
0.0965	0.1012	6.906	6.670
0.1225	0.1263	8.882	8.701
0.1351	0.1381	9.866	9.725
0.1475	0.1495	10.855	10.762
0.1721	0.1713	12.826	12.860
0.1956	0.1915	14.799	14.979
0.2178	0.2102	16.778	17.110
0.2395	0.2279	18.751	19.260

Table 4.8: Regressed and Experimental Solubility Data of Carbon Dioxide in [(ETO)2IM][Tf2N]at 298.15 K

Experimental Mole Fraction of CO_2	Regressed mole fraction of CO_2	Experimental P/(ATM)	Regressed P / (ATM)
0.0033	0.0032	0.099	0.102
0.0150	0.0150	0.491	0.493
0.0292	0.0292	0.984	0.982
0.0566	0.0575	1.975	1.948
0.1079	0.1116	3.947	3.844
0.1777	0.1824	6.908	6.782
0.2211	0.2240	8.882	8.806
0.2411	0.2429	9.869	9.823
0.2613	0.2614	10.855	10.853
0.2989	0.2957	12.830	12.914
0.3345	0.3276	14.803	14.986
0.3676	0.3570	16.772	17.055

Table 4.9: Regressed and Experimental Solubility Data of Carbon Dioxide in [(ETO)2IM][Tf2N]at 313.15 K

Experimental Mole Fraction of CO_2	Regressed mole fraction of CO_2	Experimental P/(ATM)	Regressed P / (ATM)
0.0029	0.0028	0.097	0.102
0.0115	0.0115	0.493	0.495
0.0218	0.0219	0.987	0.985
0.0438	0.0445	1.973	1.946
0.0847	0.0877	3.946	3.834
0.1395	0.1443	6.907	6.737
0.1762	0.1793	8.883	8.777
0.1916	0.1942	9.868	9.779
0.2073	0.2090	10.856	10.798
0.2377	0.2370	12.828	12.854
0.2667	0.2630	14.803	14.929
0.2947	0.2876	16.777	17.021
0.3220	0.3110	18.749	19.128

Table 4.10: Regressed and Experimental Solubility Data of Carbon Dioxide in [(ETO)2IM][Tf2N]at 323.15 K

Experimental Mole Fraction of CO_2	Regressed mole fraction of CO_2	Experimental P/(ATM)	Regressed P / (ATM)
0.0025	0.0024	0.099	0.103
0.0093	0.0092	0.491	0.493
0.0179	0.0179	0.986	0.984
0.0368	0.0373	1.973	1.948
0.0718	0.0742	3.946	3.841
0.1177	0.1220	6.907	6.723
0.1473	0.1511	8.881	8.723
0.1618	0.1648	9.869	9.744
0.1772	0.1787	10.856	10.793
0.2042	0.2034	12.826	12.859
0.2299	0.2264	14.804	14.947
0.2547	0.2481	16.780	17.054
0.2779	0.2681	18.754	19.156

Table 4.11: Regressed and Experimental Solubility Data of Carbon Dioxide in [BMIM][TfO] at 298.15 K

Experimental Mole Fraction of CO_2	Regressed mole fraction of CO_2	Experimental P/(ATM)	Regressed P / (ATM)
0.0037	0.0035	0.098	0.104
0.0124	0.0123	0.495	0.497
0.0227	0.0227	0.986	0.986
0.0427	0.0436	1.974	1.931
0.0806	0.0847	3.946	3.784
0.1327	0.1386	6.907	6.695
0.1655	0.1705	8.883	8.708
0.1816	0.1855	9.868	9.732
0.1979	0.2002	10.855	10.774
0.2279	0.2271	12.830	12.859
0.2567	0.2520	14.802	14.962
0.2849	0.2756	16.780	17.096
0.3123	0.2977	18.750	19.240

Table 4.12: Regressed and Experimental Solubility Data of Carbon Dioxide in [BMIM][TfO] at 313.15 K

Experimental Mole Fraction of CO_2	Regressed mole fraction of CO_2	Experimental P/(ATM)	Regressed P / (ATM)
0.0019	0.0018	0.099	0.104
0.0080	0.0080	0.493	0.496
0.0151	0.0151	0.986	0.988
0.0304	0.0308	1.974	1.951
0.0603	0.0624	3.947	3.827
0.1001	0.1040	6.907	6.705
0.1264	0.1297	8.882	8.713
0.1390	0.1418	9.869	9.730
0.1516	0.1535	10.857	10.763
0.1761	0.1758	12.829	12.846
0.1991	0.1962	14.805	14.944
0.2212	0.2153	16.777	17.060
0.2423	0.2332	18.752	19.186

Table 4.13: Regressed and Experimental Solubility Data of Carbon Dioxide in [BMIM][TfO] at 323.15 K

Experimental Mole Fraction of CO_2	Regressed mole fraction of CO_2	Experimental P/(ATM)	Regressed P / (ATM)
0.0018	0.0017	0.100	0.106
0.0066	0.0066	0.495	0.497
0.0125	0.0125	0.986	0.987
0.0259	0.0262	1.973	1.951
0.0510	0.0529	3.946	3.821
0.0851	0.0887	6.908	6.688
0.1069	0.1104	8.882	8.679
0.1181	0.1209	9.868	9.706
0.1286	0.1308	10.855	10.732
0.1504	0.1501	12.830	12.845
0.1704	0.1676	14.804	14.960
0.1890	0.1837	16.776	17.076
0.2085	0.1994	18.750	19.252

Table 4.14: Regressed and Experimental Solubility Data of Carbon Dioxide in [DMIM][Tf2N] at 298.15 K

Experimental Mole Fraction of CO_2	Regressed mole fraction of CO_2	Experimental P/(ATM)	Regressed P / (ATM)
0.0027	0.0026	0.097	0.101
0.0125	0.0124	0.493	0.495
0.0242	0.0242	0.986	0.987
0.0474	0.0482	1.974	1.944
0.0919	0.0951	3.948	3.836
0.1532	0.1574	6.907	6.764
0.1908	0.1944	8.883	8.766
0.2091	0.2119	9.871	9.781
0.2266	0.2285	10.854	10.794
0.2615	0.2607	12.826	12.854
0.2942	0.2903	14.807	14.929
0.3253	0.3179	16.774	17.006
0.3555	0.3441	18.748	19.102

Table 4.15: Regressed and Experimental Solubility Data of Carbon Dioxide in [DMIM][Tf2N] at 313.15 K

Experimental Mole Fraction of CO_2	Regressed mole fraction of CO_2	Experimental P/(ATM)	Regressed P / (ATM)
0.0024	0.0023	0.098	0.103
0.0096	0.0096	0.493	0.495
0.0182	0.0182	0.985	0.985
0.0366	0.0372	1.973	1.942
0.0716	0.0743	3.947	3.824
0.1187	0.1230	6.907	6.721
0.1499	0.1533	8.881	8.738
0.1654	0.1678	9.867	9.767
0.1800	0.1815	10.857	10.798
0.2073	0.2066	12.828	12.854
0.2332	0.2301	14.803	14.932
0.2582	0.2521	16.779	17.026
0.2831	0.2733	18.754	19.149

Table 4.16: Regressed and Experimental Solubility Data of Carbon Dioxide in [DMIM][Tf2N] at 323.15 K

Experimental Mole Fraction of CO_2	Regressed mole fraction of CO_2	Experimental P/(ATM)	Regressed P / (ATM)
0.0018	0.0017	0.099	0.104
0.0073	0.0073	0.494	0.496
0.0142	0.0142	0.986	0.986
0.0306	0.0309	1.973	1.952
0.0603	0.0621	3.946	3.844
0.1005	0.1037	6.906	6.737
0.1259	0.1289	8.883	8.728
0.1393	0.1415	9.868	9.754
0.1516	0.1532	10.857	10.778
0.1780	0.1768	12.828	12.890
0.1987	0.1962	14.805	14.926
0.2198	0.2153	16.777	17.003
0.2405	0.2334	18.748	19.101

Table 4.17: Regressed and Experimental Solubility Data of Carbon Dioxide in [BMPIP][Tf2N] at 298.15 K

Experimental Mole Fraction of CO_2	Regressed mole fraction of CO_2	Experimental P/(ATM)	Regressed P / (ATM)
0.0029	0.0028	0.098	0.101
0.0142	0.0141	0.494	0.497
0.0279	0.0279	0.986	0.986
0.0543	0.0555	1.974	1.931
0.1038	0.1074	3.946	3.834
0.1713	0.1755	6.907	6.782
0.2128	0.2159	8.883	8.793
0.2324	0.2346	9.867	9.803
0.2514	0.2526	10.856	10.821
0.2879	0.2866	12.828	12.867
0.3218	0.3177	14.803	14.919
0.3539	0.3468	16.778	16.981
0.3847	0.3743	18.748	19.050

Table 4.18: Regressed and Experimental Solubility Data of Carbon Dioxide in [BMPIP][Tf2N] at 313.15 K

Experimental Mole Fraction of CO_2	Regressed mole fraction of CO_2	Experimental P/(ATM)	Regressed P / (ATM)
0.0028	0.0026	0.099	0.104
0.0110	0.0109	0.493	0.496
0.0207	0.0207	0.988	0.986
0.0418	0.0428	1.974	1.928
0.0808	0.0840	3.947	3.820
0.1340	0.1381	6.907	6.750
0.1677	0.1708	8.882	8.765
0.1837	0.1860	9.868	9.781
0.1992	0.2006	10.856	10.802
0.2287	0.2280	12.829	12.853
0.2575	0.2540	14.800	14.932
0.2851	0.2782	16.777	17.028
0.3096	0.3001	18.749	19.100

Table 4.19: Regressed and Experimental Solubility Data of Carbon Dioxide in [BMPIP][Tf2N] at 323.15 K

Experimental Mole Fraction of CO_2	Regressed mole fraction of CO_2	Experimental P/(ATM)	Regressed P / (ATM)
0.0024	0.0023	0.100	0.105
0.0091	0.0090	0.494	0.497
0.0175	0.0175	0.986	0.984
0.0361	0.0368	1.973	1.934
0.0698	0.0724	3.946	3.820
0.1152	0.1192	6.907	6.727
0.1454	0.1483	8.882	8.751
0.1596	0.1619	9.868	9.770
0.1734	0.1748	10.855	10.793
0.1994	0.1990	12.831	12.848
0.2264	0.2228	14.804	14.962
0.2489	0.2432	16.775	17.018
0.2719	0.2633	18.750	19.121

4.4 Non-random Two Liquid Segment Activity Coefficient Model (NRTL)

4.4.1 Non-random Two Liquid Segment Equation

Renon and Prausnitz (1968) further developed Wilson's concept of local concentrations (Eq. 4.35) with the view of obtaining a general equation that would be applicable to partially miscible liquid and gas.

$$x_{ii} = \frac{x_i \exp(-\frac{g_{ii}}{RT})}{\sum_j x_i \exp(-\frac{g_{ji}}{RT})} \quad (4.35)$$

where x_i denotes the mole fraction of species j in the binary solution and x_{ji} the local mole fraction of J in the neighborhood of a molecule of species i. The interation energy between the pair ij is g_{ij}.

In analogy to Equation 4.35, they suggest Equation 4.36 and 4.37 for the local mole fractions in a binary system:

$$x_{21} = \frac{x_2 \exp[-\frac{\alpha_{12}(g_{21}-g_{11})}{RT}]}{x_1 + x_2 \exp[-\frac{\alpha_{12}(g_{21}-g_{11})}{RT}]} \quad (4.36)$$

$$x_{12} = \frac{x_2 \exp[-\frac{\alpha_{12}(g_{12}-g_{22})}{RT}]}{x_2 + x_1 \exp[-\frac{\alpha_{12}(g_{12}-g_{22})}{RT}]} \quad (4.37)$$

The factor α is assumed to be a constant for a binary system. Thus,

$\alpha_{12}=\alpha_{21} = \alpha_{11} = \alpha_{22}$.

The partial contribution of component 1 to the Excess Gibbs energy of the solution is assumed to be of the form:

$$g^E = g^1 - g^0 \quad (4.38)$$

Similarly for component 2, the quantity g^1expresses the free energy of molecule 1 located in its own neighborhood in the solution and is given by:

$$g^1=x_{11}g_{11}+x_{21}g_{21} \quad (4.39)$$

For pure liquid state, equation 4.39 can be simplified as:

$$g^0=g_{11} \quad (4.40)$$

The working equation for the activity coefficient is obtained upon substituting Eqs. 4.36, 4.37, 4.39, and 4.40 into Eq. 4.38:

$$\text{Ln}\gamma_1 = x_2^2\{\tau_{21}\frac{\exp(-2\alpha_{12}\tau_{21})}{[x_1+x_2\exp(-\alpha_{12}\tau_{21})]^2}+\tau_{12}\frac{\exp(-\alpha_{12}\tau_{12})}{[x_2+x_1\exp(-\alpha_{12}\tau_{12})]^2}\} \quad (4.41)$$

$$\text{Ln}\gamma_2 = x_1^2\{\tau_{12}\frac{\exp(-2\alpha_{12}\tau_{12})}{[x_2+x_1\exp(-\alpha_{12}\tau_{12})]^2}+\tau_{21}\frac{\exp(-\alpha_{12}\tau_{21})}{[x_1+x_2\exp(-\alpha_{12}\tau_{21})]^2}\} \quad (4.42)$$

where:

$$\tau_{12}=a_{12}+\frac{b_{12}}{T}=\frac{g_{12}-g_{22}}{RT} \quad (4.43)$$

$$\tau_{21}=a_{21}+\frac{b_{21}}{T}=\frac{g_{21}-g_{11}}{RT} \quad (4.44)$$

where τ_{ij} and g_{ij} are zero for ideal solution and a_{ij} and b_{ij} are asymmetrical binary parameters that were regressed with α in this work.

The NRTL equation contains five constants for each binary system, i.e.,a_{12}, a_{21}, b_{21} , b_{12}, and α, that are adjustable in fitting data. To simplify the calculations, Ren and Prausnitz (1968) empirically recommended values of α for broad classes of mixture systems. Their values range from 0.2 to 0.5, and generally increase with the complexity of the ij molecular interaction, but most importantly, it needs to fit the consistency test.

4.4.2 Model Parameters and Regression

The experimental solubility results were regressed with the NRTL equation (Aspen, 2012) as one solvent and three isotherms together. The regressed five binary parameters a_{12}, a_{21}, b_{21} , b_{12}, and α all meet the consistency test, and for molecule-molecule and molecule-ion pair and ion-pair are expressed as a function of temperature, as shown in Equations 4.43 and 4.44. To reduce the number of interaction parameters, the nonrandomness factor (α) was fixed at 0.3, (same value was obtained if factor was used as a regression parameter). Equation 4.34 was used to calculate deviation between experimental and regressed solubility data. The regressed specific solubility values are presented at certain pressure and temperature in Tables 4.21 to 4.35 and Figures 4.16 to 4.30. Regressed binary parameters and deviations are shown in Table 4.20.

Table 4.20: Regressed Binary Parameters and Deviation by NRTL Equation

Binary Interaction Param -eters / Binary Systems	a_{12},	a_{21}	b_{12}	b_{21}	α	Temperature (K)	AAD`%
[(ETO)2IM][Tf2N]---Carbon Dioxide	-0.13153	-0.09877	-42.72690	-31.65150	0.3	298.15	3.74
						313.15	5.48
						323.15	6.65
[BMIM][DBP] --- Carbon Dioxide	-11.4268	3.56820	2587.81700	-1290.31250	0.3	298.15	1.39
						313.15	0.65
						323.15	1.75
[BMIM][TfO]--- Carbon Dioxide	-1.74468	-2.03142	-123.40906	25.46189	0.3	298.15	1.43
						313.15	3.04
						323.15	4.13
[DMIM][Tf2N]--- Carbon Dioxide	1.05039	-0.05213	-463.00200	-435.97452	0.3	298.15	1.62
						313.15	0.83
						323.15	0.46
[BMPIP][Tf2N]--- Carbon Dioxide	0.65552	-1.12420	280.01130	-224.85900	0.3	298.15	1.29
						313.15	0.82
						323.15	0.67

Table 4.21: Regressed and Experimental Solubility Data of Carbon Dioxide in [BMIM][DBP] at 298.15 K

Experimental Mole Fraction of CO_2	Regressed mole fraction of CO_2	Experimental P/(ATM)	Regressed P / (ATM)
0.0025	0.0024	0.095	0.097
0.0114	0.0114	0.492	0.492
0.0222	0.0223	0.986	0.982
0.0434	0.0440	1.974	1.952
0.0842	0.0858	3.947	3.895
0.1408	0.1432	6.907	6.822
0.1767	0.1796	8.882	8.777
0.1950	0.1980	9.867	9.754
0.2124	0.2157	10.856	10.734
0.2458	0.2495	12.829	12.689
0.2778	0.2819	14.804	14.643
0.3085	0.3131	16.779	16.596
0.3379	0.3429	18.752	18.543

Table 4.22: Regressed and Experimental Solubility Data of Carbon Dioxide in [BMIM][DBP] at 313.15 K

Experimental Mole Fraction of CO_2	Regressed mole fraction of CO_2	Experimental P/(ATM)	Regressed P / (ATM)
0.0023	0.0022	0.098	0.100
0.0092	0.0092	0.493	0.493
0.0174	0.0175	0.985	0.984
0.0354	0.0354	1.974	1.971
0.0688	0.0687	3.948	3.952
0.1145	0.1140	6.907	6.930
0.1446	0.1437	8.882	8.925
0.1599	0.1587	9.868	9.923
0.1771	0.1755	10.858	10.933
0.2022	0.2004	12.831	12.921
0.2283	0.2262	14.804	14.915
0.2539	0.2515	16.777	16.909
0.2793	0.2766	18.751	18.903

Table 4.23: Regressed and Experimental Solubility Data of Carbon Dioxide in [BMIM][DBP] at 323.15 K

Experimental Mole Fraction of CO_2	Regressed mole fraction of CO_2	Experimental P/(ATM)	Regressed P / (ATM)
0.0025	0.0024	0.098	0.100
0.0078	0.0078	0.495	0.496
0.0146	0.0145	0.986	0.989
0.0306	0.0303	1.973	1.986
0.0581	0.0573	3.946	3.986
0.0965	0.0948	6.906	7.005
0.1225	0.1201	8.882	9.032
0.1351	0.1323	9.866	10.044
0.1475	0.1443	10.855	11.061
0.1721	0.1681	12.826	13.092
0.1956	0.1909	14.799	15.122
0.2178	0.2125	16.778	17.152
0.2395	0.2337	18.751	19.172

Table 4.24: Regressed and Experimental Solubility Data of Carbon Dioxide in [DMIM][Tf2N] at 298.15 K

Experimental Mole Fraction of CO_2	Regressed mole fraction of CO_2	Experimental P/(ATM)	Regressed P / (ATM)
0.0027	0.0026	0.097	0.099
0.0125	0.0124	0.493	0.494
0.0242	0.0243	0.986	0.984
0.0474	0.0479	1.974	1.957
0.0919	0.0939	3.948	3.881
0.1532	0.1571	6.907	6.779
0.1908	0.1954	8.883	8.730
0.2091	0.2140	9.871	9.710
0.2266	0.2316	10.854	10.688
0.2615	0.2665	12.826	12.658
0.2942	0.2991	14.807	14.635
0.3253	0.3301	16.774	16.603
0.3555	0.3601	18.748	18.579

Table 4.25: Regressed and Experimental Solubility Data of Carbon Dioxide in [DMIM][Tf2N] at 313.15 K

Experimental Mole Fraction of CO_2	Regressed mole fraction of CO_2	Experimental P/(ATM)	Regressed P / (ATM)
0.0024	0.0023	0.098	0.101
0.0096	0.0096	0.493	0.495
0.0182	0.0182	0.985	0.987
0.0366	0.0367	1.973	1.968
0.0716	0.0723	3.947	3.916
0.1187	0.1202	6.907	6.839
0.1499	0.1515	8.881	8.808
0.1654	0.1669	9.867	9.798
0.1800	0.1815	10.857	10.789
0.2073	0.2087	12.828	12.760
0.2332	0.2346	14.803	14.738
0.2582	0.2595	16.779	16.717
0.2831	0.2841	18.754	18.706

Table 4.26: Regressed and Experimental Solubility Data of Carbon Dioxide in [DMIM][Tf2N] at 323.15 K

Experimental Mole Fraction of CO_2	Regressed mole fraction of CO_2	Experimental P/(ATM)	Regressed P / (ATM)
0.0018	0.0017	0.099	0.103
0.0073	0.0073	0.494	0.497
0.0142	0.0142	0.986	0.991
0.0306	0.0305	1.973	1.980
0.0603	0.0603	3.946	3.946
0.1005	0.1008	6.906	6.889
0.1259	0.1263	8.883	8.861
0.1393	0.1395	9.868	9.854
0.1516	0.1518	10.857	10.847
0.1780	0.1777	12.828	12.849
0.1987	0.1985	14.805	14.816
0.2198	0.2196	16.777	16.792
0.2405	0.2402	18.748	18.770

Table 4.27: Regressed and Experimental Solubility Data of Carbon Dioxide in [(ETO)2IM][Tf2N] at 298.15 K

Experimental Mole Fraction of CO_2	Regressed mole fraction of CO_2	Experimental P/(ATM)	Regressed P / (ATM)
0.0033	0.0031	0.099	0.104
0.0150	0.0144	0.491	0.513
0.0292	0.0280	0.984	1.024
0.0566	0.0544	1.975	2.050
0.1079	0.1039	3.947	4.084
0.1777	0.1714	6.908	7.129
0.2211	0.2134	8.882	9.157
0.2411	0.2329	9.869	10.167
0.2613	0.2525	10.855	11.179
0.2989	0.2891	12.830	13.197
0.3345	0.3240	14.803	15.208
0.3676	0.3566	16.772	17.206

Table 4.28: Regressed and Experimental Solubility Data of Carbon Dioxide in [(ETO)2IM][Tf2N] at 313.15 K

Experimental Mole Fraction of CO_2	Regressed mole fraction of CO_2	Experimental P/(ATM)	Regressed P / (ATM)
0.0029	0.0027	0.097	0.106
0.0115	0.0108	0.493	0.524
0.0218	0.0207	0.987	1.040
0.0438	0.0414	1.973	2.085
0.0847	0.0800	3.946	4.158
0.1395	0.1321	6.907	7.251
0.1762	0.1667	8.883	9.327
0.1916	0.1815	9.868	10.350
0.2073	0.1965	10.856	11.377
0.2377	0.2256	12.828	13.427
0.2667	0.2535	14.803	15.473
0.2947	0.2805	16.777	17.515
0.3220	0.3068	18.749	19.552

Table 4.29: Regressed and Experimental Solubility Data of Carbon Dioxide in [(ETO)2IM][Tf2N] at 323.15 K

Experimental Mole Fraction of CO_2	Regressed mole fraction of CO_2	Experimental P/(ATM)	Regressed P / (ATM)
0.0025	0.0022	0.099	0.109
0.0093	0.0087	0.491	0.526
0.0179	0.0168	0.986	1.048
0.0368	0.0343	1.973	2.108
0.0718	0.0670	3.946	4.207
0.1177	0.1101	6.907	7.333
0.1473	0.1379	8.881	9.420
0.1618	0.1515	9.869	10.465
0.1772	0.1658	10.856	11.516
0.2042	0.1913	12.826	13.592
0.2299	0.2156	14.804	15.671
0.2547	0.2392	16.780	17.743
0.2779	0.2614	18.754	19.801

Table 4.30: Regressed and Experimental Solubility Data of Carbon Dioxide in [BMIM][TfO] at 298.15 K

Experimental Mole Fraction of CO_2	Regressed mole fraction of CO_2	Experimental P/(ATM)	Regressed P / (ATM)
0.0037	0.0037	0.098	0.098
0.0124	0.0121	0.495	0.506
0.0227	0.0222	0.986	1.006
0.0427	0.0419	1.974	2.008
0.0806	0.0793	3.946	4.006
0.1327	0.1307	6.907	7.001
0.1655	0.1631	8.883	8.997
0.1816	0.1791	9.868	9.993
0.1979	0.1951	10.855	10.991
0.2279	0.2251	12.830	12.977
0.2567	0.2539	14.802	14.952
0.2849	0.2822	16.780	16.927
0.3123	0.3099	18.750	18.885

Table 4.31: Regressed and Experimental Solubility Data of Carbon Dioxide in [BMIM][TfO] at 313.15 K

Experimental Mole Fraction of CO_2	Regressed mole fraction of CO_2	Experimental P/(ATM)	Regressed P / (ATM)
0.0019	0.0018	0.099	0.106
0.0080	0.0078	0.493	0.504
0.0151	0.0147	0.986	1.009
0.0304	0.0296	1.974	2.026
0.0603	0.0583	3.947	4.062
0.1001	0.0970	6.907	7.107
0.1264	0.1224	8.882	9.142
0.1390	0.1348	9.869	10.156
0.1516	0.1470	10.857	11.171
0.1761	0.1710	12.829	13.189
0.1991	0.1937	14.805	15.194
0.2212	0.2157	16.777	17.186
0.2423	0.2369	18.752	19.164

Table 4.32: Regressed and Experimental Solubility Data of Carbon Dioxide in [BMIM][TfO] at 323.15 K

Experimental Mole Fraction of CO_2	Regressed mole fraction of CO_2	Experimental P/(ATM)	Regressed P / (ATM)
0.0018	0.0017	0.100	0.108
0.0066	0.0064	0.495	0.509
0.0125	0.0121	0.986	1.015
0.0259	0.0249	1.973	2.047
0.0510	0.0487	3.946	4.110
0.0851	0.0813	6.908	7.198
0.1069	0.1024	8.882	9.251
0.1181	0.1131	9.868	10.278
0.1286	0.1233	10.855	11.299
0.1504	0.1443	12.830	13.346
0.1704	0.1639	14.804	15.369
0.1890	0.1824	16.776	17.370
0.2085	0.2015	18.750	19.377

Table 4.33: Regressed and Experimental Solubility Data of Carbon Dioxide in [BMPIP][Tf2N] at 298.15 K

Experimental Mole Fraction of CO_2	Regressed mole fraction of CO_2	Experimental P/(ATM)	Regressed P / (ATM)
0.0029	0.0029	0.098	0.099
0.0142	0.0142	0.494	0.494
0.0279	0.0280	0.986	0.982
0.0543	0.0551	1.974	1.952
0.1038	0.1065	3.946	3.871
0.1713	0.1756	6.907	6.788
0.2128	0.2172	8.883	8.761
0.2324	0.2367	9.867	9.749
0.2514	0.2554	10.856	10.743
0.2879	0.2912	12.828	12.731
0.3218	0.3245	14.803	14.721
0.3539	0.3560	16.778	16.713
0.3847	0.3862	18.748	18.701

Table 4.34: Regressed and Experimental Solubility Data of Carbon Dioxide in [BMPIP][Tf2N] at 313.15 K

Experimental Mole Fraction of CO_2	Regressed mole fraction of CO_2	Experimental P/(ATM)	Regressed P / (ATM)
0.0028	0.0027	0.099	0.101
0.0110	0.0109	0.493	0.495
0.0207	0.0207	0.988	0.987
0.0418	0.0421	1.974	1.961
0.0808	0.0821	3.947	3.899
0.1340	0.1360	6.907	6.830
0.1677	0.1696	8.882	8.808
0.1837	0.1855	9.868	9.799
0.1992	0.2008	10.856	10.794
0.2287	0.2298	12.829	12.784
0.2575	0.2579	14.800	14.785
0.2851	0.2847	16.777	16.793
0.3096	0.3088	18.749	18.783

Table 4.35: Regressed and Experimental Solubility Data of Carbon Dioxide in [BMPIP][Tf2N] at 323.15 K

Experimental Mole Fraction of CO_2	Regressed mole fraction of CO_2	Experimental P/(ATM)	Regressed P / (ATM)
0.0024	0.0023	0.100	0.103
0.0091	0.0090	0.494	0.498
0.0175	0.0174	0.986	0.989
0.0361	0.0361	1.973	1.972
0.0698	0.0701	3.946	3.929
0.1152	0.1159	6.907	6.875
0.1454	0.1457	8.882	8.867
0.1596	0.1597	9.868	9.865
0.1734	0.1732	10.855	10.864
0.1994	0.1987	12.831	12.864
0.2264	0.2247	14.804	14.887
0.2489	0.2467	16.775	16.878
0.2719	0.2690	18.750	18.889

4.4.3 Consistency Test for the Results of NRTL Model

Unlike EoS, the NRTL model belongs to the so-called local composition models, like the Wilson, UNIQUAC, and UNIFAC models. The results of these local composition models have thermodynamically poor consistency due to the assumption that the local composition around molecule i is independent of the local composition around molecule j. Therefore, consistency of the results should be tested. Numerous forms of consistency test exist; most of them are based on the area test of the Gibbs-Duhem equation. The Gibbs-Duhem equation for the activity coefficients of a binary system can be written as:

$$x_i \frac{\partial ln\gamma_i}{\partial x_i})_{TP} + x_j \frac{\partial ln\gamma_j}{\partial x_j})_{TP} = 0 \quad (4.45)$$

At sufficiently low pressure, such as the cases in this study, the pressure dependence of the activity coefficients could be neglected, and then it would be re-written as:

$$x_i \frac{\partial ln\gamma_i}{\partial x_i})_{T} + x_j \frac{\partial ln\gamma_j}{\partial x_j})_{T} = 0 \quad (4.46)$$

Hence

$$\frac{x_i}{\gamma_i}\frac{\partial ln\gamma_i}{\partial x_i})_{T} + \frac{x_j}{\gamma_j}\frac{\partial ln\gamma_j}{\partial x_j})_{T} = 0 \quad (4.47)$$

The way of checking isothermal phase behaviour data for a binary system is to calculate activity coefficients and to plot $ln\frac{\gamma_i}{\gamma_j}$, $ln\gamma_i$, $log\gamma_i$or γ_i as a function of mole fraction of i. $ln\frac{\gamma_i}{\gamma_j}$ is plotted as a function of mole function over the entire

composition range $(0 \rightarrow 1)$ for a given temperature and pressure in the liquid phase. If the phase boundary data are mutually consistent, the areas A and B above and below the curve should be equal. The vertical line through each point indicates the uncertainty in the calculated value of $ln\frac{\gamma_i}{\gamma_j}$ arsing from the anticipated uncertainties in the experimentally determined quantities x_i, y_i(1-x_i) at certain pressure and temperature in a binary system. It could be possible to draw a smooth curve through the vertical lines at area A=B, especially for the ideal binary systems.

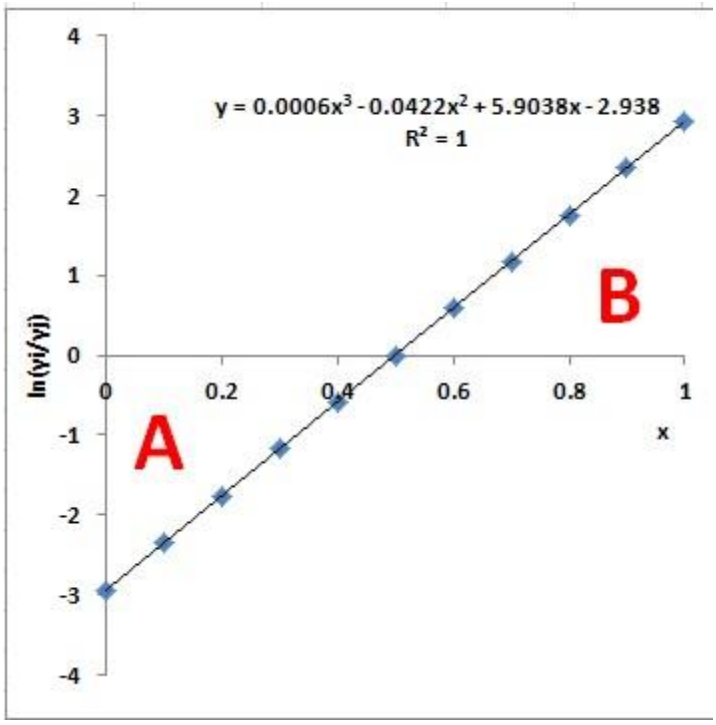

Figure 4.1: The Equal Area Test (Original in colour)

Area A=B means:

$$G^E = x_i RT ln\gamma_i + x_j RT ln\gamma_j \quad (4.48)$$

Then,

$$(\frac{1}{RT})\frac{\partial G^E}{\partial x_i})_{TP} = ln\frac{\gamma_i}{\gamma_j} + x_i(\frac{\partial ln\gamma_i}{\partial x_i})_{TP} + x_j(\frac{\partial ln\gamma_j}{\partial x_j})_{TP} = 0 \quad (4.49)$$

If we plot Eq. 4.45 in to Eq. 4.49, then it is re-written as:

$$(\frac{1}{RT})\frac{\partial G^E}{\partial x_i})_{TP} = ln\frac{\gamma_i}{\gamma_j} \quad (4.50)$$

where G^E is, by definition, zero, both when x_i=0 and x_i=1, so the integral of $\frac{\partial G^E}{\partial x_i})_{TP}$ with respect to mole fraction over the entire composition range (0→1) also must be zero. Then, Eq. 4.50 could be:

$$\int_0^1 ln\frac{\gamma_i}{\gamma_j}\mathrm{d}x_i = 0]_{TP} \quad (4.51)$$

For the binary isothermal data at low or moderate pressure, the effect of pressure can be neglected, and then, it can be simplified as:

$$\int_0^1 ln\frac{\gamma_i}{\gamma_j}\mathrm{d}x_i = 0]_{T} \quad (4.52)$$

In this study, the area thermodynamic consistency test was performed for the phase result of ionic liquid +CO_2. The value of the $ln\frac{\gamma_i}{\gamma_j}$ versus mole fraction x_i in liquid phase was plotted, and the areas of both sections (area A and B) were calculated. Appendix C shows the area test for both mixtures at several temperatures together with values area A and B. One of the most common criteria to determine if data are thermodynamically consistent or not is to compare the net area with the totally area as:

$$\Delta=\frac{|A-B|}{|A+B|}*100 \quad (4.54)$$

Δ should be as low as possible, indicating perfect data when it is zero. However, obtaining zero value is not always realistic due to experimental error. It can be considered as “respectable” as long as it is less than 5 percent or so.

Patricia et al., (2012) got the value ∆= 11, 0.062 ,7.9 for an acetonitrile+toluene binary system at temperatures 298.15, 323.15, and 343.15 K ,respectively, and 0.58, 1.5, and 1.9 for ethylacetate+ isooctane under the same conditions.

CHAPTER 5

CONCLUSION AND FUTURE WORK

5.1 Conclusion

The major conclusions drawn from this study are listed as follows:

1. Solubility of carbon dioxide was measured in 1,3-Diethoxyimidazolium bis(trifluoromethylsulfonyl)imide [[(ETO)2IM][Tf2N]], 1,3-Dimethoxy imidazolium bis(trifluoromethylsulfonyl)imide [[DMIM][Tf2N]], 1-Butyl-1-methylpiperidinium bis(trifluoromethylsulfonyl)imide [[BMPIP][Tf2N]], 1-Butyl-3-methylimidazolium trifluoromethanesulfonate [[BMIM][TfO]] and 1-Butyl-3 methylimidazolium dibutyl phosphate [[BMIM][DBP]] at 298.15, 313.15 and 323.15 K over a pressure range from 100 mbar to 20000 mbar. The experimental results show the capacity for absorbing carbon dioxide ranked from high to low as: [(ETO)2IM][Tf2N] >[BMPIP][Tf2N]>[DMIM][Tf2N]>[BMIM][DBP] >[BMIM][TfO].
2. [(ETO)2IM][Tf2N] has the most competitive affinity for carbon dioxide among any other ionic liquids that absorb carbon dioxide physically but has lower solubility, at low pressure, than ionic liquids that absorb CO_2 chemically which in turn requires more significant amount of energy to be regenerated.
3. Several thermo-physical properties of different ionic liquids were predicted including, critical temperature, pressure, acentric factors. Densities of ionic

liquids were measured and found to range from 0.800 g/cm^3 to 1.700 g/ cm^3 at temperatures from 228.5 K to 358.15 K at atmospheric pressure; densities decreased dramatically with increasing temperatures.

4. The solubility data were successfully correlated using the Peng-Robinson equation of state. The non-random two-liquid (NRTL) activity model also correlated the data quit well. Data is shown to be thermodynamically consistent.

5.2 Future Work

We propose that more Functionalized Task Specific Ionic Liquids (FTSIL) be tested as they seem more promising than conventional Ionic Liquids in terms of their absorption capacity for CO_2.

REFERENCES

Aki, S. N. V. K., Mellein, B. R., Saurer, E. M., and Brennecke, J. F., “High-pressure phase behaviour of carbon dioxide with imidazolium-based ionic liquids,” J. Phys. Chem. B, 108, 20355-20365, 2004.

Anderson, J. L., “Characterizing ionic liquids on the basis of multiple solvation interactions,” J. Am. Chem. Soc.,124, 14247–14254, 2002.

Revelli, A-L., “High carbon dioxide solubilities in imidazolium-based ionic liquids and in poly(ethylene glycol) dimethyl ether,” J. Phys. Chem. B, 114, 12908-12913, 2010.

Anthony, J. L., Maginn, E. J., and Brennecke, J. F., “CO_2 as a separation switch for ionic liquid/organic mixtures,” J. Phys. Chem. B, 106, 7315-7320, 2002.

Anthony, J. L., Anderson, J. L., Maginn, E. J., and Brennecke, J. F., “Anion effects on gas solubility in ionic liquids,” J. Phys. Chem. B, 109, 6366-6374, 2005.

Bara, J. E., “Guide to CO_2 separations in imidazolium-based room-temperature ionic liquids,” Ind. Eng. Chem. Res., 48 (6): 2739-2751, 2009.

Bates, E.D., Mayton, R. D., Ntai, I., and Davis, J.H., “CO_2 capture by a task-specific ionic liquid,” J. Am. Chem. Soc.,124(6): 926-927, 2002.

Blanchard, L. A., and Brennecke, J. F., “Recovery of organic products from ionic liquids using supercritical carbon dioxide,” Ind. Eng. Chem. Res., 40(1): 287-292, 2001**.** .

Blath, J., Christ, M., Deubler, N., Hirth, T., and Schiestel, T., “Gas solubilities in

room temperature ionic liquids – Correlation between RTiL-molar mass and Henry's law constant.," Chemical Engineering Journal, 172,167– 176, 2011.

Gurkan, B.E, J.C. Fuente, D.L., Mindrup, E.M., Goodrich, B.F., Price, E.A., Schneider, W.F., Brennecke, J.F., "Equimolar CO_2 absorption by anion functionalized ionic liquids," J. Am. Chem. Soc., 132, 2116 –2119, 2010.

Carmichael, A. J., and Seddon, K. R. J., "Polarity study of some 1-alkyl-3-methylimidazolium ambient-temperature ionic liquids with the solvatochromic dye, Nile Red," Phys. Org. Chem.,13: 591–595, 2000.

Cadena, C., Anthony, J. L., Jin, K.S., Timothy I. Morrow, J.F., Brennecke, and Edward J., Maginn, J. A., "Why is CO_2 so soluble in imidazolium-based ionic liquids," J. Am. Chem. Soc.,126, 5300-5308,2003.

Crowhurst, L., Mawdsley, P. R., Perez, J. M., Salter, P. A., and Welton,T., "Solvent-solute interactions in ionic liquids," Phys. Chem. Chem.,5: 2790-2794, 2003.

Energy Information Administration (EIA), "Annual energy outlook 2006," http://www.eia.doe.gov/oiaf/aeo/, 2006a.

Energy Information Administration (EIA), "International energy outlook 2006," http://www.eia.doe.gov/oiaf/ieo/index.html, 2006b.

Energy Information Administration (EIA), "Emissions of greenhouse gases in the United States" 2006c.

Finotello, A., Bara, J. E., Camper, D., and Noble, R. D., “Article room-temperature ionic liquids: temperature dependence of gas solubility selectivity,” Ind. Eng. Chem. Res., 47, 3453-3459.2008.

Freemantle, M., “Ionic liquids may boost clean technology development,” Chemical Engineering Journal, 76, 32-35, 1998.

Gregg, J., Andres,R., and Marland,G., “China:emissions pattern of the world leader inCO_2 emissions from fossil fuel consumption and cement production,” Geophysical Research Letters, 35, 2008.

Gutkowski, K. I., Shariati, A., and Peters, C. J. J.,” High-pressure phase behaviour of the binary ionic liquid system 1-octyl-3-methylimidazolium tetrafluoroborate + carbon dioxide,” J. of Supercritical Fluids, 39, 187-191, 2006.

Klara, S.M., Srivastava, R.D., and McIlvried, H.G., “Integrated collaborative technology development program for CO_2 sequestration in geologic formations—United States,” Energy Conversion and Management, 44, 2699–2712, 2003.

Kohl, A. and Nielsen, R., “Gas Purification”, 5th Edition, Gulf Publishing Company: Houston Texas, 1997.

Hamilton, D. J., “Continuous flow hydroformylation of alkenes in supercritical fluid-ionic liquid biphasic systems,” J. Am. Chem. Soc., 125, 15577-15588, 2003.

Marsh, K. N.; Boxall, J.A. and Lichtenthaler, R., “Room temperature ionic liquids and their mixtures, a review,” Fluid Phase Equilibria, 219, 93-98, 2004.

Mathias, P.M., and Thomas W., “Extension of the Peng-Robinson equation of state to complex mixtures: evaluation of the various forms of the local composition concept,” Fluid Phase Equilibria, 13, 91-108, 1983.

Heintz, A., “Recent developments in thermodynamics and thermophysics of nonaqueous mixtures containing ionic liquids,” J. Chem. Thermo-dynamics, 37, 525-535, 2005.

Moore, D. D., “Experimental studies of gas adsorption on microporous materials,” M.S. Thesis, Department of Chemical Engineering, University of Notre Dame, Notre Dame, IN, 2000.

Muldoon, M.J., Sudhir, N. V. K., Aki, J.L., JaNeille K. D., and Brennecke, J.F., “Improving carbon dioxide solubility in ionic liquids,” Phys. Chem.,111, 9001-9009, 2007.

Netherlands Environmental Assessment Agency (NEAA), “Global CO_2 emissions: annual increase 2008”http://www.pbl.nl/en/news/pressreleases/2009/20090625-Global-CO_2-emission s_-annual-increase-halved-in-2008.htmlS, 2009.

Patricia, L., Wouters, C., Sweygers, N., Creemers, C., and Bruggen ,B. V., “The potential of head-space gas chromatography for VLE measurements,” J. Chem. Thermodynamics, 49, 128–136, 2009.

Pinkerton, E. P., Meyer, M. S., Tibbetts, G. G., and Chahine, R.,“High-pressure gravimetric measurement of hydrogen capacity in vapour-grown carbon

Nano fibers and related materials, Proceedings of the 11th Canadian Hydrogen Conference," Victoria, BC, 633-642, 2001.

Poling, B. E., Prausnitz, J. M., and O'Connell, J. P., "The Properties of Gases and Liquids", 5th ed., McGraw-Hill: New York, 1987.

Prausnitz, J. M., and Renon, H., "Molecular thermodynamic fluid phase equilibrium", Inst. Chem. Eng. J(14),135, 1968.

Scovazzo, P., Kieft, J., Finan, D. A., Koval, C., DuBois, D., and Noble, R., "Gas separations using non-hexafluorophosphate [PF6]− anion supported ionic liquid membranes," Journal of Membrane Science, 238, 57-63, 2004.

Seddon, K. R., "Room-temperature ionic liquids: Neoteric solvents for clean catalysis," Kinet. Catal., 37(5), 693-697, 1996.

Shen, K.P., and Li, M.H, "Solubility of carbon dioxide in aqueous mixtures of monoethanolamine with methyldiethanolamine" J. Chem. Eng., 37, 96-100, 1992.

Shiflett, M. B., and Yokozeki, A., "Solubilities and diffusivities of carbon dioxide in ionic liquids: [bmim][PF_6] and [bmim][BF_4]," Ind. Eng. Chem. Res., 44, 4453-4464, 2005.

Shiflett, M. B., and Yokozeki, A., "Solubility of CO_2 in room temperature ionic liquid [hmim][Tf_2N]," J. Phys. Chem. B, 111, 2070-2074, 2007.

Singh, R., Reddy, M. K., Wilson, S., Joshi, K., Diniz, C., and Webley, P., "High temperature materials for CO_2 capture," Energy Procedia,1, 623–630, 2009.

Sumon, Z. K., and Henni, A. “Ionic liquids for CO_2 capture using COSMO-RS: Effect of structure, properties and molecular interactions on solubility and selectivity,” Fluid Phase Equilibria, 310, 39– 55, 2011.

Valderrama, J.O., and Robles, P. A., “Critical properties, normal boiling temperatures,and acentric factors of fifty ionic liquids,” Ind. Eng. Chem. Res., 46,1338 -1344, 2007.

Webb, P. B., Sellin, M. F., Kunene, T. E., and Williamson, S., **“**Continuous flow hydroformylation of alkenes in supercritical fluid-ionic liquid biphasic systems,” J. Am. Chem. Soc., 125, 15577-15588, 2003.

Welton, T., “Room-temperature ionic liquids: solvents for synthesis and catalysis,” Chem. Rev., 99, 2071–2033, 1999.

Wilkes, J. S., “Dialkylimidazolium chloroaluminate melts: a new class of room-temperature ionic liquids for electrochemistry, spectroscopy, and synthesis,” Inorg. Chem., 21, 1263-1264,1982.

Yang, H., Xu, Z., Fan, M., Gupta, R., Slimane, R., Bland, A., and Wright, I., “Progress in carbon dioxide separation and capture: A review,” Journal of Environmental Sciences, 20, 14-27, 2008.

Yokozeki A., Shiflett, M.B., Junk, C.P., Liane M.G., and Foo, T., “Physical and chemical absorptions of carbon dioxide in room temperature ionic liquids” J. Phys. Chem. B: 112, 16654–16663, 2008.

Yim, J-H., Song, H.N., Yoo, K-P., and Lim, J.S., “Measurement of CO_2 solubility in ionic liquids: [BMP][Tf2N] and [BMP][MeSO4] by measuring bubble-point Pressure,” J. Chem. Eng., 56,1197–1203, 2011.

APPENDICES

Appendix A1: Peng-Robinson Equation of State

$$P=\frac{RT}{v-b}-\frac{a}{v(v+b)+b(v-b)}$$

$$a_i = 0.45724\frac{R^2T_{c,i}^2}{P_{c,i}}[1+c_i(1-T_{r,i}^{0.5})]^2$$

$$b_i = 0.07780\frac{RT_{c,i}}{P_{c,i}}$$

For

ω>0.2

$$c_i = 0.3796 + 1.485\omega - 0.1644\omega^2 + 0.0166\omega^3$$

$$k_{11} = 0; k_{22} = 0$$

vdW Mixing Rules:

$$a = \sum_i \sum_j x_i x_j a_{ij}$$

$$b = \sum_i x_i b_i$$

$$a_{ij} = \left(a_i a_j\right)^{0.5}(1-k_{ij})$$

For binary system: $k_{11} = 0; k_{22} = 0;$

$a = x_1^2 a_1 + 2x_1x_2a_{12} + x_2^2a_2$; b=$x_1b_1 + x_2b_2$

$$a_{12} = (a_1a_2)^{0.5}(1-k_{12})$$

Compressibility Equation:

$$Z^3 - (1-B)Z^2 + (A-3B^2-2B)Z - (AB-B^2-B^3) = 0$$

A=$\frac{aP}{(RT)^2}$; B=$\frac{bP}{RT}$

At equilibrium, the fugacity of each component in both phases is equal.

Therefore,

$f_i^V = f_I^L$

It can be re-written as:

$f_i^V = y_i P \Phi_i^V; f_i^L = x_i P^{Sat} \Phi_i^L;$

Fugacity equation:

Vapour phase:

$$\ln\frac{f_i^V}{y_i P} = ln\Phi_i^V = \frac{b_i}{b}(Z^v - 1) - \ln(Z^v - B) - \frac{A}{2.848B}\left[\frac{2\sum_j y_j a_{ij}}{a} - \frac{b_i}{b}\right]\ln[\frac{Z^V + 2.414B}{Z^V - 2.414B}]$$

Liquid phase:

$$\ln\frac{f_i^L}{y_i P} = ln\Phi_i^L = \frac{b_i}{b}(Z^L - 1) - \ln(Z^L - B) - \frac{A}{2.848B}\left[\frac{2\sum_j y_j a_{ij}}{a} - \frac{b_i}{b}\right]\ln[\frac{Z^L + 2.414B}{Z^L - 2.414B}]$$

Appendix A2: NRTL Model

The NRTL model for a binary system is given by:

$$\frac{g^E}{RT} = x_1 x_2 \left(\frac{\tau_{21} x_{21}}{x_1 + x_2 G_{21}} + \frac{\tau_{12} G_{12}}{x_1 + x_1 G_{12}}\right)$$

$\tau_{12} = \frac{g_{12} - g_{22}}{RT} = \frac{\Delta g_{12}}{RT}$, $\tau_{12} = \frac{g_{21} - g_{11}}{RT} = \frac{\Delta g_{12}}{RT}$,

G_{12}=exp (-$\alpha_{12}\tau_{12}$), G_{21}=exp (-$\alpha_{21}\tau_{21}$),

$$\text{Ln}\gamma_1 = x_2^2 \{\tau_{21} \left(\frac{G_{21}}{x_1 + x_2 G_{21}}\right)^2 + + \frac{\tau_{12} G_{12}}{[x_2 + x_1 G_{12}]^2}\}$$

$$\text{Ln}\gamma_2 = x_1^2 \{\tau_{12} \left(\frac{G_{12}}{x_2 + x_1 G_{12}}\right)^2 + + \frac{\tau_{21} G_{21}}{[x_1 + x_2 G_{21}]^2}\}$$

Appendix B: Group Contributions for Various Properties

(Valderrama et al., 2007)

groups	ΔT_{bM}	ΔT_M	ΔP_M	ΔV_M
		Without Rings		
$-CH_3$	23.58	0.0275	0.3031	66.81
$-CH_2-$	22.88	0.0159	0.2165	57.11
>CH−	21.74	0.0002	0.1140	45.70
>C<	18.18	−0.0206	0.0539	21.78
$=CH_2$	24.96	0.0170	0.2493	60.37
=CH−	18.25	0.0182	0.1866	49.92
=C<	24.14	−0.0003	0.0832	34.90
=C=	26.15	−0.0029	0.0934	33.85
≡CH		0.0078	0.1429	43.97
≡C−		0.0078	0.1429	43.97
−OH (alcohol)	92.88	0.0723	0.1343	30.40
−O−	22.42	0.0051	0.1300	15.61
>C=O	94.97	0.0247	0.2341	69.76
−CHO	72.24	0.0294	0.3128	77.46
−COOH	169.06	0.0853	0.4537	88.60
−COO−	81.10	0.0377	0.4139	84.76
HCOO−		0.0360	0.4752	97.77
=O (others)	−10.50	0.0273	0.2042	44.03
$-NH_2$	73.23	0.0364	0.1692	49.10
>NH	50.17	0.0119	0.0322	78.96
>N−	11.74	−0.0028	0.0304	26.70
−N=	74.60	0.0172	0.1541	45.54
−CN	125.66	0.0506	0.3697	89.32
$-NO_2$	152.54	0.0448	0.4529	123.62
−F	−0.03	0.0228	0.2912	31.47
−Cl	38.13	0.0188	0.3738	62.08
−Br	66.86	0.0124	0.5799	76.60
−I	93.84	0.0148	0.9174	100.79
		With Rings		
$-CH_2-$	27.15	0.0116	0.1982	51.64
>CH−	21.78	0.0081	0.1773	30.56
=CH−	26.73	0.0114	0.1693	42.55
>C<	21.32	−0.0180	0.0139	17.62
=C<	31.01	0.0051	0.0955	31.28
−O−	31.22	0.0138	0.1371	17.41
−OH (phenol)	76.34	0.0291	0.0493	−17.44
>C=O	94.97	0.0343	0.2751	59.32
>NH	52.82	0.0244	0.0724	27.61
>N−		0.0063	0.0538	25.17
−N=	57.55	−0.0011	0.0559	42.15
		New Groups		
−B	−24.56	0.0352	0.0348	22.45
−P	34.86	−0.0084	0.1776	67.01
$-SO_2$	147.24	−0.0563	−0.0606	112.19

Appendix C: Consistency Test Results

This part of appendix includes the result of consistency test for modeling results of all five solvents in chapter 4.4.3.

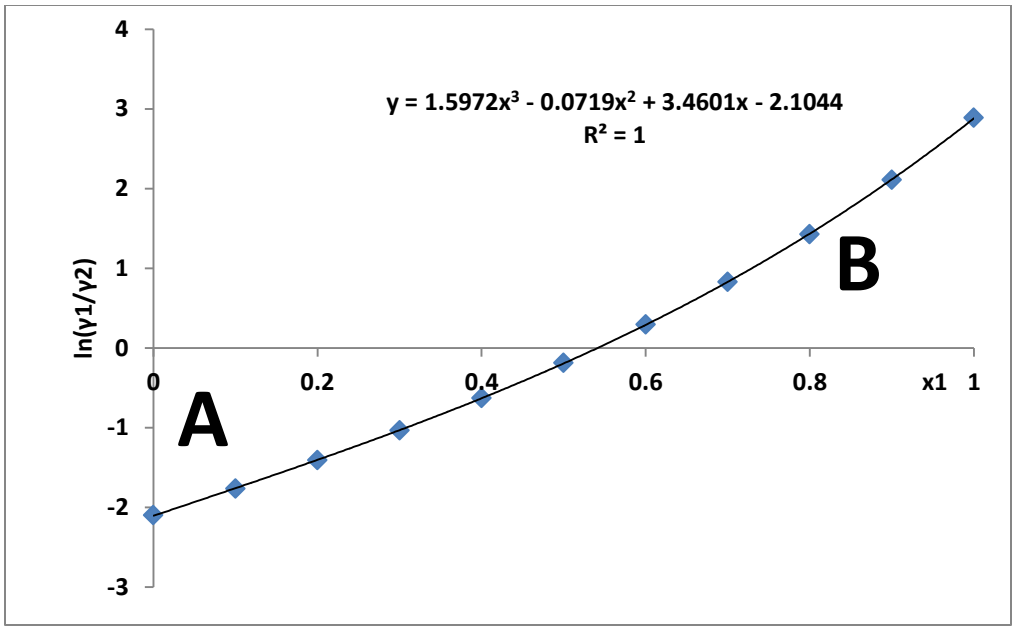

Figure C1: Area Thermodynamic Consistency Test for [DMIM][Tf2N]+Carbon Dioxide at 298.15 K

Area A: 0.601718, Area B: 0.602701, consistency Δ (%): 0.081616

Table C1: Area Thermodynamic Consistency Test for [DMIM][Tf2N]+Carbon Dioxide at 298.15 K

x1	x2	$\ln\gamma_1$	$\ln\gamma_2$	$\frac{dln\gamma_1}{dx_1}$	$\frac{dln\gamma_2}{dx_1}$	Consistency $x_1\frac{dln\gamma_1}{dx_1}+x_2\frac{dln\gamma_2}{dx_1}$
0.0	1.0	-2.09869	0.00000	5.90360	-0.00010	0.0
0.1	0.9	-1.77964	-0.01693	5.30573	-0.58954	0.0
0.2	0.8	-1.47868	-0.07025	4.70954	-1.17736	0.0
0.3	0.7	-1.19612	-0.16471	4.11501	-1.76354	0.0
0.4	0.6	-0.93303	-0.30677	3.52214	-2.34808	0.0
0.5	0.5	-0.69151	-0.50496	2.93095	-2.93100	0.0
0.6	0.4	-0.47491	-0.77056	2.34142	-3.51228	0.0
0.7	0.3	-0.28833	-1.11844	1.75357	-4.09194	0.0
0.8	0.2	-0.13918	-1.56830	1.16738	-4.66996	0.0
0.9	0.1	-0.03804	-2.14636	0.58285	-5.24634	0.0
1.0	0.0	0.00000	-2.88785	0.00000	-5.82110	0.0

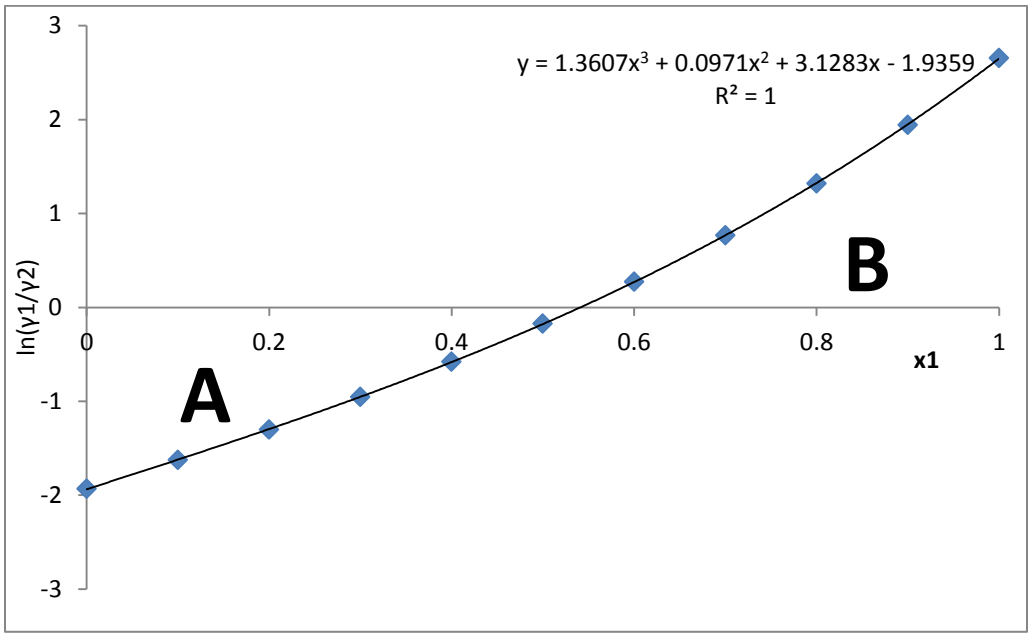

Figure C2: Area Thermodynamic Consistency Test for [DMIM][Tf2N]+Carbon Dioxide at 313.15 K

Area A: 0.555260, Area B: 0.556052, Consistency Δ (%): 0.071267

Table C2: Area Thermodynamic Consistency Test for [DMIM][Tf2N]+Carbon Dioxide at 313.15 K

x1	x2	$\ln\gamma_1$	$\ln\gamma_2$	$\frac{dln\gamma_1}{dx_1}$	$\frac{dln\gamma_2}{dx_1}$	Consistency $x_1\frac{dln\gamma_1}{dx_1}+x_2\frac{dln\gamma_2}{dx_1}$
0.0	1.0	-1.93117	0.00000	5.90320	-0.00010	0.0
0.1	0.9	-1.64049	-0.01545	5.30537	-0.58950	0.0
0.2	0.8	-1.36469	-0.06432	4.70922	-1.17728	0.0
0.3	0.7	-1.10458	-0.15129	4.11473	-1.76342	0.0
0.4	0.6	-0.86162	-0.28250	3.52190	-2.34792	0.0
0.5	0.5	-0.63817	-0.46586	2.93075	-2.93080	0.0
0.6	0.4	-0.43771	-0.71167	2.34126	-3.51204	0.0
0.7	0.3	-0.26522	-1.03327	1.75345	-4.09166	0.0
0.8	0.2	-0.12767	-1.44806	1.16730	-4.66964	0.0
0.9	0.1	-0.03477	-1.97886	0.58281	-5.24598	0.0
1.0	0.0	0.00000	-2.65583	0.00000	-5.82070	0.0

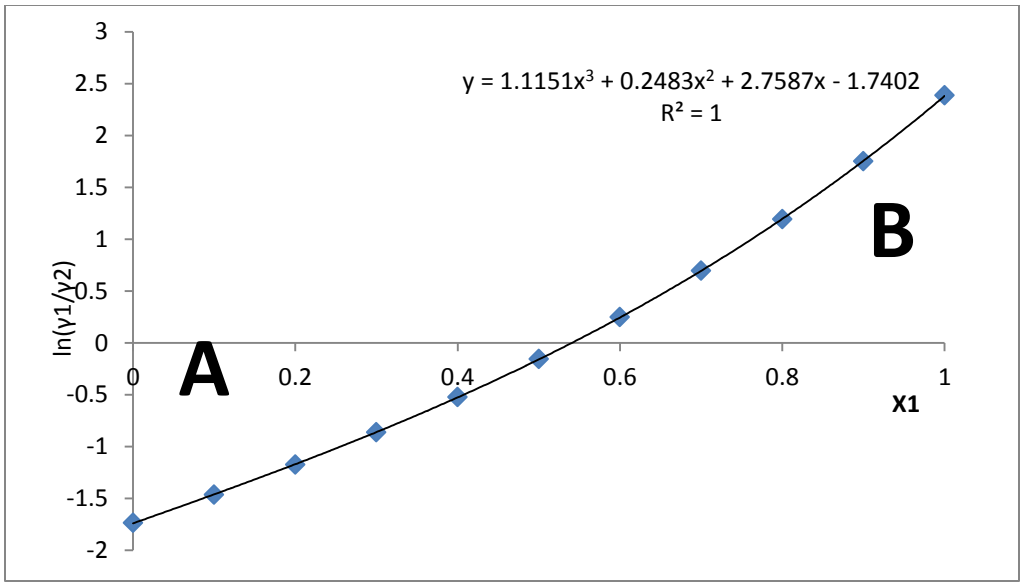

Figure C3: Area Thermodynamic Consistency Test for [DMIM][Tf2N]+Carbon Dioxide at 323.15 K

Area A**:** 0.500753, Area B: 0.501445, Consistency Δ (%): 0.069048

Table C3: Area Thermodynamic Consistency Test for [DMIM][Tf2N]+Carbon Dioxide at 323.15 K

x1	x2	$\ln\gamma_1$	$\ln\gamma_2$	$\frac{dln\gamma_1}{dx_1}$	$\frac{dln\gamma_2}{dx_1}$	Consistency $x_1\frac{dln\gamma_1}{dx_1}+x_2\frac{dln\gamma_2}{dx_1}$
0.0	1.0	-1.73653	0.00000	5.90270	-0.00010	0.0
0.1	0.9	-1.47794	-0.01376	5.30493	-0.58944	0.0
0.2	0.8	-1.23104	-0.05752	4.70884	-1.17716	0.0
0.3	0.7	-0.99702	-0.13579	4.11441	-1.76324	0.0
0.4	0.6	-0.77769	-0.25424	3.52164	-2.34768	0.0
0.5	0.5	-0.57559	-0.42010	2.93055	-2.93050	0.0
0.6	0.4	-0.39421	-0.64251	2.34112	-3.51168	0.0
0.7	0.3	-0.23833	-0.93312	1.75337	-4.09124	0.0
0.8	0.2	-0.11437	-1.30684	1.16728	-4.66916	0.0
0.9	0.1	-0.03103	-1.78289	0.58285	-5.24544	0.0
1.0	0.0	0.00000	-2.38619	0.00010	-5.82010	0.0

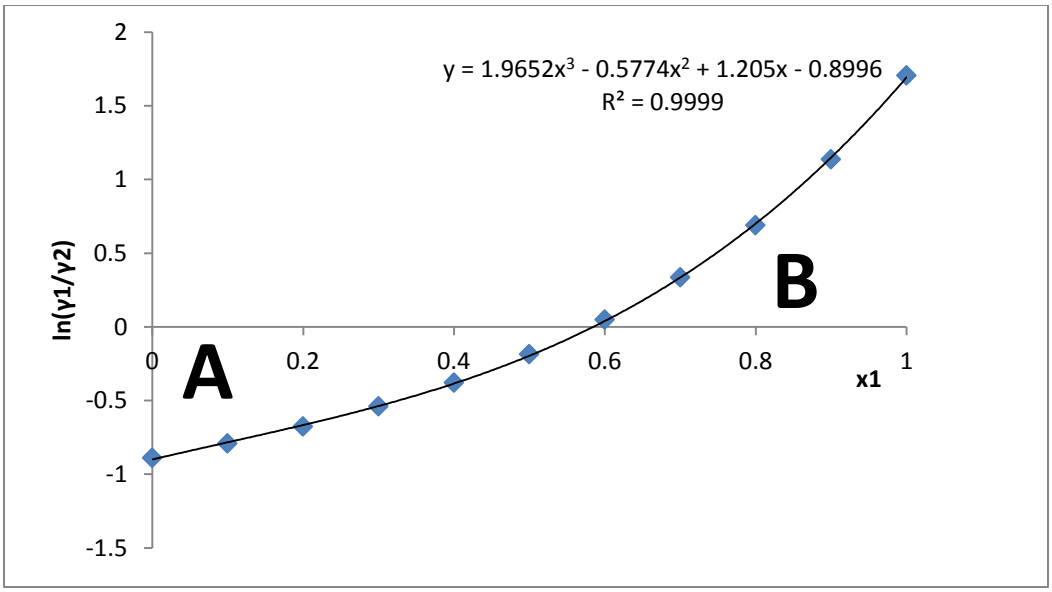

Figure C4: Area Thermodynamic Consistency Test for [BMPIP][Tf2N]+Carbon Dioxide at 298.15 K

Area A: 0.301068, Area B: 0.302801, Consistency Δ (%): 0.286982

Table C4: Area Thermodynamic Consistency Test for [BMPIP][Tf2N]+Carbon Dioxide at 298.15 K

x1	x2	$\ln\gamma_1$	$\ln\gamma_2$	$\frac{dln\gamma_1}{dx_1}$	$\frac{dln\gamma_2}{dx_1}$	Consistency $x_1\frac{dln\gamma_1}{dx_1}+x_2\frac{dln\gamma_2}{dx_1}$
0.0	1.0	-0.89	0	0.7804	4E-15	0.0
0.1	0.9	-0.80	-0.00506	0.70236	-0.07804	0.0
0.2	0.8	-0.70	-0.02251	0.62432	-0.15608	0.0
0.3	0.7	-0.60	-0.05667	0.54628	-0.23412	0.0
0.4	0.6	-0.49	-0.1134	0.46824	-0.31216	0.0
0.5	0.5	-0.39	-0.20073	0.3902	-0.3902	0.0
0.6	0.4	-0.28	-0.32988	0.31216	-0.46824	0.0
0.7	0.3	-0.18	-0.5166	0.23412	-0.54628	0.0
0.8	0.2	-0.09	-0.78348	0.15608	-0.62432	0.0
0.9	0.1	-0.03	-1.16342	0.07804	-0.70236	0.0
1.0	0.0	0.00	-1.70533	1.5E-13	-0.7804	0.0

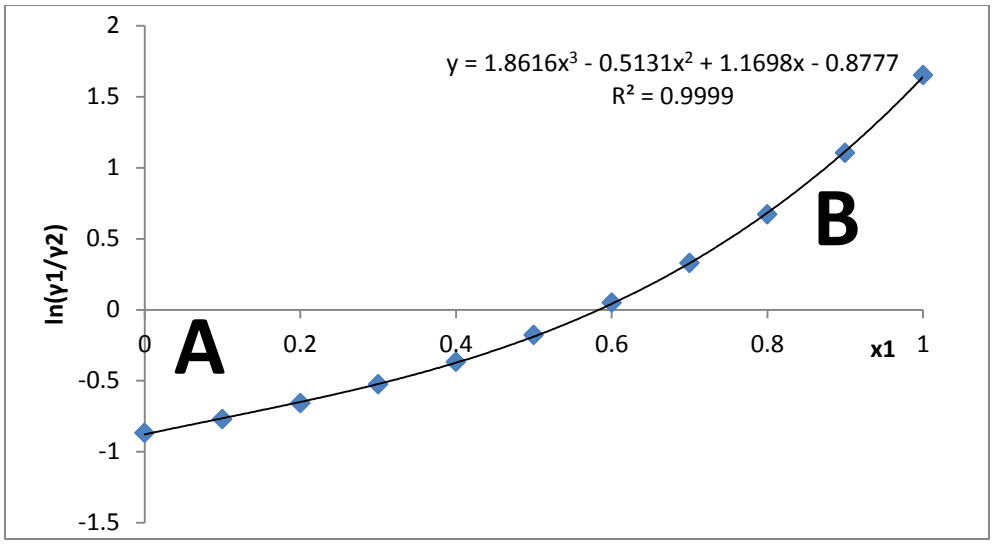

Figure C5: Area Thermodynamic Consistency Test for [BMPIP][Tf2N]+Carbon Dioxide at 313.15 K

Area A: 0.293024, Area B: 0.294591, Consistency Δ (%): 0.266671

Table C5: Area thermodynamic Consistency Test for [BMPIP][Tf2N]+Carbon Dioxide at 313.15 K

x1	x2	$\ln\gamma_1$	$\ln\gamma_2$	$\frac{dln\gamma_1}{dx_1}$	$\frac{dln\gamma_2}{dx_1}$	Consistency $x_1\frac{dln\gamma_1}{dx_1}+x_2\frac{dln\gamma_2}{dx_1}$
0.0	1.0	-0.86875	0	0.7946	6E-14	0.0
0.1	0.9	-0.77688	-0.00496	0.71514	-0.07946	0.0
0.2	0.8	-0.68085	-0.02209	0.63568	-0.15892	0.0
0.3	0.7	-0.58116	-0.05556	0.55622	-0.23838	0.0
0.4	0.6	-0.47872	-0.11108	0.47676	-0.31784	0.0
0.5	0.5	-0.37505	-0.19642	0.3973	-0.3973	0.0
0.6	0.4	-0.27267	-0.32237	0.31784	-0.47676	0.0
0.7	0.3	-0.17558	-0.50405	0.23838	-0.55622	0.0
0.8	0.2	-0.09011	-0.76296	0.15892	-0.63568	0.0
0.9	0.1	-0.02627	-1.13027	0.07946	-0.71514	0.0
1.0	0.0	0	-1.65196	1.5E-13	-0.7946	0.0

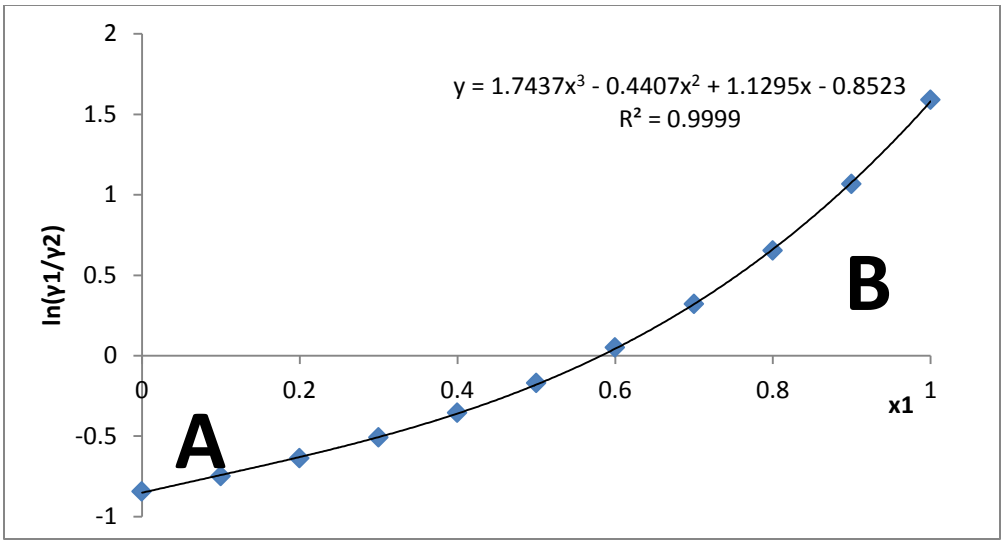

Figure C6: Area Thermodynamic Consistency Test for [BMPIP][Tf2N]+Carbon Dioxide at 323.15 K

Area A**:** 0.283688, Area B: 0.285163, Consistency Δ (%): 0.259295

Table C6: Area Thermodynamic Consistency Test for [BMPIP][Tf2N]+Carbon Dioxide at 323.15 K

x1	x2	$\ln\gamma_1$	$\ln\gamma_2$	$\frac{dln\gamma_1}{dx_1}$	$\frac{dln\gamma_2}{dx_1}$	Consistency $x_1\frac{dln\gamma_1}{dx_1}+x_2\frac{dln\gamma_2}{dx_1}$
0.0	1.0	-0.84411	0	0.8115	4E-14	0.0
0.1	0.9	-0.75421	-0.00486	0.73034	-0.08116	0.0
0.2	0.8	-0.66034	-0.02159	0.64918	-0.16232	0.0
0.3	0.7	-0.56301	-0.05428	0.56802	-0.24348	0.0
0.4	0.6	-0.46314	-0.10839	0.48686	-0.32464	0.0
0.5	0.5	-0.36228	-0.19143	0.4057	-0.4058	0.0
0.6	0.4	-0.2629	-0.31368	0.32454	-0.48696	0.0
0.7	0.3	-0.16892	-0.48951	0.24338	-0.56812	0.0
0.8	0.2	-0.08646	-0.73923	0.16222	-0.64928	0.0
0.9	0.1	-0.02513	-1.09202	0.08106	-0.73044	0.0
1.0	0.0	0	-1.59055	-1E-04	-0.8116	0.0

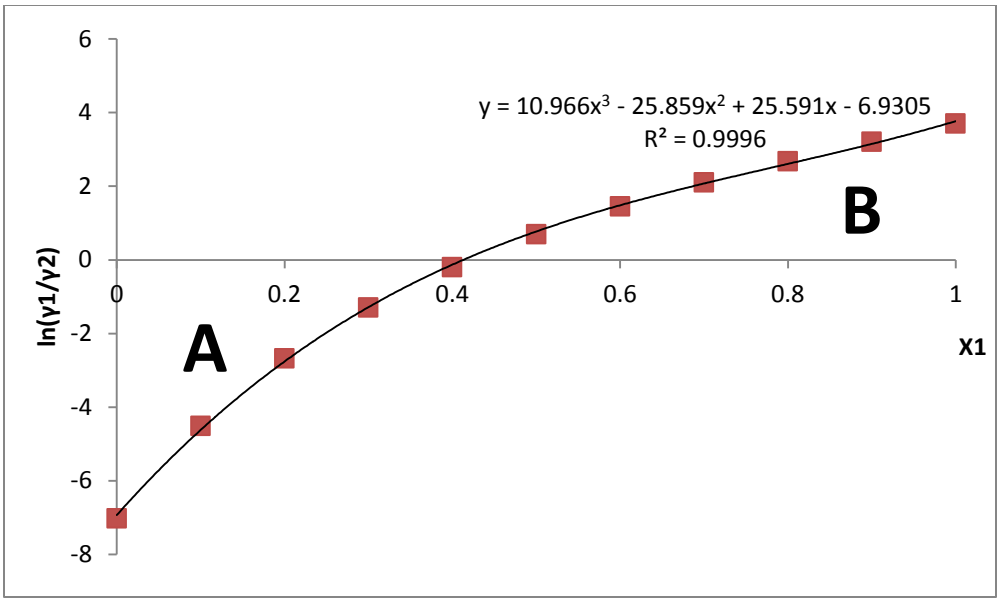

Figure C7: Area Thermodynamic Consistency Test for [BMIM][DBP] +Carbon Dioxide at 298.15 K

Area A: 1.20723, Area B: 1.19407, Consistency Δ (%): 0.548036

Table C7: Area Thermodynamic Consistency Test for [BMIM][DBP] +Carbon Dioxide at 298.15 K

x1	x2	$\ln\gamma_1$	$\ln\gamma_2$	$\frac{dln\gamma_1}{dx_1}$	$\frac{dln\gamma_2}{dx_1}$	Consistency $x_1\frac{dln\gamma_1}{dx_1}+x_2\frac{dln\gamma_2}{dx_1}$
0.0	1.0	-7.02	0	10.45	-0.1121	0.0
0.1	0.9	-4.63	-0.11854	8.978985	-1.022751	0.0
0.2	0.8	-3.07	-0.38839	7.6055	-1.874464	0.0
0.3	0.7	-2.02	-0.73274	6.329545	-2.667239	0.0
0.4	0.6	-1.31	-1.11416	5.15112	-3.401076	0.0
0.5	0.5	-0.82	-1.51484	4.070225	-4.075975	0.0
0.6	0.4	-0.48	-1.9273	3.08686	-4.691936	0.0
0.7	0.3	-0.25	-2.34971	2.201025	-5.248959	0.0
0.8	0.2	-0.10	-2.78356	1.41272	-5.747044	0.0
0.9	0.1	-0.02	-3.23237	0.721945	-6.186191	0.0
1.0	0.0	0.00	-3.70107	0.1287	-6.5664	0.0

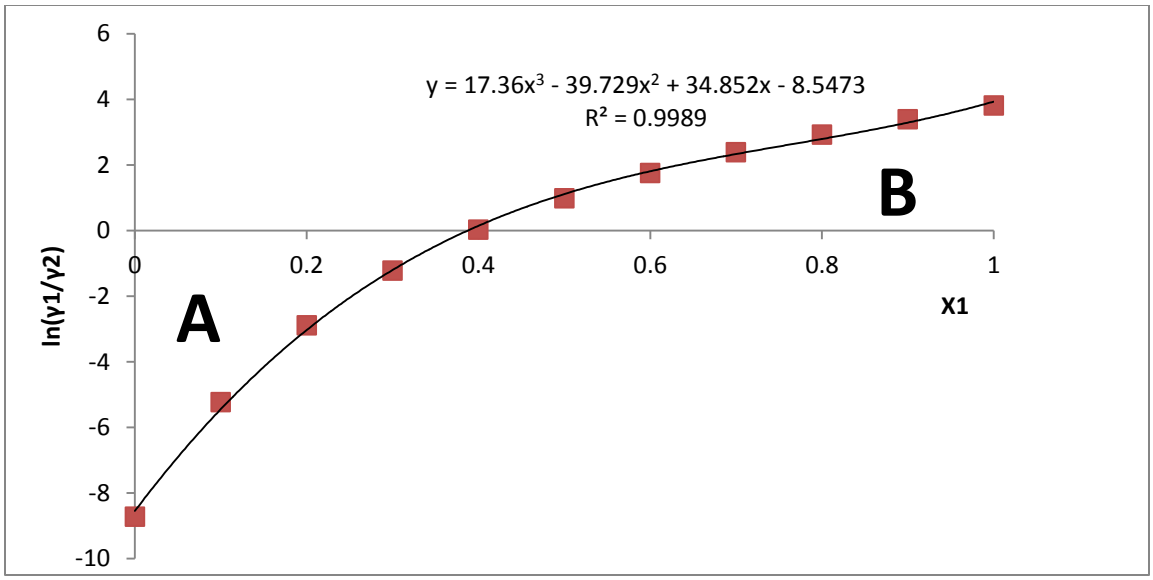

Figure C8: Area Thermodynamic Consistency Test for [BMIM][DBP] +Carbon Dioxide at 313.15 K

Area A: 1.36815, Area B: 1.34385, Consistency Δ (%): 0.896018

Table C8: Area Thermodynamic Consistency Test for [BMIM][DBP] +Carbon Dioxide at 313.15 K

x1	x2	$\ln\gamma_1$	$\ln\gamma_2$	$\frac{dln\gamma_1}{dx_1}$	$\frac{dln\gamma_2}{dx_1}$	Consistency $x_1\frac{dln\gamma_1}{dx_1}+x_2\frac{dln\gamma_2}{dx_1}$
0.0	1.0	-8.72149	0	10.45	-0.112	0.0
0.1	0.9	-5.39347	-0.1621	8.979156	-1.02258	0.0
0.2	0.8	-3.39237	-0.50683	7.605824	-1.87423	0.0
0.3	0.7	-2.13748	-0.91928	6.330004	-2.66695	0.0
0.4	0.6	-1.32817	-1.3507	5.151696	-3.40075	0.0
0.5	0.5	-0.79822	-1.78083	4.0709	-4.07563	0.0
0.6	0.4	-0.45093	-2.20238	3.087616	-4.69157	0.0
0.7	0.3	-0.22777	-2.61415	2.201844	-5.24859	0.0
0.8	0.2	-0.09229	-3.01789	1.413584	-5.74669	0.0
0.9	0.1	-0.02132	-3.41678	0.722836	-6.18586	0.0
1.0	0.0	0	-3.81466	0.1296	-6.5661	0.0

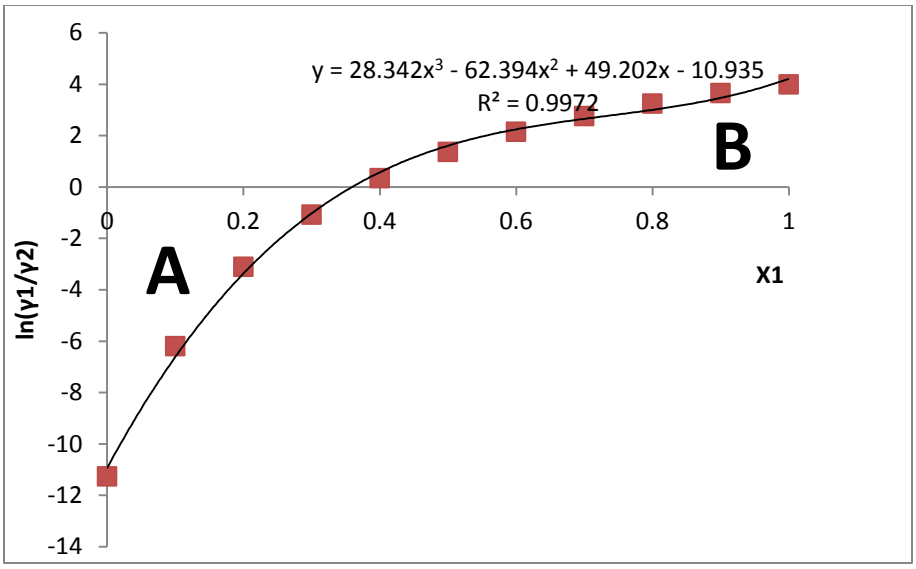

Figure C9: Area Thermodynamic Consistency Test for [BMIM][DBP] +Carbon Dioxide at 323.15 K

Area A**:** 1.59966, Area B: 1.55316, Consistency Δ (%): 1.47487

Table C9: Area Thermodynamic Consistency Test for [BMIM][DBP] +Carbon Dioxide at 323.15 K

x1	x2	$\ln\gamma_1$	$\ln\gamma_2$	$\frac{dln\gamma_1}{dx_1}$	$\frac{dln\gamma_2}{dx_1}$	Consistency $x_1\frac{dln\gamma_1}{dx_1}+x_2\frac{dln\gamma_2}{dx_1}$
0.0	1.0	-11.2721	0	10.448	-0.112	0.0
0.1	0.9	-6.42315	-0.23121	8.977384	-1.0225	0.0
0.2	0.8	-3.78601	-0.6829	7.604256	-1.87409	0.0
0.3	0.7	-2.25886	-1.18323	6.328616	-2.66677	0.0
0.4	0.6	-1.33789	-1.67306	5.150464	-3.40053	0.0
0.5	0.5	-0.76972	-2.13333	4.0698	-4.07538	0.0
0.6	0.4	-0.41741	-2.56018	3.086624	-4.69131	0.0
0.7	0.3	-0.20276	-2.95549	2.200936	-5.24833	0.0
0.8	0.2	-0.0791	-3.32316	1.412736	-5.74643	0.0
0.9	0.1	-0.0176	-3.6676	0.722024	-6.18562	0.0
1.0	0.0	0	-3.9931	0.1288	-6.5659	0.0

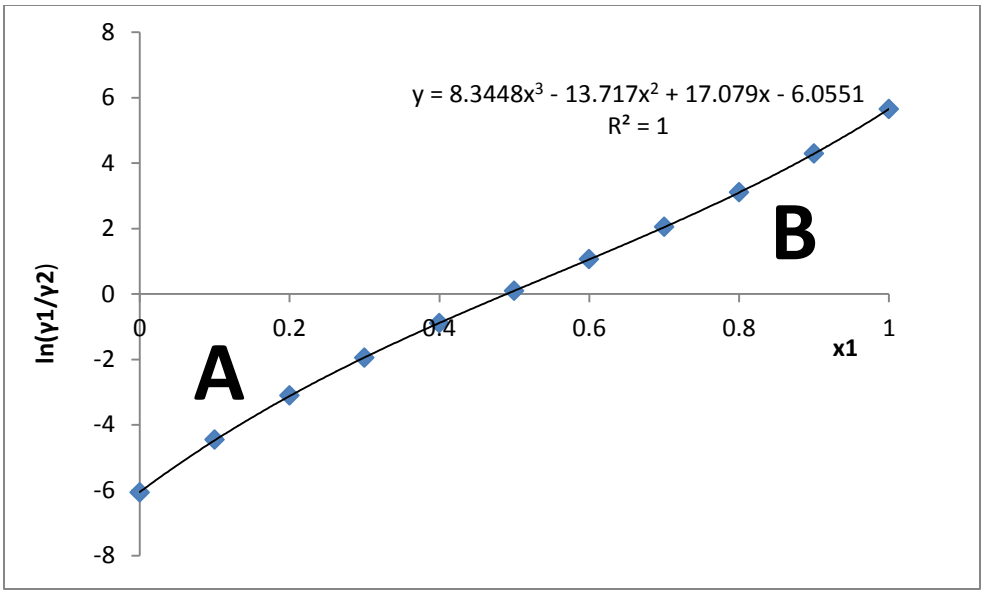

Figure C10: Area Thermodynamic Consistency Test for [BMIM][TfO]+Carbon Dioxide at 298.15 K

Area A: 1.33433, Area B: 1.33260, Consistency Δ (%): 0.064869

Table C10: Area Thermodynamic Consistency Test for [BMIM][TfO]+Carbon Dioxide at 298.15 K

x1	x2	$\ln\gamma_1$	$\ln\gamma_2$	$\frac{dln\gamma_1}{dx_1}$	$\frac{dln\gamma_2}{dx_1}$	Consistency $x_1\frac{dln\gamma_1}{dx_1}+x_2\frac{dln\gamma_2}{dx_1}$
0.0	1.0	-6.07	0	3.5954	-0.0936	0.0
0.1	0.9	-4.53	-0.07809	3.40015	-0.403481	0.0
0.2	0.8	-3.39	-0.27785	3.17016	-0.775804	0.0
0.3	0.7	-2.51	-0.56743	2.90543	-1.210569	0.0
0.4	0.6	-1.83	-0.93384	2.60596	-1.707776	0.0
0.5	0.5	-1.29	-1.37754	2.27175	-2.267425	0.0
0.6	0.4	-0.85	-1.91038	1.9028	-2.889516	0.0
0.7	0.3	-0.51	-2.55587	1.49911	-3.574049	0.0
0.8	0.2	-0.24	-3.35154	1.06068	-4.321024	0.0
0.9	0.1	-0.07	-4.35395	0.58751	-5.130441	0.0
1.0	0.0	0.00	-5.64751	0.0796	-6.0023	0.0

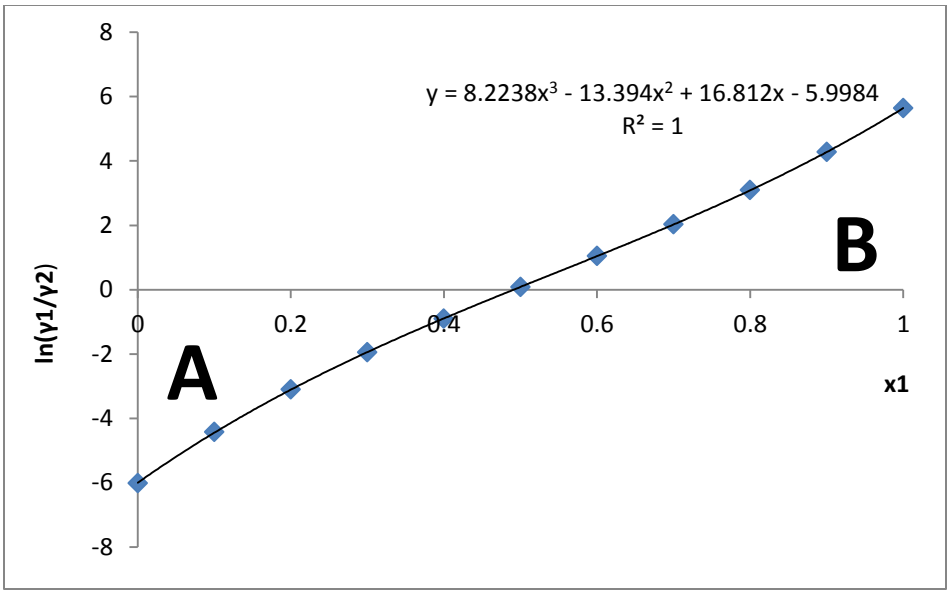

Figure C11: Area Thermodynamic Consistency Test for [BMIM][TfO]+Carbon Dioxide at 313.15 K

Area A: 1.32768, Area B: 1.32656, Consistency Δ (%): 0.042197

Table C11: Area Thermodynamic Consistency Test for [BMIM][TfO]+Carbon Dioxide at 313.15 K

x1	x2	$\ln\gamma_1$	$\ln\gamma_2$	$\frac{dln\gamma_1}{dx_1}$	$\frac{dln\gamma_2}{dx_1}$	Consistency $x_1\frac{dln\gamma_1}{dx_1}+x_2\frac{dln\gamma_2}{dx_1}$
0.0	1.0	-6.01287	0	3.5953	-0.0935	0.0
0.1	0.9	-4.49943	-0.07686	3.400033	-0.4034	0.0
0.2	0.8	-3.37013	-0.27405	3.170032	-0.77572	0.0
0.3	0.7	-2.50535	-0.56076	2.905297	-1.21048	0.0
0.4	0.6	-1.82786	-0.9245	2.605828	-1.70766	0.0
0.5	0.5	-1.28756	-1.36601	2.271625	-2.26728	0.0
0.6	0.4	-0.85293	-1.8973	1.902688	-2.88932	0.0
0.7	0.3	-0.50635	-2.54205	1.499017	-3.5738	0.0
0.8	0.2	-0.24206	-3.338	1.060612	-4.3207	0.0
0.9	0.1	-0.06633	-4.34209	0.587473	-5.13004	0.0
1.0	0.0	0	-5.63931	0.0796	-6.0018	0.0

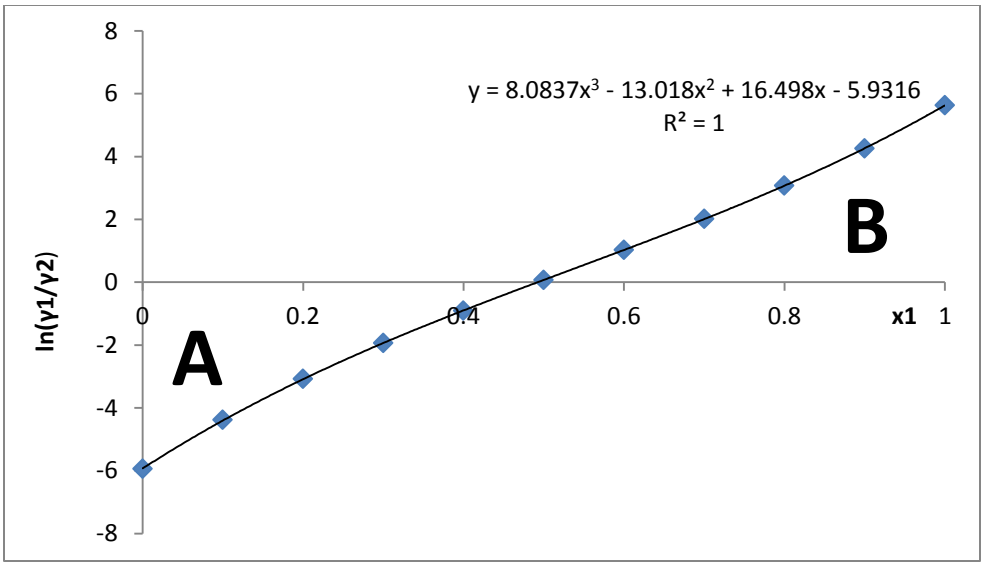

Figure C12: Area Thermodynamic Consistency Test For [BMIM][TfO]+Carbon Dioxide at 323.15 K

Area A: 1.31994, Area B: 1.31893, Consistency Δ (%): 0.038274

Table C12: Area Thermodynamic Consistency Test for [BMIM][TfO]+Carbon Dioxide at 323.15 K

x1	x2	$\ln\gamma_1$	$\ln\gamma_2$	$\frac{d\ln\gamma_1}{dx_1}$	$\frac{d\ln\gamma_2}{dx_1}$	Consistency $x_1\frac{d\ln\gamma_1}{dx_1}+x_2\frac{d\ln\gamma_2}{dx_1}$
0.0	1.0	-5.94439	0	3.5951	-0.0935	0.0
0.1	0.9	-4.46076	-0.0754	3.399816	-0.40341	0.0
0.2	0.8	-3.34909	-0.26957	3.169804	-0.77572	0.0
0.3	0.7	-2.4947	-0.55288	2.905064	-1.21045	0.0
0.4	0.6	-1.82317	-0.91345	2.605596	-1.7076	0.0
0.5	0.5	-1.28612	-1.35235	2.2714	-2.26715	0.0
0.6	0.4	-0.85304	-1.88178	1.902476	-2.88912	0.0
0.7	0.3	-0.50698	-2.52563	1.498824	-3.57349	0.0
0.8	0.2	-0.2426	-3.3219	1.060444	-4.32028	0.0
0.9	0.1	-0.06654	-4.32796	0.587336	-5.12949	0.0
1.0	0.0	0	-5.62956	0.0795	-6.0011	0.0

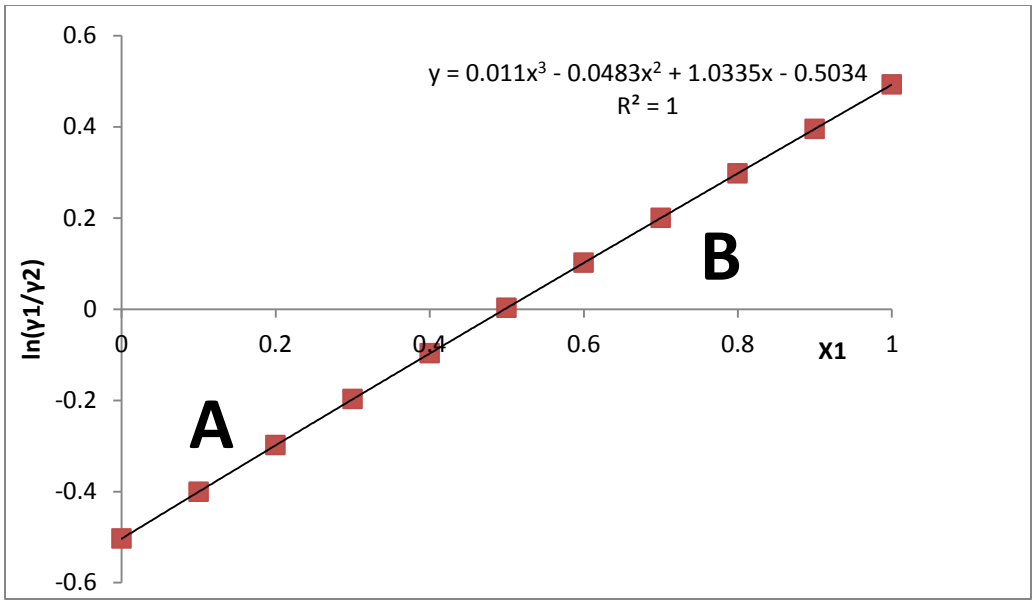

Figure C13: Area Thermodynamic Consistency Test for [(ETO)2IM][Tf2N]+Carbon Dioxide at 298.15 K

Area A: 0.124357, Area B: 0.124357, Consistency Δ (%): 0.000000

Table C13: Area Thermodynamic Consistency Test for [(ETO)2IM][Tf2N]+Carbon Dioxide at 298.15 K

x1	x2	$\ln\gamma_1$	$\ln\gamma_2$	$\frac{dln\gamma_1}{dx_1}$	$\frac{dln\gamma_2}{dx_1}$	Consistency $x_1\frac{dln\gamma_1}{dx_1}+x_2\frac{dln\gamma_2}{dx_1}$
0.0	1.0	-0.50	0	6.7306	-0.0242	0.0
0.1	0.9	-0.41	-0.00514	5.978	-0.670012	0.0
0.2	0.8	-0.32	-0.02043	5.24364	-1.305528	0.0
0.3	0.7	-0.24	-0.0457	4.52752	-1.930748	0.0
0.4	0.6	-0.18	-0.08083	3.82964	-2.545672	0.0
0.5	0.5	-0.12	-0.12567	3.15	-3.1503	0.0
0.6	0.4	-0.08	-0.18014	2.4886	-3.744632	0.0
0.7	0.3	-0.04	-0.24413	1.84544	-4.328668	0.0
0.8	0.2	-0.02	-0.3176	1.22052	-4.902408	0.0
0.9	0.1	0.00	-0.40048	0.61384	-5.465852	0.0
1.0	0.0	0.00	-0.49276	0.0254	-6.019	0.0

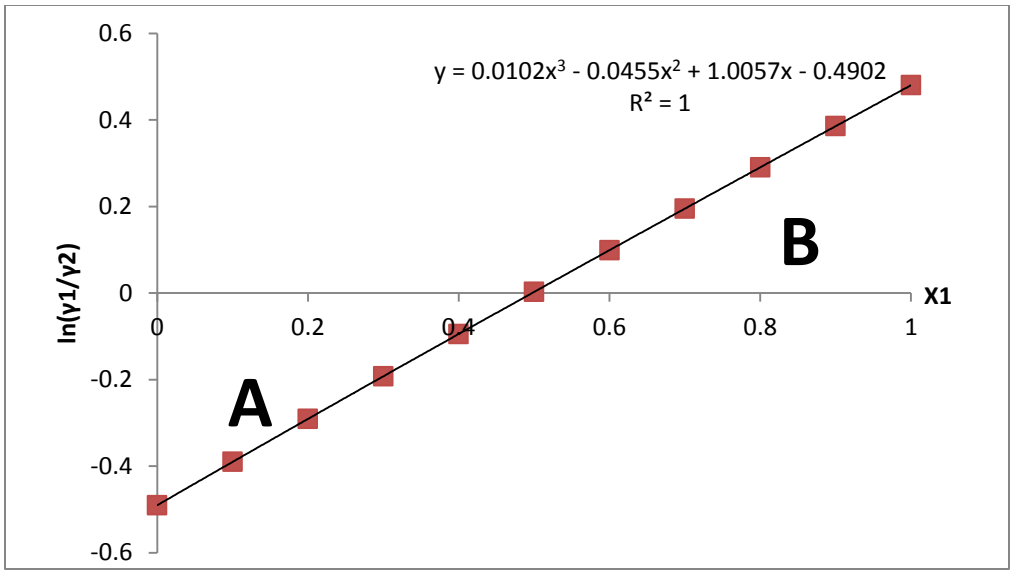

Figure C14: Area thermodynamic consistency test for [(ETO)2IM][Tf2N]+Carbon Dioxide at 313.15 K

Area A: 0.121127, Area B: 0.121161, Consistency Δ (%): 0.014000

Table C14: Area Thermodynamic Consistency Test for [(ETO)2IM][Tf2N]+Carbon Dioxide at 313.15 K

x1	x2	$\ln\gamma_1$	$\ln\gamma_2$	$\frac{d\ln\gamma_1}{dx_1}$	$\frac{d\ln\gamma_2}{dx_1}$	Consistency $x_1\frac{d\ln\gamma_1}{dx_1}+x_2\frac{d\ln\gamma_2}{dx_1}$
0.0	1.0	-0.49025	0	6.7301	-0.0242	0.0
0.1	0.9	-0.39511	-0.005	5.977577	-0.66997	0.0
0.2	0.8	-0.31072	-0.01988	5.243288	-1.30545	0.0
0.3	0.7	-0.23685	-0.0445	4.527233	-1.93063	0.0
0.4	0.6	-0.17329	-0.07871	3.829412	-2.54551	0.0
0.5	0.5	-0.11989	-0.1224	3.149825	-3.1501	0.0
0.6	0.4	-0.07646	-0.17547	2.488472	-3.74439	0.0
0.7	0.3	-0.04287	-0.23783	1.845353	-4.32839	0.0
0.8	0.2	-0.019	-0.30943	1.220468	-4.90209	0.0
0.9	0.1	-0.00474	-0.39022	0.613817	-5.46549	0.0
1.0	0.0	0	-0.48016	0.0254	-6.0186	0.0

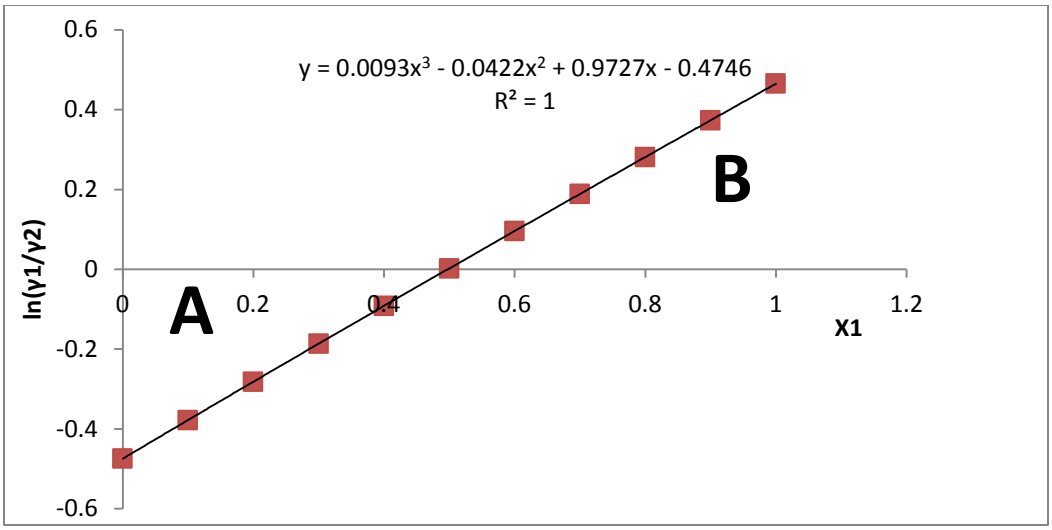

Figure C15: Area Thermodynamic Consistency Test for [(ETO)2IM][Tf2N]+Carbon Dioxide at 323.15 K

Area A**:** 0.11733, Area B: 0.11734, Consistency Δ (%): 0.00384

Table C15: Area Thermodynamic Consistency Test for [(ETO)2IM][Tf2N]+Carbon Dioxide at 323.15 K

x1	x2	$\ln\gamma_1$	$\ln\gamma_2$	$\frac{dln\gamma_1}{dx_1}$	$\frac{dln\gamma_2}{dx_1}$	Consistency $x_1\frac{dln\gamma_1}{dx_1}+x_2\frac{dln\gamma_2}{dx_1}$
0.0	1.0	-0.474613	0	6.7295	-0.0242	0.0
0.1	0.9	-0.382581	-0.00484	5.977074	-0.66992	0.0
0.2	0.8	-0.300914	-0.01924	5.242876	-1.30534	0.0
0.3	0.7	-0.229406	-0.04307	4.526906	-1.93048	0.0
0.4	0.6	-0.167873	-0.07619	3.829164	-2.54532	0.0
0.5	0.5	-0.116147	-0.11851	3.14965	-3.14988	0.0
0.6	0.4	-0.07408	-0.16991	2.488364	-3.74414	0.0
0.7	0.3	-0.041539	-0.23033	1.845306	-4.32812	0.0
0.8	0.2	-0.018409	-0.29971	1.220476	-4.9018	0.0
0.9	0.1	-0.00459	-0.37799	0.613874	-5.4652	0.0
1.0	0.0	0	-0.46516	0.0255	-6.0183	0.0